Republic of Iraq
Ministry of Higher Education and Scientific Research
University of Babylon
College of Materials Engineering
Department of Polymer and Petrochemical Industries

Comparing Study for PEDOT:PSS/Graphene and PEDOT:PSS/Graphene with Isopropyl Alcohol Nanocomposite Thin Films by Spin Coating Technique

A Thesis

Submitted to the Council of the College of Materials Engineering/ University of Babylon in Partial Fulfillment of the Requirements for the Master Degree in Materials Engineering/ Polymer

By

Sura Kamel Jebur Zamel

(B. Sc. in materials engineering, 2017)

Supervised by

Prof. Dr. Auda Jabbar Braihi

Assist. Prof. Dr. Ali Salah Hassan

2021 A.D. 1443 A.H.

بِسْمِ ٱللَّهِ ٱلرَّحْمَٰنِ ٱلرَّحِيمِ

۞ ٱللَّهُ نُورُ ٱلسَّمَٰوَٰتِ وَٱلْأَرْضِ ۚ مَثَلُ نُورِهِۦ كَمِشْكَوٰةٍ فِيهَا
مِصْبَاحٌ ۖ ٱلْمِصْبَاحُ فِى زُجَاجَةٍ ۖ ٱلزُّجَاجَةُ كَأَنَّهَا كَوْكَبٌ دُرِّىٌّ
يُوقَدُ مِن شَجَرَةٍ مُّبَٰرَكَةٍ زَيْتُونَةٍ لَّا شَرْقِيَّةٍ وَلَا غَرْبِيَّةٍ يَكَادُ
زَيْتُهَا يُضِىٓءُ وَلَوْ لَمْ تَمْسَسْهُ نَارٌ ۚ نُّورٌ عَلَىٰ نُورٍ ۚ يَهْدِى ٱللَّهُ
لِنُورِهِۦ مَن يَشَآءُ ۚ وَيَضْرِبُ ٱللَّهُ ٱلْأَمْثَٰلَ لِلنَّاسِ ۗ وَٱللَّهُ بِكُلِّ شَىْءٍ
عَلِيمٌ ﴿٣٥﴾

سورة النور الآية 35

Dedication

To my Mom and Dad;

The reason of what I become today. Thanks for your great support and conditions care through my life.

To my brothers;

Mustafa
Mohammed

To my sisters;

Dhuha
Nabaa
Wadaq

With Respect

Sura kamel

Acknowledgment

I would like to express my deepest sense of gratitude to my supervisors, ***Proff. Dr. Auda Jabbar Braihi*** and ***Assist. Proff. Dr. Ali Salah Hasan*** for their continuous advice and encouragement throughout the course of this work. I thank them for the guidance and great effort they made in supervising this scientific field.

Additionally, I would like to thank ***Assist. Proff. Dr. Ammar emad, Proff. Dr. Akram Jebur, Proff. Dr Khaled Haneen*** and ***Omer Ahmed*** for their help in carrying out the research. With the utmost gratitude, I would like to thank ***Sara Kareem, eng Ali Dadush*** and ***Mr. Hussin Abd Alabas*** for their continuous support during the research period. Sincere thanks are also expressed to the staff of the college of Materials Engineering especially in Polymers laboratories (***Ban Juad, Ali Yhea and Fadaa Ather)*** for the encouragement during this work.

Finally, I would like to express my appreciation and love to the members of my family and my friends for their support, inspiration, and care during this work.

Sura 2021

Abstract

A low-cost, long-wavelength optical sensor has been manufactured using Spin Coating technology on a glass substrate. The sensor consists of a polymeric nanocomposite composed of PEDOT:PSS polymer, in addition to nano-graphene in different weight ratios (0.5, 1, 1.5, 2). Also, Isopropyl Alcohol (IPA) was added as a dispersant to improve the diffusion of graphene nano-filler within the main phase of the complex and it was compared with the initial compound (PEDOT:PSS/Graphene)

To ensure good adhesion between the glass substrate and the components of the nanocomposite, the surface of the substrate was prepared according to international contexts and chemically etched using Piranha solution consisting of hydrogen peroxide (H_2O_2) and concentrated sulfuric acid (H_2SO_4). Roughness and Wettability tests were carried out before and after the etching of the prepared substrates. The optical method was adopted to measure the thickness of the prepared films and to ensure that all the prepared films were of equal thickness.

A zeta potential test was conducted to ascertain the role of the proposed dispersant material (IPA) to increase the diffusion of the nano-graphene filler, as this dispersant material was used for the first time with nano-graphene and it was proposed to overcome the problem of graphene deposition after a few hours of preparing the suspension, which was Do not use the same suspension the next day of laboratory work.

Infrared spectroscopy (FTIR) was employed to determine the type of bonding between the components and to suggest a model for the bonding, while the X-ray diffraction (XRD) technique was used to study crystalline variables. The effect of the nano-filler on thermal transitions was monitored using a differential scanning calorimeter (DSC), and scanning electron microscopy (SEM) and atomic forces (AFM) studied the morphological properties. As for the optical properties, they were studied

by UV-Vis spectroscopy. Visible spectrometer The electrical conductivity was measured by DC Keithley device, while wettability was studied according to the principle of contact angle.

The results confirmed the success of the surface preparation and chemical etching processes in changing the topography and surface roughness of the substrate, in a way that ensures efficient adhesion of it with the nanocomposite. It was also found that the method of rotary coating used has the ability to produce films of close thickness. It was 245 ± 5 nm. The results also showed the ability of the proposed dispersant material (IPA) to bring about the desired change in preventing the deposition of graphene nano-filler and increasing the stability of the suspension from good stability to excellent stability, as the zeta potential changed from -48.04 to -168.38 Millivolts as well as mobility changed from -2.27 to - / (V/cm) 1.6 (μ/s).

The results of infrared spectroscopy showed that no chemical reaction occurred between the components of the compound, and only the occurrence of hydrogen bonding's, and accordingly a model of the attraction between the components was proposed, which is achieved in three steps. A new bonding occurs between the oxygen (which is present at 1% in the graphene sheets) with the hydrogen available in the polymer, thus increasing the surface activity of the graphene (it has hydroxyl groups), which qualifies it to bond with the available water.

The addition of graphene caused noticeable effects on the crystallinity, as it transformed the semi-crystalline structure of the pure polymer into a crystalline structure. At position 2Θ= 550. The increase in crystallinity was enhanced by accompanying calculations such as the crystallite size according to the Scherrer equation, which increased from 0.1 to 2.8487 nanometers, and the scattering function, which increased from 0.25783 to 0.29921. The addition of graphene also caused an increase

in the degree of glass transition (Tg) by 35% and a shift from the hydrophilic nature to the hydrophobic nature, as the contact angle changed from 74.6450 to 136.6240.

The results of the AFM showed an increase in the roughness coefficients, as the average roughness (Sa) increased by about 92% and the density of the peaks (Sds) by 45%. These results matched with the SEM images, which showed that the PEDOT:PSS films without graphene have a relatively smoother surface than the surfaces of the nanocomposites. . The fluid retention index (Sci) increased by 7.23% due to the formation of very small compartments that store fluids in the superimposed as a result of the aforementioned hydrogen bonding, in the same context. The surface bearing index (Sbi) increased by a very high (525%), which indicates the expected improvement in the mechanical specifications of the prepared films.

The spectroscopy of UV-visible rays proved that the addition of graphene, (especially with IPA) an increase in the absorbance in all three regions of the spectrum (UV region, infrared region, and visible region) and the increase is at its peak in the UV region, which indicates the possibility of the prepared sensor resisting deterioration. Ultraviolet radiation (because it will absorb it and dissipate it inside it in the form of a slight heat) and its ability to work within a long wavelength that includes the three regions. The spectroscopy itself proved that the band gab energy decreased, especially after the addition of the dispersant material, and that the gap values are within the working range of the sensors. This spectrometry also showed clear changes in the excitation and damping coefficients and the dielectric constant. The electrical conductivity measurements showed a significant increase by adding Nano graphene.

Table contents

List of Figures

List of Tables

List of English Symbols

Symbol	Meaning
X	spacing of the fringes
ΔX	displacement
λ	Laser light wavelength.
L_{hkl}	grain size
k	constant
β	line broadening at half the maximum intensity
θ	Bragg angle
ω	Angular frequency in (rad)
ω_o	critical angular frequency (rad)
E_g	energy gap
λ_c	critical wavelength
r	exponential modulus
A'	proportionality constant
α	absorption coefficient
T_{op}	Transmission
R	reflectivity
t	thickness of the film
A	Absorbance
k	Extinction coefficient
n	Refractive Index
ε_τ	dielectric constant

N	complex refractive index
ρ	film resistivity
R	resistance (Ω)
σ	electric conductance (S/cm)

List of Abbreviations

Abbreviate	Meaning
PEDOT:PSS	Poly(3,4-ethylenedioxythiophene)polystyrene sulfonate
IPA	Isopropyl Alcohol
PNC	Polymer Nano Composites
PVA	Poly vinyl alcohol
PMMA	Poly methyl methacrylate
PE	Polyethylene
TCF	transparent conductive films
POSS	Polyhedral Oligomeric Silsesquioxane
PVD	Physical Vapor Deposition
PVD	Chemical vapor Deposition
LEDS	Light-emitting diodes
PLD	Pulsed laser deposition
ALD	Atomic layer deposition
CVD	Chemical vapor deposition
LDR	light dependent resister
CCDs	charge coupled devices
Rx	receiver
Tx	Transmitter
ITO	Indium Tin Oxide
FTO	Fluorine doped Tin Oxide

1.1 General Introduction

Thin-film technologies have advanced significantly over the last several decades, becoming one of the major components of electronic, medical or energy related industries [1 and 2]. As freestanding structures, two-dimensional thin films have advantages over bulk materials due to their large surface-to volume ratios, which are desirable for applications requiring enhanced surface interactions. Thin films, can also be employed as coatings over bulk materials to achieve application-specific properties that are unattainable in the substrate material. With the advance of polymer thin-film deposition techniques, polymer films continue to garner more recognition in the thin-film industry that historically has been dominated by inorganic films [3].

A polymer is a long chain organic molecule composed of one or more types of monomers. The organic nature of the polymer thin films makes them invaluable for biomedical applications and the ability to tune the response of the films by functionalization significantly expands the application areas of the polymer thin films [4]. Furthermore, the mechanical robustness, ease of processing and the low cost of polymer thin films are desirable characteristics for industrial applications.

Polymer thin films are ubiquitous in contemporary life. Most commonly, they can be found as protective or optical coatings, but the last few decades has witnessed the birth of organic electronics, thus furthering incorporation of polymer thin films into cutting edge technologies and exponential growth of the field. Whether a film is utilized for its optical, electronic, chemical, or surface properties, in-depth understanding of its structural properties is often crucial to development of a successful product [5].

PEDOT:PSS is a conductive polymer used successfully in commercial applications due to its outstanding properties. On the other hand, graphene attracted enormous attention because of its unique electronic, thermal, and optical properties [6 and 7]. Carbon atoms in graphene are sp^2 hybridized and covalently bonded to form a honeycomb structure [8].

PEDOT: PSS is a mixed polymer comprising of two ionomers: polythiophene based conjugated polymer; poly (3, 4-ethylenedioxythiophene) having a positive charge and polystyrenesulfonate with the sulfonyl group being deprotonated and carries a negative charge [9].

PEDOT itself is insoluble in water, which means dealing with PEDOT alone was quite difficult. Therefore, PSS was added to PEDOT to made the PEDOT: PSS water soluble material. PSS is insulator in nature therefore; it reduces the overall electrical conductivity of the polymer mixture. Alternatively, it is possible to tune up the electrical conductivity through chemical treatment. In addition, it has higher mechanical flexibility, processability, thermal stability and transparency [10].

As a conductive polymer, PEDOT:PSS is commonly used in production of electrodes in many electronic devices due to its low cost [11].

In current work, thin films of Graphene/ PEDOT:PSS were prepared on glass substrates for sensor by spin coating technique. Graphene were added by (0.5, 1, 1.5, and 2) wt.%. Structural, optical and morphological properties were steadied by XRD, FTIR, AFM, SEM and UV-Visible techniques.

1.2 Aims of the current work:

This work aims to:

1. Study the structural, morphological and optical properties for thin film for photo sensor application.

2. Prepare thin film from PEDOT:PSS/Graphene and with .

3. Study the effect of Graphene addition by simple technique in different concentrations on the thin film properties.

1.3 Scope of the current work:

To achieve the above aims, the following activities has been done:

1. Literature survey on the relating topics.

2. Choose simple technique, which is spin coating method.

3. Increasing the substrate surface reactivity by treating the glass substrates by Piranha solution.

4. Carrying out the required structural, morphological and optical tests to determine various properties, such as interaction type, crystallinity state, band gap, roughness, UV-degradation and so on.

2.1 Introduction

Polymers, being a highly diverse class of materials, are widely used in daily life. So far, the significance of polymeric materials has been much more accentuated due to their applications in different domains of science, technology, and industry. Furthermore, the demand for high strength polymeric materials and their lightweight composites is continuously increasing owing to their excellent mechanical properties, low processing temperature, high performances, low cost, and good environmental stability [12].

Polymers have limited use for the manufacture of goods and structures on their own, since their properties are not very high when compared to other materials, for example, most metals. Their properties can be improved when the polymer system (matrix) is combined with reinforcing material (filler)، producing that way a "composite". In connection to matrix properties, the properties of the composite are strongly depended on the filler characteristics among which the size of the filler plays dominant role. Polymer composites with the size of the filler in the nanoscale regime generates the polymer Nano composites (PNC) and the related technology, the nanotechnology [13 and 14].

The area of nanotechnology has been a very hot topic and it has the potential to make our lives better and to make the world a better place to live in [15].

Nanotechnology refers to the research and development of materials that contain structures or features that have at least one length up to approximately 100 nm، which exhibit improved or novel properties that are the direct result of their small size. These novel properties result from the tremendous amount of surface area that can occur between phases.

Globally, in addition to the traditionally used microfillers, nanofillers has also been of tremendous academic and industrial interest. Depending on the combination of matrix-Nano filler a variety of PNC can be produced even on demand. During recent years, these Nano composites have generated much research interest owing to remarkable enhancements in the various composite properties at very low cost and thereby entered in our everyday life [16].

The polymer/Nano filler compatibility leads to synergistic improvements in the composite properties, where the achieved properties are superior to those of the individual components.

Polymer/graphene Nano composites synthesized and also polymers that doped with the graphene like"Poly vinyl alcohol (PVA)", epoxy, Polyethylene (PE)," Poly(methyl methacrylate (PMMA)" [17 and 18]. The polymer/graphene nanocomposite showing greater properties that attributed of the special properties of graphene, therefore appearing superior characterizes like: thermal, electrical, optical and mechanical associated to pure of polymer. This special properties of these nanocomposite enable them to use in many applications, such as aerospace, automotive, electronics and piezoelectric [19]. Because the great specific surface region and the strong graphene-graphene intermolecular van der Waals interactions, therefore the graphene incline to great clusters in polymer network and solvents, subsequently this restrictions diffusion and exfoliation [20].

These clusters poorer the proficiency of graphene for back, as most noteworthy stack exchange and most reduced filling stack can as it were be done when the graphene is spread at the atomic level within the polymer network [21].

2.2 Nanomaterials

Nanomaterials are classified into four types as shown in Figure (2.1) depending on material dimensionality (MD), which are in nanometric range:-

1- Zero dimensions nanomaterials (0D) have all dimensions with nanometric range, such as gold nanoparticles.

2- One dimensions nanomaterials (1D) have needle like –shaped materials within range of nanometer. 1D nanomaterial includes nanotube, nanorods, nanoclays and metallic nanorods.

3- Two dimensions nanomaterials (2D) have two dimensions in the nanometer range and the third long, such as graphene sheets.

4- Three dimensions nanomaterials (3D) have all three dimensions in nanoscale. Such as polycrystalline [22].

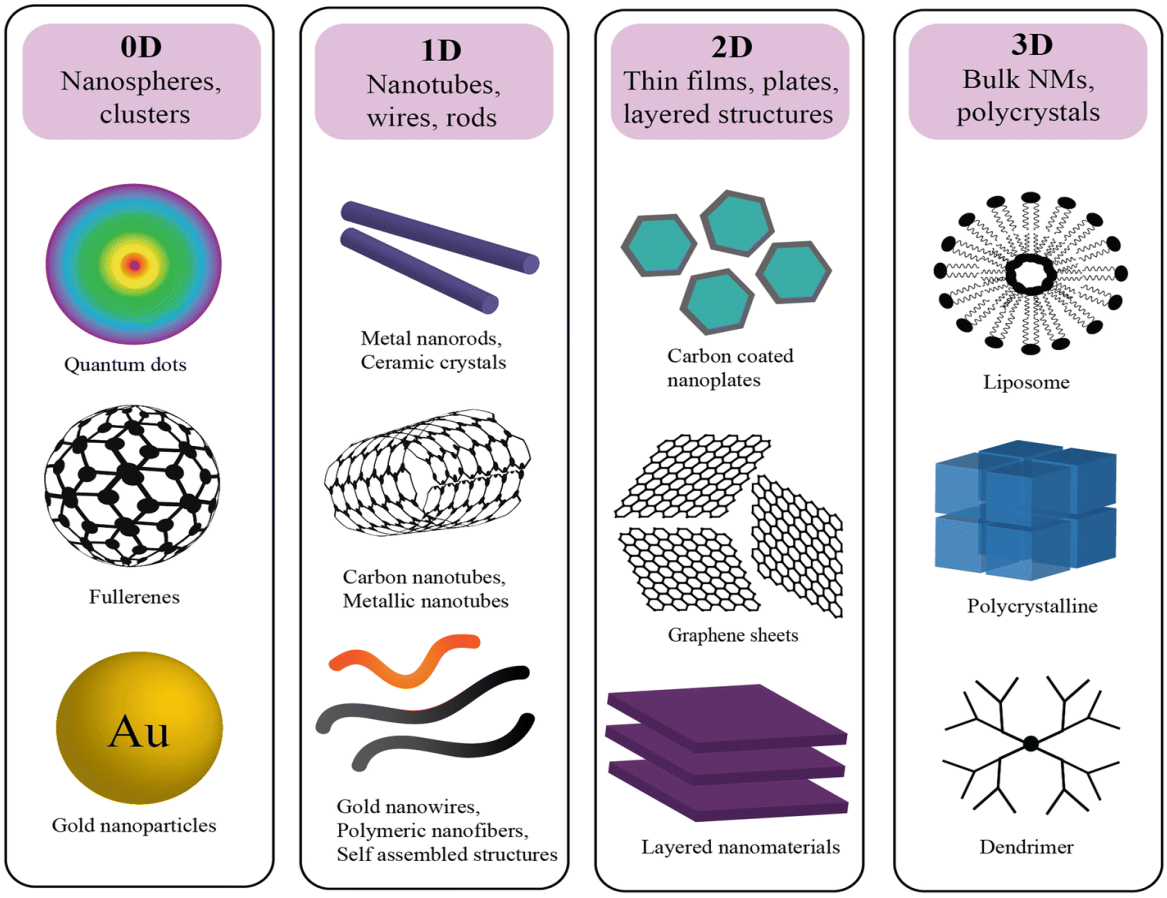

Figure 2.1: Dimensions of nanomaterials [22]

2.3 Nanocomposite

A nanocomposite is a structure that has nano-scale repeat distances between the different phases that make up the material or a multiphase solid material where one of the phases has one, two or three dimensions of less than 100 (nm). Nanocomposites are widely used in electronics and semiconductor application due to their desirable electrical properties. They are considered a viable replacement for IoT (Internet of things) transparent conductors in electronics applications. Fabricated as transparent conductive films (TCF), nanocomposite can be used as a highly conductive, transparent, and cost-efficient alternative in flexible displays and touch screens. The growth of the Nano composites market is significantly higher than that of conventional materials; the market volume in 2018 be 3.5–5 times higher than the volum achieved in 2010, as show in Figure (2.2) [23].

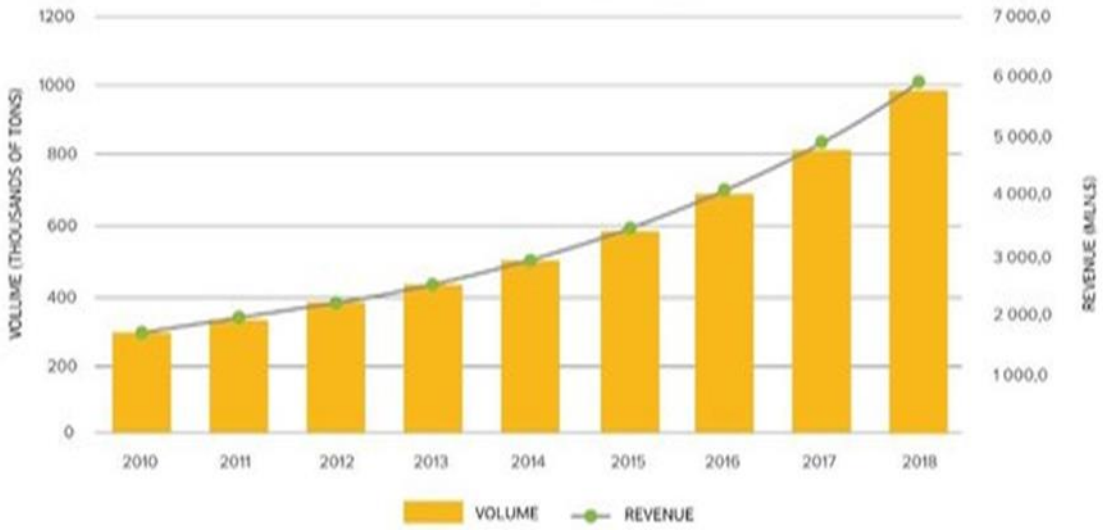

Figure 2.2: The growth of the Nano composites market [23]

2.3.1 Types of nanocomposite

Nanocomposites are classified into three categories according to the nature of matrix [24] composite with metal matrix, composite with ceramic matrix and composite with polymer matrix.

Nanocompsites can be divided also to:

1. **Nanoparticle-Reinforced Composites**

Particulate composites reinforced with micron-sized particles of various materials are perhaps the most widely utilized composites in everyday materials. Particles, are typically added to enhance the matrix elastic modulus and yield strength [25]. By scaling the particle size down to the nanometer scale, it has been shown that novel material properties can be obtained [26].

2. **Nanoplatelet-Reinforced Composites**

Nano clay and nano graphite are the famous two types of nanoplatelet-reinforced composites. In their bulk state, both clay and graphite can exist as layered materials. In order to utilize these materials most efficiently, the layers must be separated and dispersed throughout the matrix phase. In the conventional miscible state, the interlayer spacing in a clay particle is at its minimum. When polymer resin is inserted into the gallery between the adjacent layers, the spacing expands, and it is known as the intercalated state. When the layers are fully separated, the clay is considered to be exfoliated [27].

Different types of fillers are utilized, the most common is a nanoclay material called montmorillonite. Clays, in a natural state, are hydrophilic while polymers are hydrophobic [28]. To make the two compatible, the clay's polarity must be modified to be more

"organic" to interact successfully with polymers. Additional nanofillers include carbon nanotubes, graphite platelets, graphene platelets, carbon nanofibers, as well as other fillers being investigated such as synthetic clays, natural fibers (hemp or flax), and POSS (Polyhedral Oligomeric Silsesquioxane) MCarbon nanotubes, offer superb electrical and thermal conductivity properties [29]. Figure (2.3) illustrates two ways that polymer can access the surface of all or most of these plates in such clays (a) and Graphene nanoplates (b) into a semi crystalline matrix. In intercalated Nano composites, the polymer enters the gallery between the layers of clay and the clay layers maintain their registration and the increase in spacing between. In exfoliated Nano composites, individual clay plates become dispersed in the polymer [30].

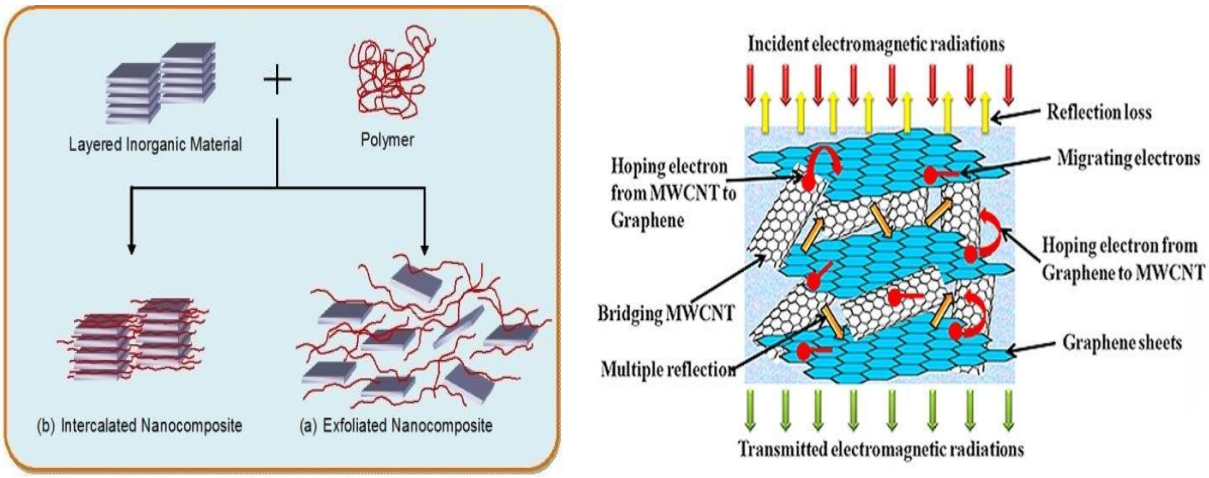

Figure 2.3: (a) Polymer/Clay Nanocomposite and (b) Graphene plates [30]

3. Nanofibers-Reinforced Composites

Vapor grown carbon nanofibers have been used to reinforce a variety of polymers, including polypropylene, polycarbonate, nylon, poly(ether sulfone), poly(ethylene terephthalate), poly(phenylene sulfide), acrylonitrile–butadiene– styrene, and epoxy. Carbon nanofibers are known to have wide-

ranging morphologies, from structures with a disordered bamboo-like structure to highly graphitized ‘cup stacked’ structures where the conical shells of the nanofiber are nested within each other. Carbon nanofibers typically have diameters on the order of 50–200 nm [31].

2.4 Nano thin films

Materials with thicknesses ranging from nanometres to micrometres and high surface-to-volume ratios are called thin films; they behave differently from bulk materials of the same chemical composition in several different ways. Thin films are becoming increasingly important as means of altering the properties of surfaces and interfaces. The first use of thin films for optical purposes can be dated back to 1912. Pohl and Pringsheim published the well-known work about the production of mirrors in which they vaporize metals like Ag and Al in high vacuum [32].

In general, thin films are produced by vapour deposition processes which can principally be divided into Physical Vapour Deposition (PVD) and chemical vapourdeposition (CVD). PVD involves purely physical processes such as high temperature vacuum evaporation with subsequent condensation. The overall process involves four different steps: evaporation, transportation, reaction and deposition [33].

2.4.1 Classification of nanostructured thin films

The term “thin films” is ambiguous and usually used to describe “coating” layers with thicknesses ranging from a single atomic layer to films that are a significant fraction of a millimeter thick. Nanostructured thin films are commonly classified by their crystallinity, morphology, and functionalities [34]. Thin films are categorized by their composition and morphology, and classified in six different groups as show in Figure (2.4).

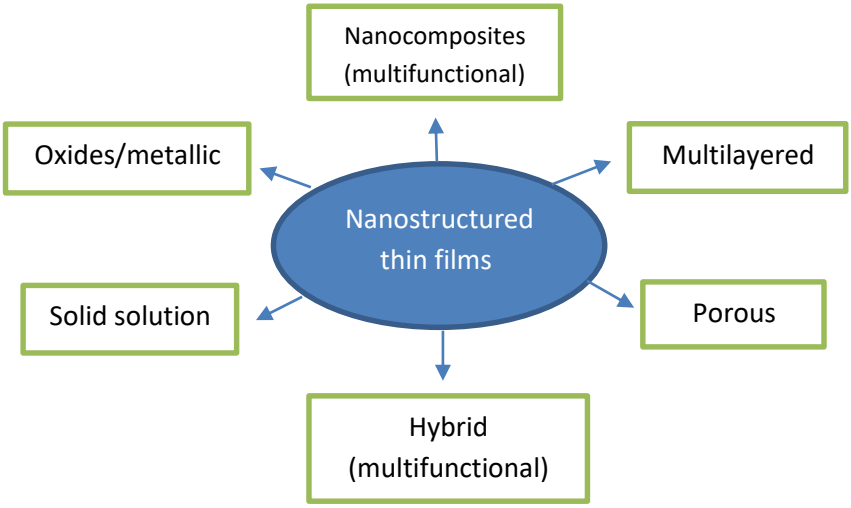

Figure 2.4: Classification of nanostructured thin films [34].

Atomically thin films known as two-dimensional materials (or 2D materials) constitute layers whose thicknesses are comparable to one or a few atomic layers. An adsorbed monolayer of gas or impurity atoms on a surface is an example of atomically thin layers. In this case, the response of the thin layer is likely to be more influenced by interatomic potentials and surface energy than by macroscopic properties [35].

2.4.2 Thin film applications

In considering the different applications of deposited thin films, the following generic categories can be identified [48].

1. Electronic components: The fabrication of electronic components, especially solid-state devices and microelectronic integrated circuits, have undoubtedly found the widest and most demanding applications for thin- film depositions. These films typically consist of semiconductor materials, dielectric and insulating materials, and metal or refractory metal silicide conductors.

2. Electronic displays: They used for interfacing electronic equipment with human operators. Different components and device structures are required, such as:

   Liquid-crystal displays

   Light-emitting diodes (LEDS)

   Electroluminescent displays

   Plasma and fluorescent

   electrochromic displays

   The fabrication of these displays requires conductive films, transparent, luminescent or fluorescent films as well as dielectric and insulating layers.
3. Optical coatings: These coatings are applied for antireflection purposes, as interference filters on solar panels, as plate glass infrared solar reflectors, and for laser optics. In the fabrication of filter optics, thin films with refractive index gradients are deposited on preforms from which the optical fibers are drawn. These coatings require dielectric materials with precisely defined indices of refraction and absorption coefficients. Laser optics require metal reflective coatings which can withstand high radiation intensities without degradation. Infrared reflecting coatings are applied to filament lamps to increase the luminous flux intensity.
4. Magnetic films for data storage: Thin films of magnetic materials have found wide commercial applications for data storage in computers and control systems. The substrates can be metal, glass or plastic polymeric materials. Thin film deposition processes for magnetic materials and for materials with a high degree of hardness are required.
5. Optical data storage devices: Thin films are finding increasing commercial use for optical data storage devices in compact disks and

computer memory applications. Processes for the deposition of organic polymer materials as storage media and as protective overcoats are required for this technology.

6. Antistatic coatings: Thin films of conductive or semiconductive materials are deposited to provide protection from electrostatic discharges. Thin film coatings of carbides, silicides, nitrides, and borides are finding increased uses to improve the wear characteristics of metal surfaces for tools, bearings, and machine parts. of particularly great current interest are films of diamond-like carbon because of this material's heat dissipation properties, electrical insulation, hardness, and resistance to high temperature and high energy radiation [36].

2.4.3 Thin films manufacturing processes

The fabrication techniques can be divided into two categories representing gas phase and liquid phase. The gas phase fabrication methods involve the deposition of materials either from small particles of bulk solid materials or chemical precursors in vapor form whereas the liquid phase fabrication methods refer to the methods involving a reaction between a substrate and a chemical precursor in a liquid state.

2.4.3.1 Gas phase processes

1. Magnetron sputtering

This is one of the most well-established techniques that is widely used in the industries to fabricate coatings of many different materials, including metals, semiconductors, and alloys [37]. Thin films fabricated via magnetron sputtering prove to be of superior quality in comparison to those fabricated using other gas phase methods [38].The schematic representation of the magnetron sputtering set-up is shown in Figure (2.5).

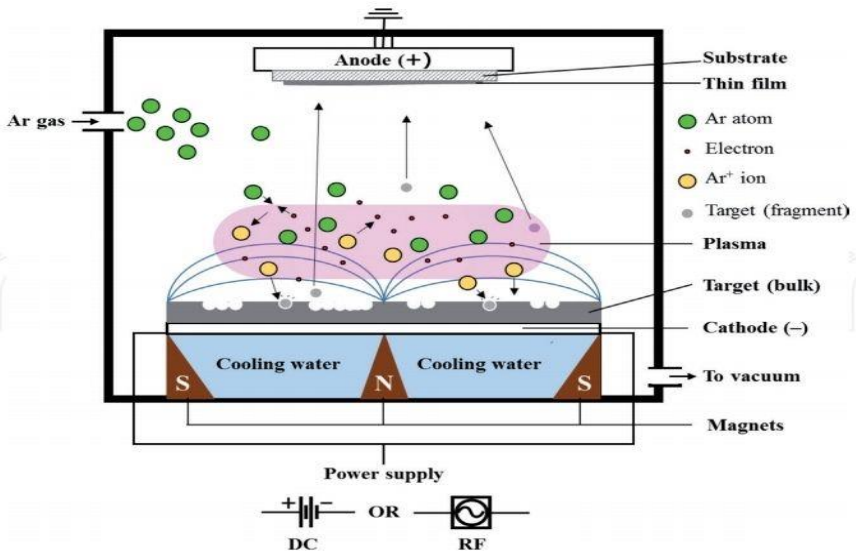

Figure 2.5: Schematic representation of a magnetron sputtering equipment and deposition process [39]

2. Pulsed laser deposition (PLD)

The schematic representation of a PLD setup is shown in Figure (2.6) The PLD technique employs the ablation of a target material with a strong, pulsed laser beam to produce a plume of vaporized materials which is then recondensed and deposited onto a substrate, placed opposite the target, under a reduced pressure atmosphere of ca. 10^{-1}–10^{-5} kPa [40]. Depending on the target material, its morphology, and the laser pulse wavelength and duration, there is a specific threshold power density that is required to cause ablation [41].

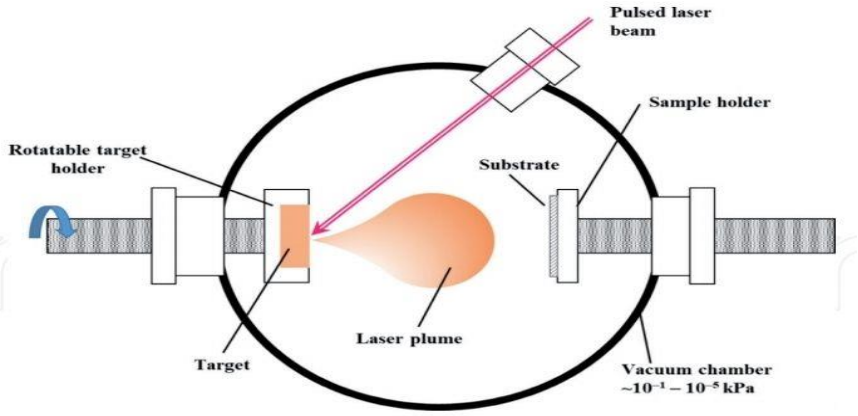

Figure 2.6: Schematic representation of PLD setup [39]

3. Atomic layer deposition (ALD)

The ALD technique is based on sequential and self-limiting reactions of a chemical precursor in vapor form, with an activated or functionalized surface of the substrate [42 and 43]. The self-limiting property of this technique is realized in a sense that, if all functional sites on the substrate have reacted, no further reaction between the chemical precursor and the substrate will take place [42 and 44]. Figure (2.7) illustrates the concept of ALD in the fabrication of a TiO_2 thin film. The steps are defined as follows: (a) precursor exposure, (b) purge, (c) reactant exposure, and (d) purge. By repetition of step (a)–(d), layers of TiO2 can be easily formed and the thickness can be controlled at the atomic level.

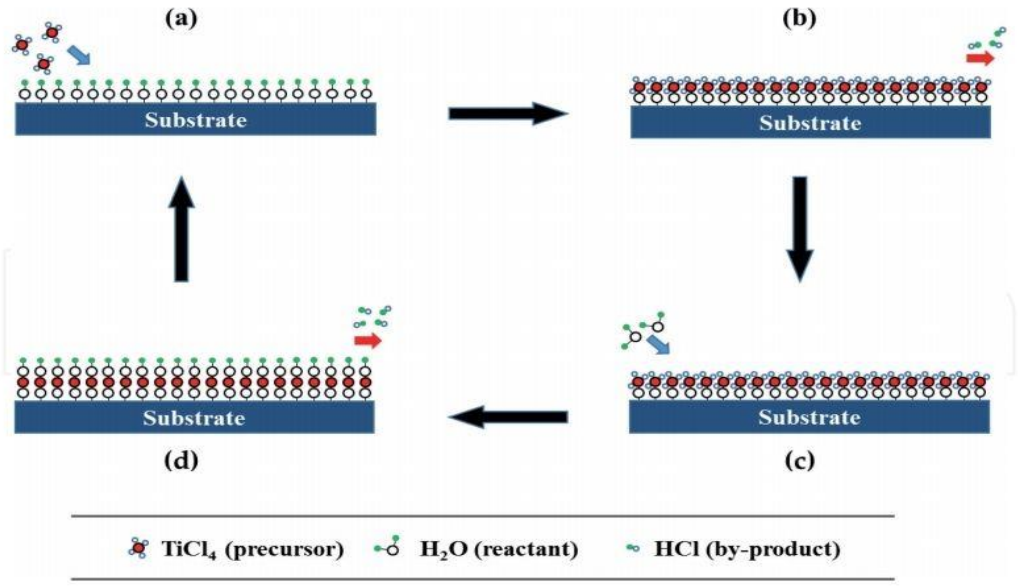

Figure 2.7: Schematic representation of 1 cycle of an ALD process for the deposition of a TiO2 thin film from titanium tetrachloride and water [39].

4. Chemical vapor deposition (CVD)

Defined as the deposition of solids onto heated substrates from chemical reactions in vapor phase [45], CVD represents a versatile deposition technique of thin films for a wide range of materials, under vacuumed atmospheres and temperatures over 600°C as shown in Figure (2.8).

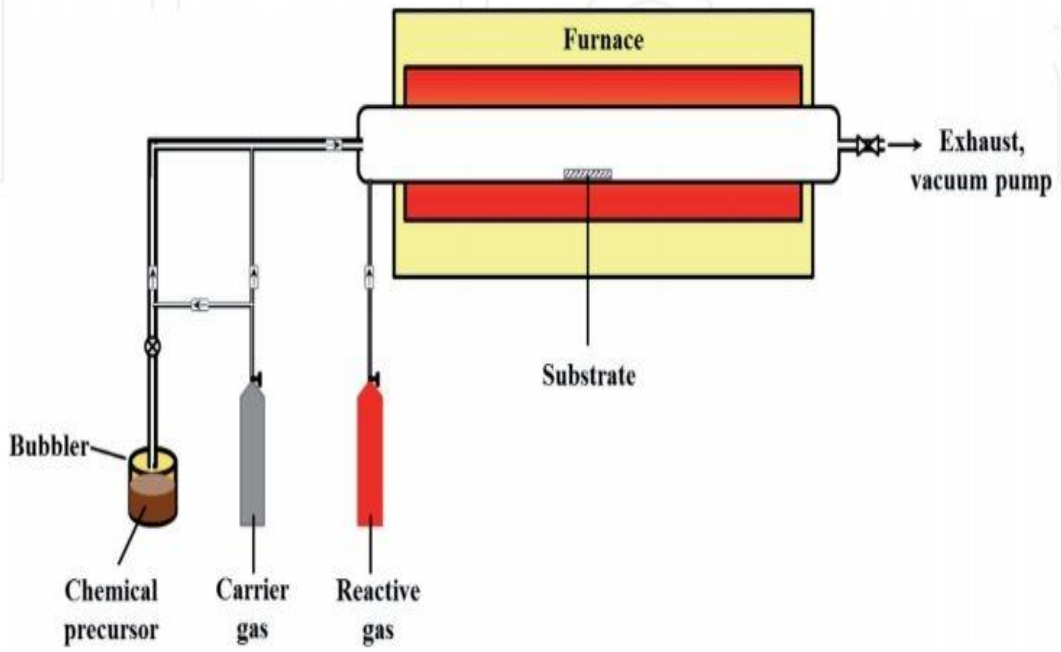

Figure 2.8: Schematic representation of a CVD setup [39].

2.4.3.2 Liquid phase processes

1. Sol-gel method

The sol-gel method has emerged as a method of choice for the fabrication of ceramics and glasses and, it is considered as a cost effective alternative to the wellestablished gas phase processes. The sol-gel method is a two-chemical processes technique based on the hydrolysis and condensation of molecular precursors and has since been considered to be capable of offering new routes for the low temperature fabrication of oxide materials [46] as show in Figure (2.9). Because all gel products may contain nanoparticles or are nano-composites, the sol-gel method has been deemed as typical nanotechnology [47].

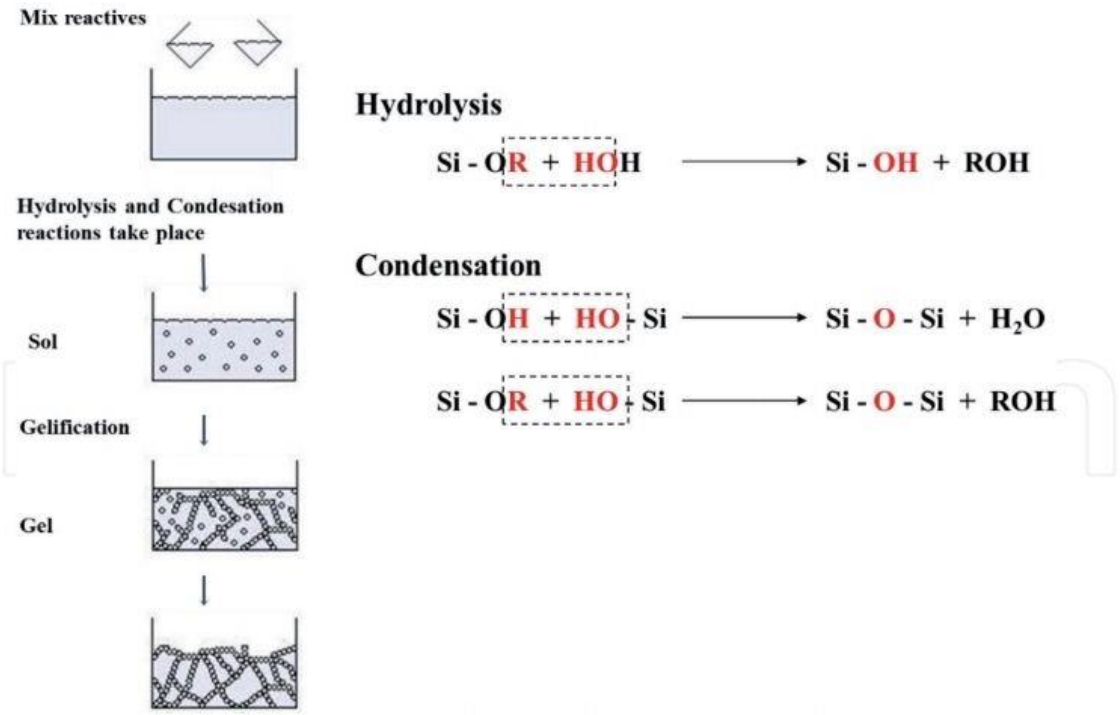

Figure 2.9:Typical sol-gel process for SiO2 formation from silicon alkoxides [48].

2. Coating

The formation of organic and polymer coatings on conducting substrates has always been of great interest. The coatings can be applied for purposes of surface decoration, optical activity alteration, heat and corrosion protection .Other important applications include improvement of interfacial laminar shear strength and toughness of brittle composites originally, organic and polymer coatings were applied manually or mechanically on substrates. However, Manual or mechanical application of coatings had inherent disadvantages and gave rise to additional problems [49].

The coating process can be classification in to:

A. Spin coating

Spin coating is used for the fabrication of thin films to deposit uniform coating of organic materials on flat surfaces [50]. Fu et al, developed a transparent superhydrophobic transparent coating via spin coating [51]. Spin

coating is performed in four steps, deposition, spin up, spin off, and evaporation, as shown in Figure (2.10).

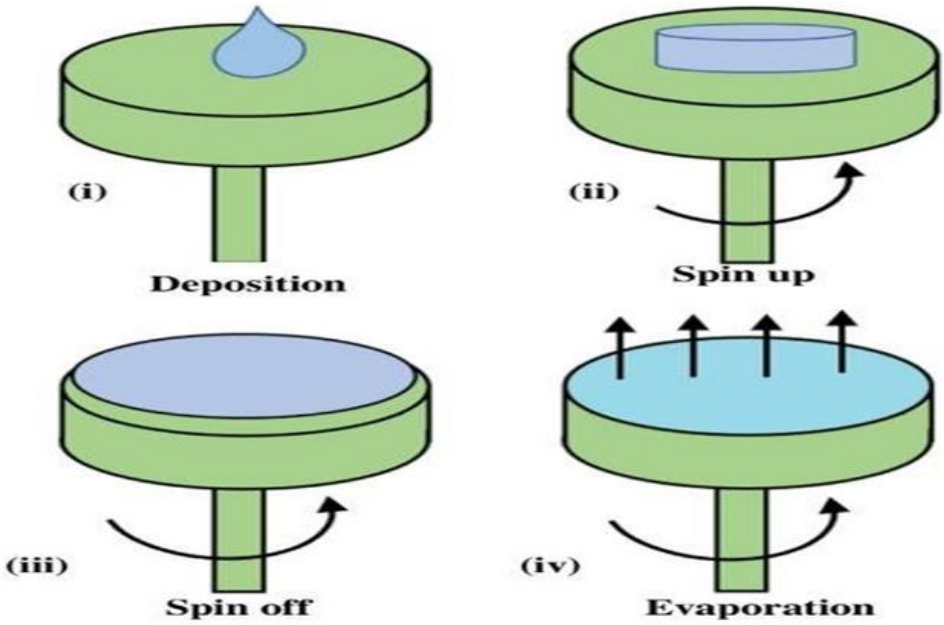

Figure 2.10: Stages of spin coating on substrate [50].

In the first stage the material is deposited on the turntable and then spin up and spin off occur in sequence while the evaporation stage occurs throughout the process. The applied solution on the turntable is distributed via centrifugal force. High spinning speed results in thinning of the layer. This stage is followed by drying of the applied layer. Uniform evaporation of the solvent is possible because of rapid rotation. High volatile components are removed from the substrate because of the evaporation or simply drying and the low volatile components of the solution remain on the surface of the substrate. Thickness of the deposited layer is controlled by the viscosity of the coating solution and the speed of rotation [52].

One of the main disadvantages of spin coating is the size of the substrate. As the size increases, the high-speed spinning becomes difficult, because film thinning becomes difficult. The material efficiency of spin coating is very low. In general, (95-98)% of material is flung off and disposed

of during the process and only (2-5)% of material is dispensed onto the substrate [53].

B. Spray Coating

In industry, for the coating of complex-shaped polymeric substrates spray coating is used [54]. Atomizers or nebulizers, as shown in Figure (2.11).

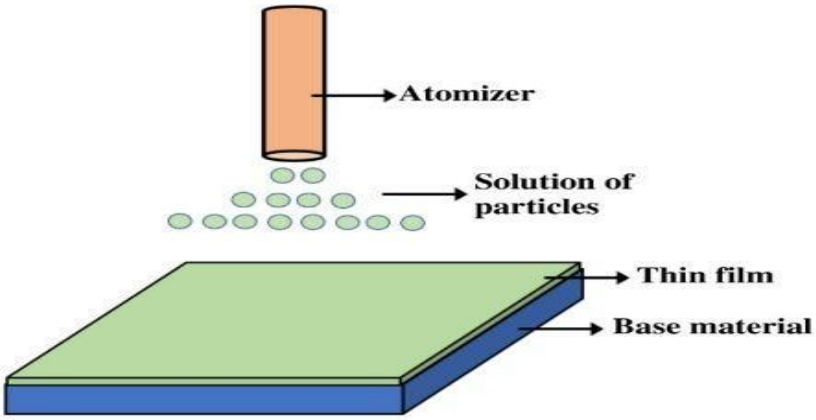

Figure 2.11: Spray coating on substrate [50].

C. Dip Coating

In the dip-coating process, the substrate is coated by immersing it in a liquid [52]. A typical schematic view of the dip-coating process is shown in Figure (2.12).

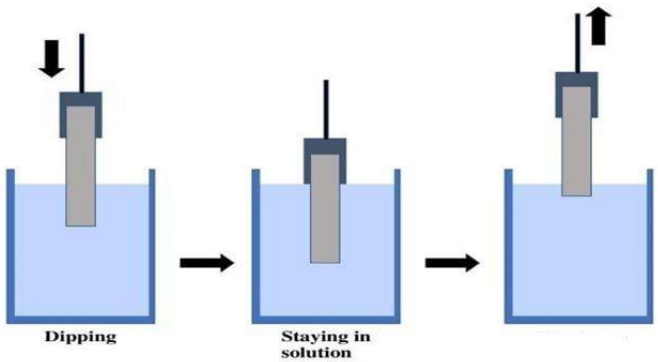

Figure 2.12: A schematic view of the steps in dip coating [50].

2.5 Sensors

The sensor is a device that receives different kinds of signal i.e. physical, chemical or biological signal and converts them into an electric signal. A sensor is a device that receives a signal or stimulus and responds to the stimulus in the form of an electrical signal. The output signals correspond to some forms of electrical signal, such as current or voltage. The sensors are classified into different types based on the applications, input signal and conversion mechanism (Figure 2.13) [51].

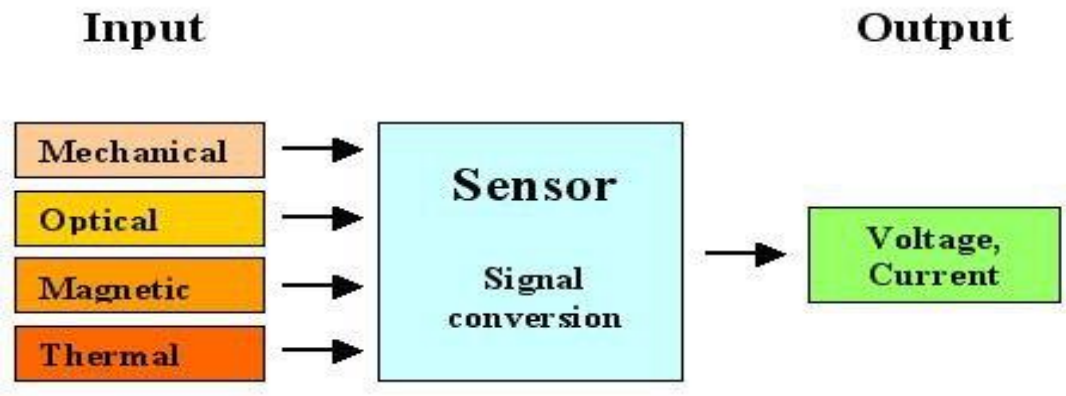

Figure 2.13: Sensors principal [52].

Sensors can be find everywhere, and the whole world is full of sensors and their applications. There are many types of sensors available around Figure (2.14), in our offices, gardens, shopping malls, homes, cars, toys etc. These sensors make our lives so easy and comfortable, starting from applications,

such as switching on the lights, fans, television (TV), automatic adjustment of the room temperature by air conditioning (AC), fire alarm, detecting obstacles when the car is reversing, making a thumb impression etc. A sensor is a device which receives signals as well as responding to a signal or stimulus. The stimulus signals can be defied by the measure, property, or state which is sensed. [53].

All the sensors are categorized on the basis of their uses, applications, material used and some production technologies. Some sensors are classified also by their characteristics, such as cost, accuracy or range of sensor. There are two main types of sensors: passive sensor and active sensor. A passive

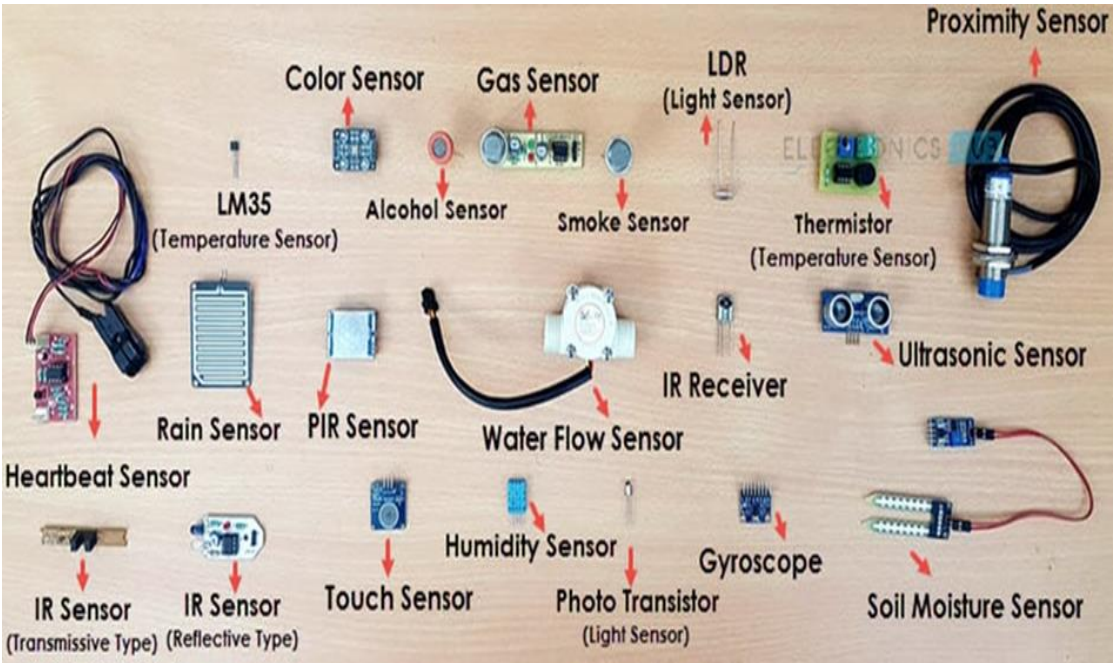

Figure 2.14: sensors type [54].

sensor does not require any extra energy source and electric signal is produced directly in reply to stimulus of external sources. This means that the sensor converts input energy to output signal energy [54 and 55].

2.5.1 Sensors characteristics

Upon receiving the input stimuli, the sensor produces output which is obtained from several conversion steps before it produces an electric signal [56].

The performance of sensors is described in terms of relationship between input and output signals. Sensors are characterized depending on the values of some of the important parameters. The characteristics of sensors are described in table (2.1).

Table 2.1. Sensors based on their detection properties [53].

Types	Properties
Thermal sensor	Temperature, heat, flow of heat etc
Electrical sensor	Resistance, current, voltage, inductance, etc
Magnetic sensor	Magnetic flux density, magnetic moment, etc
Optical sensor	Intensity of light, wavelength, polarization, etc
Chemical sensor	Composition, pH, concentration, etc
Pressure sensor	Pressure, force etc
Vibration sensor	Displacement, acceleration, velocity, etc
Rain/moisture sensor	Water, moisture, etc
Tilt sensors	Angle of inclination, etc
Speed sensor	Velocity, distance etc

2.5.2 Types of sensors

There are many sensors commonly used in various applications. All these sensors are categorized as per their physical properties like temperature, resistance, pressure, heat flow etc. The following is a brief discussion on different types of sensors [57].

2.5.2.1 Photo sensors

A photo sensor is a photoelectric passive sensor which changes the light energy into an electrical signal output. It measures the ambient light which is surrounding light, room light and reflected light. The major component of a light sensor is the light dependent resister (LDR) or photoresistor. It is a resistor that depends on the light which changes its resistance depending on the amount of light incident on it [58] .

The sensors are made up of semiconductor materials and therefore when light is incident on semiconductor material it becomes low conductive

and therefore has less resistance. When we increase the light intensity, its resistance decreases and vice versa which is shown in Figure (2.15).

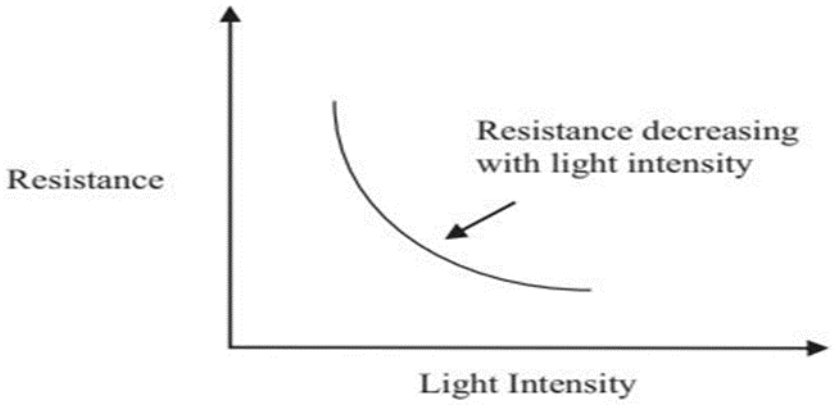

Figure 2.15: Resistance decreases with light intensity

Intensity of light falling on an LDR is measured in lux. There are different kinds of light sensors such as photoresistors, photodiodes, photovoltaic cells, phototubes, photomultiplier tubes, phototransistors, charge coupled devices (CCDs) etc [57].

2.5.2.2 Photoelectric Sensors

Photoelectric Sensors detect objects, changes in surface conditions, and other items through a variety of optical properties (as show in Figure 2.16).

A photoelectric sensor consists primarily of an Emitter for emitting light and a receiver for receiving light. When emitted light is interrupted or

Figure 2.16: Photoelectric sensors

reflected by the sensing object, it changes the amount of light that arrives at the Receiver. The Receiver detects this change and converts it to an electrical output. The light source for the majority of photoelectric sensors is infrared or visible light (generally red, or green/blue for identifying colors) [59].

2.5.2.3 Gas sensor

Thin films can be used to determine the concentration of a wide range of gaseous molecules and volatile organic compounds (VOCs) in an environment, including oxygen, nitrogen dioxide, organic amines, ammonia and ethanol, to name a few. Thin films have a high surface area for gaseous molecules to bind to, and upon absorption, a change in the conductivity and/or resistivity occurs within the thin film. This change is measurable even with small localized changes, and the number of absorbed molecules is relative to the change in conductivity/resistivity (i.e. a greater amount of absorption equates to a greater electrical change, and vice versa), which enables the concentration of these gases to be deduced [60]. To fabricate the nanostructured gas sensors, semiconducting metal oxides are the most widely used material. The schematic diagram of semiconducting metal oxide thin film gas sensor is shown in Figure (2.17) [61].

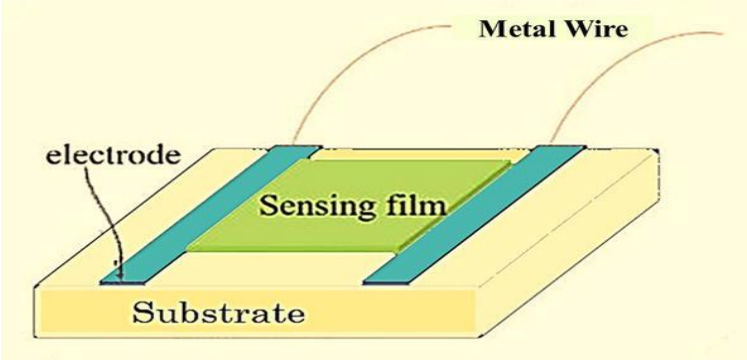

Figure 2.17: [61].

2.5.2.4 Strain sensor

The thin nature of thin films enables them to be flexed and strained much more than bulk materials. They are also a lot more stable and resistant to fracture than bulk materials. Thin films can be used to measure localized strain, such as in some wearable devices or strain gauges in the construction industry. As the film becomes strained, the deformation causes the electronic properties of the film to change, which enables any strains, stress or abnormal movements to be measured and monitored[62].

2.5.2.5 Heat-Flux Sensors

Thin films have been employed in a few different types of heat-flux sensors; namely, thermopile-type and RTD-based heat flux sensors. In the case of thermopile-type sensors, thin film thermocouples are used to measure the temperature difference across an insulating area with a defined thickness, and higher sensitivities can be achieved by using more thermocouple pairs along the temperature monitoring path. In RTD-based sensors, thin film RTD's are used to measure the temperature difference across a defined area of insulating material. RTD-based thin film sensors are easier to fabricate and possess a larger signal than thermopile-type thin film sensors[63].

2.5.2.6 Humidity Sensors

In a similar fashion to gas sensors, thin films can be used as the sending component to measure the relative humidity of an environment. As relative humidity is dependent upon how many water molecules are in the atmosphere, the high surface area adsorbs water molecules, which causes a measurable and quantifiable change in the conductivity/resistivity of the thin film. This enables the relative humidity of an environment to be processed as a function of the concentration of water molecules[64].

2.6 The used materials

2.6.1 Poly(3,4-ethylenedioxythiophene) polystyrene sulfonate (PEDOT:PSS)

PEDOT:PSS, or Poly (3,4-ethylenedioxythiophene) polystyrene sulfonate, is a transparent conductive polymer consisting of a mixture of two ionomers, which are poly (3,4-ethylenedioxythiophene) and polystyrene sulfonate. Due to its unique combination of conductivity, transparency, ductility, and ease of processing, PEDOT:PSS has become a benchmark material in thin-film electronic fabrication [65]. The conducting polymer of (PEDOT:PSS) is one of the most important and intensively investigated organic conducting materials [66]. Figure (2.18) shows the chemical structure of PEDOT:PSS.

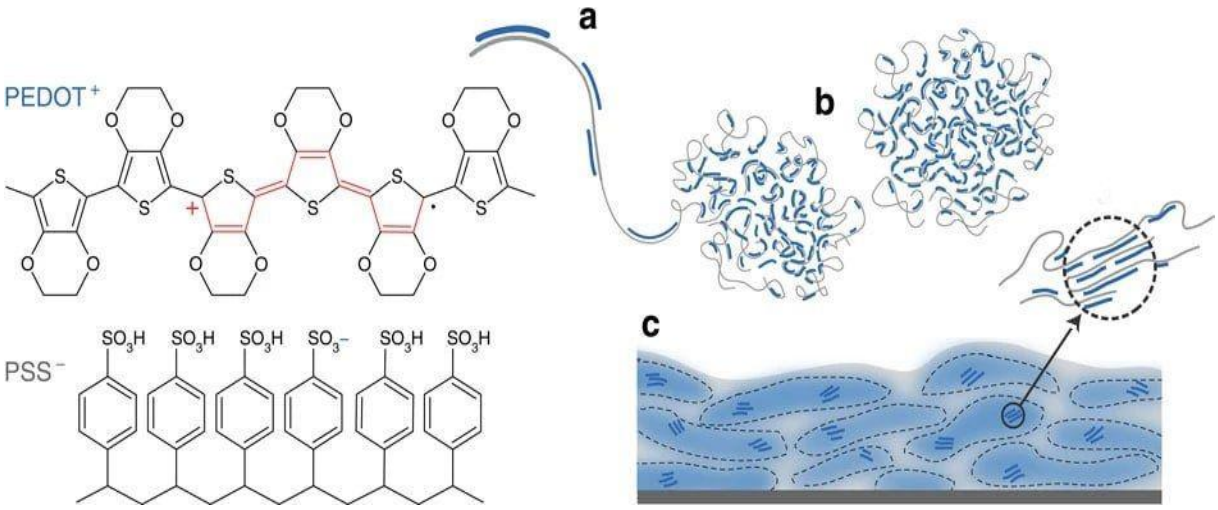

Figure 2.18: PEDOT:PSS structure and morphology. The chemical structure of PEDOT:PSS and commonly described microstructure of the conducting polymer system (a) synthesis onto PSS template, (b) formation of colloidal gel particles in dispersion and (c) resulting film with PEDOT:PSS-rich (blue) and PSS-rich (grey) phases [67].

Poly (3,4 ethylenedioxythiophene) polystyrene sulfonate can be used as an interfacial layer for hole transport in organic light emitting diodes, organic photovoltaics, and perovskite photovoltaics [68]. It can also be used as a replacement for transparent conductors, such as ITO (Indium Tin Oxide) or FTO (Fluorine Tin Oxide) and is used commonly in applications where the underlying substrate is flexible. Poly (3,4-ethylenedioxythiophene) (PEDOT) has attracted considerable interest as it is water soluble, and is stable in the p-doped state, with a relatively high conductivity, good film-forming properties, and environmental stability [69and 70].

The use of poly (3,4-styrene sulfonate) (PSS) enhances the solubility of PEDOT in aqueous media since the solubility of PEDOT itself in aqueous media is not adequate to form a film [71]. The polyelectrolyte complex of PEDOT and PSS, with an excess of the latter component, is produced and negatively charged, which stabilizes them in the aqueous media [72]. The good film-forming property, high electrical conductivity, high transparency in the visible region, and excellent thermal and environmental stability make PEDOT:PSS useful for potential applications in electronic devices, such as sensors, hole-injection layer of organic light emitting diodes, antistatic coatings, transistors, electro chromic displays, and flexible electrodes. In particular, inclusion of nanosized electrically conductive fillers, such as carbon nanotubes and graphite particles can significantly increase the electrical conductivity of the polymer beyond a threshold level of loading [73].

The various types of sensors reported in the context of chemical sensor, perhaps the most competitive type is based on the change in electrical resistance or conductance. It is recognized that sensors based on conductivity changes are potentially advantageous in cost and convenience because they

could eliminate the complexity and power consumption inherent to optical instruments. There is a little studies on the use of PEDOT:PSS /nanographene composites as sensors to detect nitroaromatic compounds, where there is an attempts to synthesize polymer NCs to develop a portable system based on chemiresistive sensors that can sense and identify nitro-based explosive vapors [74].

PEDOT:PSS properties can be classified:

2.6.1.1 PEDOT:PSS Conductivity

The electrical conductivity of oxidized polythiophenes has been known about for nearly 40 years. The origins of this conductivity are due to the presence of radical states which are formed due to the oxidation of the thiophene units. These reduced states are delocalized across the polymer chain, and in the presence of the oxidizer, these radicalized states can be stabilized [75].

In PEDOT:PSS, the PEDOT is oxidized during the polymerisation reaction by the polystyrene sulfonate. This produces an emulsion where the PSS present stabilizes the radical states on the PEDOT. Although PEDOT itself is conductive, the PSS present within the blend is insulator. The quantity of PSS and the microsctructure of the film therefore have a significant impact on the electronic properties of PEDOT:PSS. In a water based dispersion, the PEDOT and PSS form a micelle structure in which the hydrophobic PEDOT core is surrounded by a shell of hydrophilic PSS. During deposition this structure is retained forming localized regions of conductive PEDOT surrounded by insulating regions of PSS. It is this core-shell structure which results in the low conductivity values that can arise for standard formulations of PEDOT:PSS [76].

2.6.1.2 PEDOT:PSS work function

As work function is a surface property of a material, the work function of the PEDOT:PSS blend will be determined by the percentage of each component at the surface of the film. PSS has a significantly deeper work function than PEDOT, therefore a higher presence of PSS at the surface will result in a deeper work function. This means that, for formulations with higher percentages of PSS, the work function will be higher than those with lower percentages. In addition, the processing of the PEDOT:PSS film can result in changes to the work function [77].

The PEDOT:PSS forms a core-shell structure resulting in PEDOT being surrounded by PSS. In this case the work function will be dominated by PSS. If the film has been treated such that the components are more homogenously dispersed, the work function will become more shallow as the surface becomes richer with PEDOT [78].

2.6.1.3 Application of PEDOT:PSS

1. Perovskite photovoltaics

PEDOT:PSS has been used as a hole extraction material in inverted devices in order to facilitate the extraction of charge carriers at the interface between the transparent conductive oxide and the active perovskite layer. Inverted perovskite devices using PEDOT:PSS typically show lower hysteresis than standard architecture devices [79].

2. Organic photovoltaics

PEDOT:PSS has long been used as a standard material in device fabrication to form the backbone of fundamental research into polymer solar

cells. In addition PEDOT:PSS is still used in combination with the state of the art organic photovoltaic materials to push new efficiency limits [80].

3. Organic light emitting diodes

The use of PEDOT:PSS in organic light emitting diodes has been widespread for over a decade now and is a well-established standard hole injection material. More recent work still uses PEDOT:PSS due to its deep work function allowing for efficient charge injection into white emitting polymers and also host materials for thermally activated delayed fluorescence materials [81].

4.Transparent conductors

PEDOT:PSS has been seen as a potential replacement for expensive transparent metal oxides such as ITO (Indium Tin Oxide) and FTO (Fluorine_doped Tin Oxide) and has been shown in both organic photovoltaic and perovskite photovoltaic devices to be an effective replacement. In addition, in combination with metallic grid structures sheet resistances comparable to metallic films are possible [82].

2.6.2 Graphene

Graphene is a novel nanomaterial which provides significant research interest in application because of its highly unique and desirable properties. These properties include very high surface area, high thermal conductivity, remarkable mechanical properties, high electrical conductivity, and exceptional chemical properties. These desirable properties have prompted the utilization of graphene in several applications like biosensing, energy storage, pharmaceuticals, nanocomposites, nanoelectronics, catalysis, etc [83].

Graphene is a 2D planar sheet of sp^2-bonded carbon atoms where the atoms are arranged in a honeycomb crystal structure. The carbon–carbon bonds have length of 0.142 nm and 120 degrees angle apart [84]. The bonds between carbon atoms are responsible for their thermal and mechanical properties. Graphene has the advantage of repairing any holes in its plates in case it is exposed to particles containing carbon. This is a very important feature for many applications. This property works by bombing the pure carbon atom on the graphene sheet, where the carbon atoms apply perfectly to the hexagonal graphene structure and thus fill the holes as shown in Figure (2.19) [85].

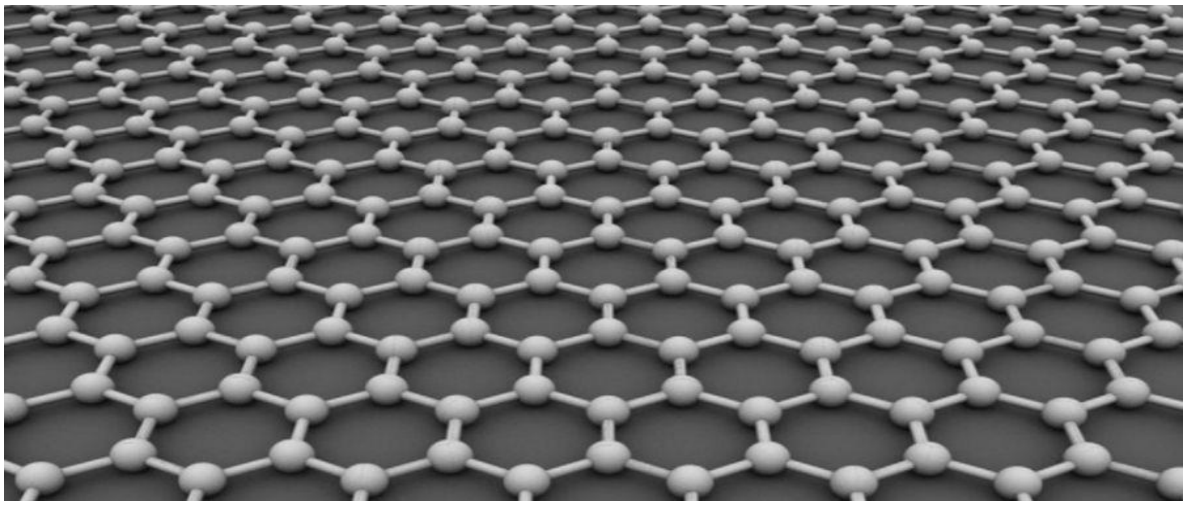

Figure 2.19: Structure of grapheme [83].

Graphene is a highly conductive allotrope of carbon whose atoms are arranged in a mesh- like form a single atom thick. Graphene is a wonder material. It has gained enormous interest amongst scientists since its discovery due to its excellent properties.

In 1980, only three basic allotropes of carbon, namely diamond, graphite, and amorphous carbon were known. Later on, fullerenes and carbon nanotubes were discovered and, in 2004, Figure (2.20)

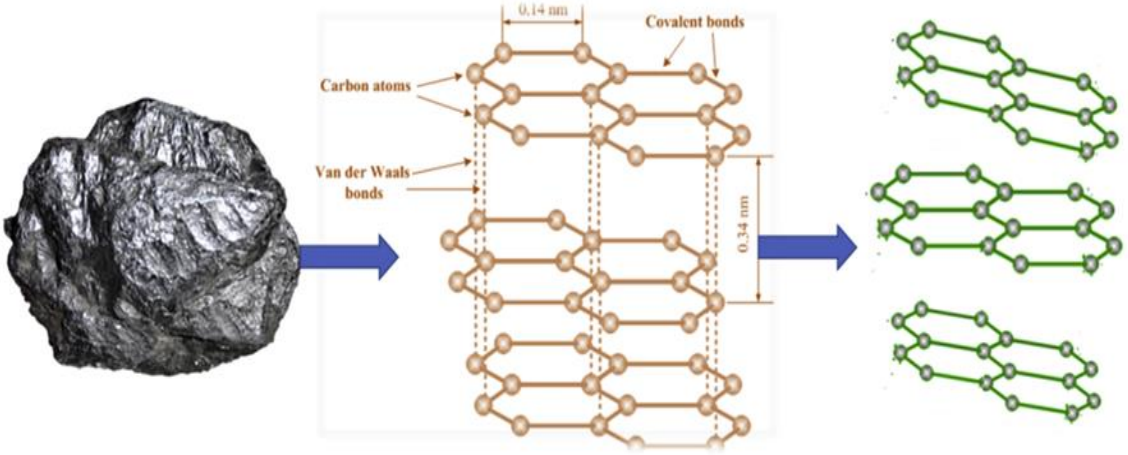

Figure 2.20 Schematic depictions about the Origin (presenting the transformation) of graphene from graphite and peculiar structure of graphite and graphene [86].

graphene came into the picture. Graphene can be seen as a 2D aromatic macromolecule. It is the basic building block of other graphitic allotropes. It can be wrapped into 0D fullerenes, rolled into 1D nanotubes, and stacked into 3D graphite as shown in Figure (2.21).

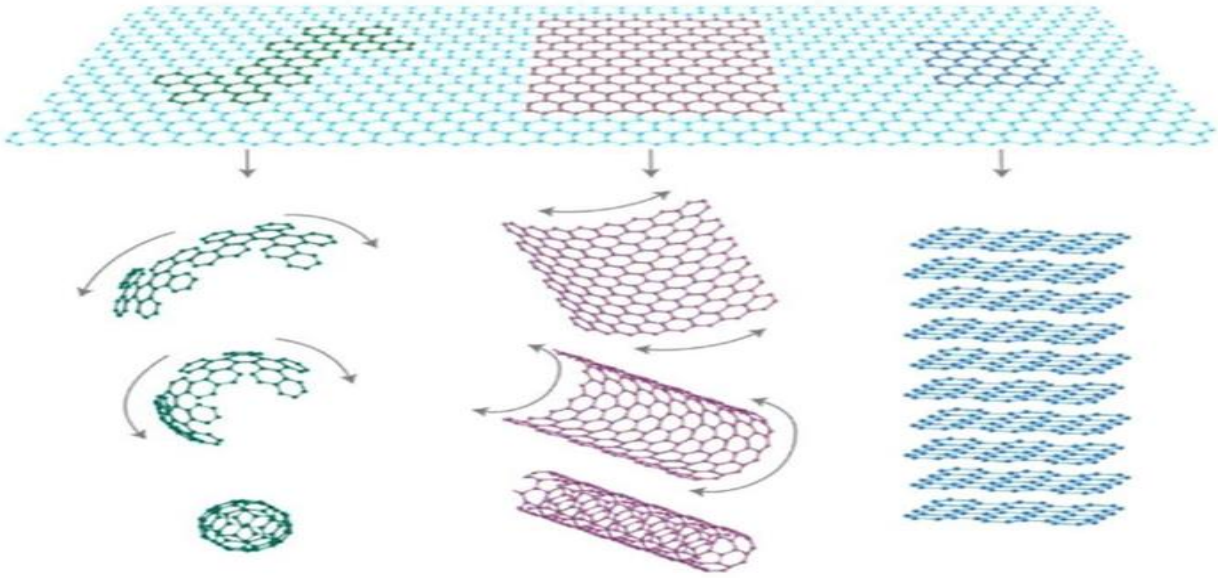

Figure 2.21: Graphene wrapped up into 0D fullerene, rolled into 1D nanotubes, or stacked into 3D graphite.

Carbon is one of the most abundant elements inside the human body. Moreover it is also one of the most abundant elements by mass in the universe. So, all living materials have a chemical basis made up of carbon. So, graphene can be an ecologically friendly material for numerous applications. The band structure of graphene is unique. The valence and the conduction bands touch each other at six direct points exhibiting a zero band gap semiconductor behavior. It has high fracture strength, excellent electrical and thermal conductivity, fast mobility of charge carriers ($2*10^5$ cm^2/Vs, 200 times higher than silicon), large specific surface area (2600 m^2) and biocompatibility [87].

Layers of graphene stacked on top of each other form graphite. The molecular bond length is 0.142 nm. The interplanar spacing is 0.335 nm.were able to isolate graphene sheets using a simple micro mechanical exfoliation method placing scotch-tape over commercial highly ordered pyrolytic graphite as shown in Figure (2.22).The latter technique allowed scientists all over the world to isolate single- and double-layered graphene flakes. Subsequently, other methods to obtain graphene flakes were reported, including its epitaxial growth over SiC substrates, and chemical vapor deposition growth over thin metal layers [88].

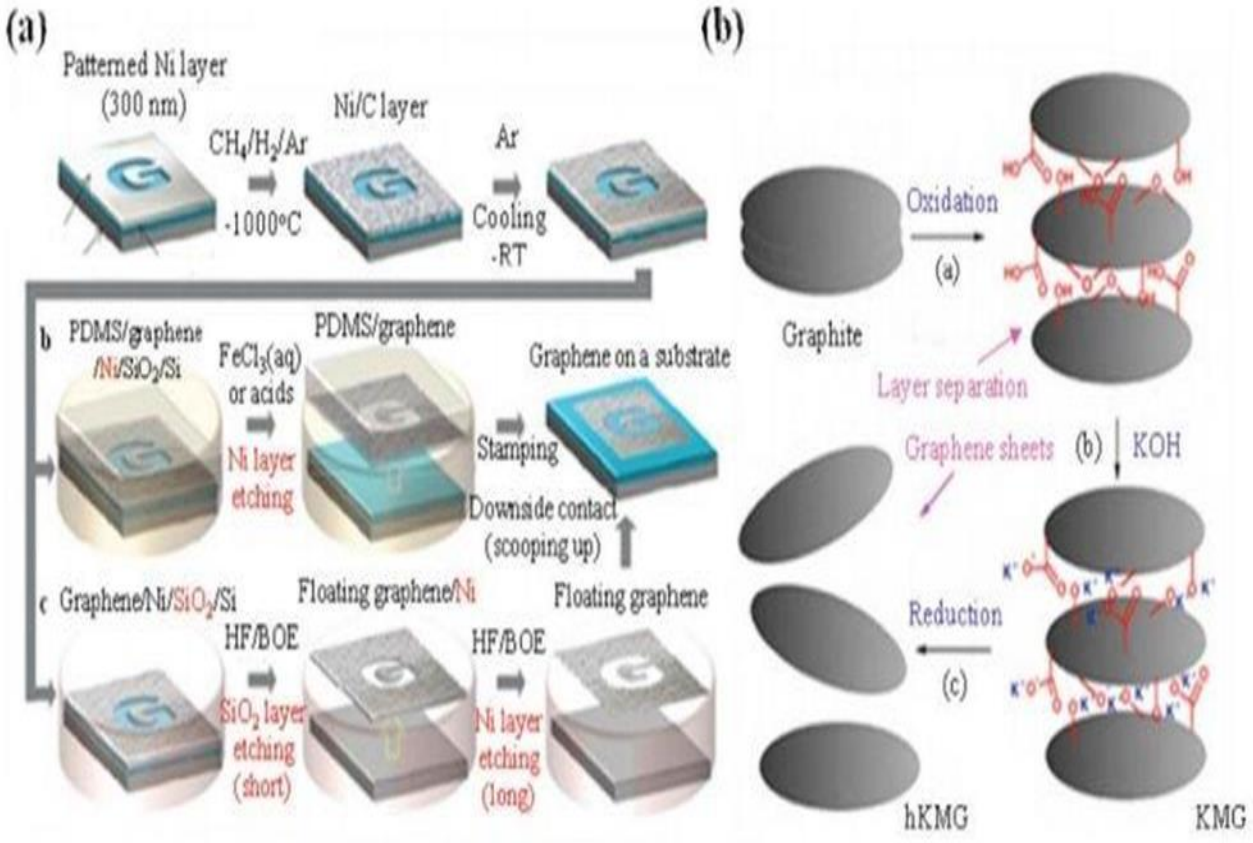

Figure 2.22: Synthesis method of graphene: (a) chemical vapor deposition method and (b) chemically exfoliation method [89].

Graphene is about 300 times stronger than steel. It is the lightest material known so far. One square meter weighs about 0.77 mg. It is the best conductor of heat at room temperature. Graphene is reported to have an exceptionally high value of thermal conductivity. It has low coefficient of thermal expansion and high optical transmittance [90].

Graphene, due to its exceptional chemical and physical properties, has attracted attention in a wide range of application areas. Due to the remarkable electronic properties of graphene, such as high charge transport mobility [91].

It is a key material particularly in the manufacture of sensitive nanodevices, nanoelectronics, and nanosensors. Further, graphene is a promising building block for high performance electronics, sensors, and energy storage devices. Graphene nanostructures are integrated into a variety of electronic and optoelectronic applications, such as sensors, transistors, solar cells, and liquid crystal elements, due to its low electrical noise, and ballistic transport properties [92]. Figure (2.23) shows some of the main existing and potential application areas of graphene.

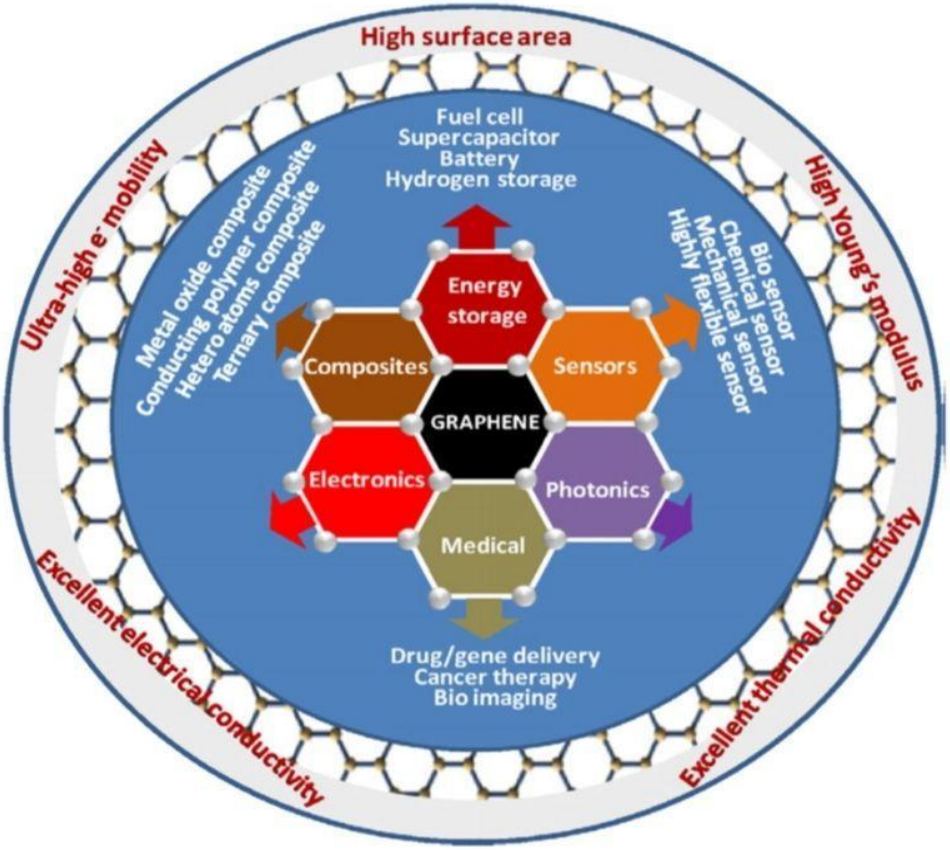

Figure 2.23: Existing and potential applications of graphene in different fields [93].

Table 2.2 gives a comparative chart on the mechanical, thermal, and electrical properties of graphene with carbon nanotube, steel, plastic, rubber, and fiber. The tensile strength of graphene is similar or slightly higher than

carbon nanotube, but much higher than steel, Kevlar, high-density polyethylene, and natural rubber. The thermal conductivity of graphene is higher than all these materials. The electrical conductivity of graphene is also higher than these materials except for steel [94].

Table 2.2. properties of Graphene, carbon Nanotube, Nanosized steel and Polymer.

Materials	Tensile strength	Thermal conductivity (W/m k) at room temperature	Electrical conductivity (S/m)
Graphene	130 ± 10 GPa	$(4.84 \pm 0.44) \times 10^3$ to $(5.30 \pm 0.48) \times 10^3$	7,200
Carbon nanotube	60–150 GPa	3,500	3,000–4,000
Nanosized steel	1,769 GPa	5–6	1.35×10^6
Plastic (high-density polyethylene)	18–20 GPa	0.46–0.52	Insulator
Rubber (nature rubber)	20–30 GPa	0.13–0.142	Insulator
Fiber (Kevlar)	3,620 MPa	0.04	Insulator

2.6.2.1 Properties of Graphene

As mentioned above, graphene is considered a 2D material with a one atom-thick planar sheet of sp^2 bonded carbon atoms that are densely packed in a honeycomb crystal lattice. It is regarded as the 'thinnest material with tremendous application potential. Graphene is predicted to have remarkable properties, such as high thermal conductivity, superior mechanical properties, and excellent electronic transport properties. These intrinsic properties of graphene as shown in Table (2.3) have generated enormous interest for its possible implementation in a myriad of devices [95]. These include future generations of high speed and radio frequency logic devices, thermally and electrically conducting reinforced Nano composites, ultra-thin carbon films,

electronic circuits, sensors, and transparent and flexible electrodes for displays and solar cells.

Table 2.3. The physical properties of the graphene

Property	Value
Charg carier	- 200 000 $cm^2/V.$
Transparency	-97.4%
Specific surface area	-2630 m^2/g
Band gap	Zero
Specific density	2.26 g/cm^3
Resistivity	2.26 Ω.cm
Thermal stability	450-650°C
Melting points	3527 °C
Current density	> 10^8 A/cm^2

The electronic properties of graphene change with the number of layers and by the relative position of atoms in adjacent layers (stacking order). For bilayer graphene, the stacking order can be either AA, with each atom on top of another atom; or AB, where a set of atoms in the second layer sits on top of the empty center of a hexagon in the first layer. As the number of layers increase, the stacking order can become more complicated. For graphite, there are three common types of stacking: (i) AB or Bernal stacking, (ii) ABC or rhombohedral stacking, and (iii) no discernible stacking order or turbostatic stacking. The most stable stacking is AB, thus it has been studied more than other graphene-based stacks. However, the other stacking orders are certainly possible, especially in few-layer graphene [96].

2.7 Isopropyl Alcohol (IPA)

Isopropyl alcohol, also known as isopropanol, 2-propanol, dimethylcarbinol, and sec-propyl alcohol, is a colorless, volatile, and flammable liquid, having a molecular weight of 60.09 and a slight odor

resembling a mixture of ethyl alcohol and acetone. Isopropyl, the lowest member of the class of secondary alcohols, is generally known as the first petrochemical. of the lower (C_1–C_5) alcohols, isopropyl alcohol is third in commercial production, behind methanol (qv) and ethyl alcohol. The 1993, U.S. production was 5.4 × 105 metric tons (1). Production of isopropyl alcohol has been declining at an average annual rate of 3% since 1980, mostly because of the declining use of isopropyl alcohol as an acetone (qv) feedstock. An estimated 50% of isopropyl alcohol was used in solvent applications in 1992 (see Solvents, industrial). Isopropyl alcohol is used for the manufacture of agricultural chemicals, pharmaceuticals (qv), process catalysts, and solvents. Properties, preparation, and uses of isopropyl alcohol have been discussed (2) [97].

2.7.1 Physical properties

Physical properties of isopropyl alcohol are characteristic of polar compounds because of the presence of the polar hydroxyl, –OH, group. Isopropyl alcohol is completely miscible in water and readily soluble in a number of common organic solvents such as acids, esters, and ketones. It has solubility properties similar to those of ethyl alcohol (qv). There is a competition between these two products for many solvent applications. Isopropyl alcohol has a slight, pleasant odor resembling a mixture of ethyl alcohol and acetone, but unlike ethyl alcohol, isopropyl alcohol has a bitter, unpotable taste. Physical and chemical properties of isopropyl alcohol reflect its secondary hydroxyl functionality. For example, its boiling and flash points are lower than n-propyl alcohol [98], whereas its vapor pressure and freezing point are significantly higher. Isopropyl alcohol boils only 4◦C higher than ethyl alcohol. Anhydous and 91 vol % alcohol, the two main grades of isopropyl alcohol marketed in the United States, differ mainly in water content. The latter represents the azeotrope with water and is usually referred

to as constant boiling mixture (CBM) isopropyl alcohol. Because of its tendency to associate in solution, isopropyl alcohol forms azeotropes with compounds from a variety of classes, including hydrocarbons, esters, halocarbons, amines, ketones (qv), and aromatics[99].

2.7.2 Chemical Properties

Chemical properties of isopropyl alcohol are determined by its functional hydroxyl group in the secondary position. Except for the production of acetone, most isopropyl alcohol chemistry involves the introduction of the isopropyl or isopropoxy group into other organic molecules by the breaking of the C–OH or the O–H bond in the isopropyl alcohol molecule.

Isopropyl alcohol undergoes reactions typical of an active secondary alcohol. It can be dehydrogenated, oxidized, esterified, etherified, aminated, halogenated, or otherwise modified at the OH moiety more readily than primary alcohols such as n-propyl or ethyl alcohol. Manufacture of the commercially important aluminum isopropoxide and isopropyl halides illustrates this reactivity [97].

2.8 Literatures Review

In 2015, Suhana et al. [100] development of high efficiency organic thermoelectric materials to harness energy from ambient sources such as solar and domestic heat. In this present work, poly (3, 4-ethylenedioxythiophene)/(poly)styrenesulfonate (PEDOT: PSS) was post treated using nitric acid in order to increase its electrical conductivity, hence the efficiency. A maximum electrical conductivity of 197.51 S/cm was achieved which was approximately 115 times than that of the untreated material. Improvement of the electrical conductivity after post-treatment is due to the depletion of the non-conducting PSS after the acid treatment. Hence, it is concluded that it is an easy method to achieve comparatively good thermoelectric properties which can find its uses in flexible thermoelectric applications.

In 2015, Yong Zhang *et al.* [101] A thin layer of PEIE (polyethylene emine ethoxylate) film was spin-coated onto the surface on the PEDOT:PSS films, thus substantially changing their charge selectivity from supporting hole transport to supporting electron transport. It was also found that the PEDOT:PSS/PEIE ETL exhibited higher interfacial contact, a more favorable active morphology, and improved charge mobility. By virtue of these beneficial properties, inverted PSCs based on low-bandgap semiconducting photoactive layers achieved a notably improved power conversion efficiency (PCE) of 7.94%, superior even to the corresponding performance of devices with only a ZnO layer. Surpassing our expectations, compared with the extreme degradation of device stability observed when pure PEDOT:PSS is used, PEIE-modified PEDOT:PSS can considerably suppress device degradation because of the hydrophobic and alkaline nature of PEIE, which not only reduces the hygroscopicity of the PEDOT:PSS but also neutralizes the acidic PEDOT:PSS and thus prevents the corrosion of the ITO cathode.

These results demonstrate the potential of PEIE-modified PEDOT:PSS for use as an efficient ETL in commercial printed electronic devices.

In 2016, Joseph Palathinkal Thomas and Kam Tong [102] prepared a mixed co-solvent of EG (ethylene glycol) and methanol (MeOH) to used for engineer the PEDOT:PSS grains to dramatically enhance their conductivity.

As a result, engineering of PEDOT:PSS by mixed co-solvent addition of an appropriate amount is extremely beneficial for modifying the bulk and structural properties that lead to the low sheet resistance films. The 16 wt% mixed co-solvent added PEDOT:PSS film provides a very high Voc of 620 mV and the highest PCE performance (14.6%) reported to date for a PEDOT:PSS/planar-Si single junction solar cell. This remark able performance is made possible by the partial removal of the PSS chain network around the grain boundaries of PEDOT, the extended linear chain network of the quinoas structure that results in the enlargement of PEDOT grains, and the improved close packing of PEDOT grains by the mixed co-solvent, which are consistent with the observed reduction in the sheet resistance. Post-treatment could be used to further reduce the surface resistivity of these films. Mixed co-solvent engineering therefore promises a facile approach to produce highly con ducting PEDOT:PSS films not just for solar cell applications but indeed for other organic electronic device fabrication.

In 2017, Park *et al.* [103] preparation polymer PVDF film with graphene sheet prepared by chemical vapor deposition (CVD) and metal electrodes (Al and Ag) were deposited via an electron beam evaporation for energy harvesting efficiency of piezoelectric. The thin of piezoelectric PVDF film was (~10 μm) with uniform roughness was synthesis well. It is indicate that thin piezoelectric film exhibits better energy conversion efficiency. The thin piezo-film was more effective in converting acoustic waves into electrical charge because free standing thin film is more flexible and more sensitive to

the acoustic waves. They found that the maximum voltage at its resonance frequencies f_r were measured as 6.6 V at 283 Hz.

In 2018, Hiroyuki *et al.* [104] Poly(3,4-ethylenedioxythiophene):poly(4-styrenesulfonate) (PEDOT:PSS) films doped with several sugar alcohols, viz. xylitol (XL), glycerol (GL), and polyglycerol (PG), at various levels have been synthesized and their thermoelectric properties studied. Among these specimens, 2.5 vol.% GL-doped films showed the best performance with electrical conductivity, Seebeck coefficient S, and power factor S2 r at room temperature reaching 1040 S/cm, 19 lV/K, and 37 lW/m-K2 , respectively. Next, synthesized films under an electric field Epr for the purpose of crystal growth. GL-doped films showed r enhancement with increase of Epr. The highest r value of 1300 S/cm was attained at Epr = 4 kV/cm. S and thermal conductivity j values were almost independent of Epr. The ZT value was calculated to be between 0.017 and 0.101 at room temperature. They also examined film flexibility. High flexibility was achieved on GL doping, and it was not deteriorated when synthesized under an electric field.

In 2018, Fukushima *et al.* [105] prepared high-responsivity graphene photodetectors operating in the middle-wavelength infrared (MWIR) spectral band were fabricated by taking advantage of the photo-gating effect. In this device, a 600 μm thick Ge-doped InSb (Indium antimonide) substrate was utilized as the photo-sensitizer and a 260 nm thick tetraethyl orthosilicate (TEOS)-SiO_2, insulator layer was deposited on the InSb substrate by plasma chemical vapor deposition. The source/drain electrodes consisted of 10 nm Graphene-based field effect transistors were fabricated on indium antimonide (InSb) substrates. The InSb generated photo-carriers in response to incident IR light modulated the graphene channel gate voltage and induced a large photocurrent. These graphene-based photodetectors exhibited a clear photoresponse during irradiation with 4.6 μm MWIR laser light and an

ultrahigh responsivity of 33.8 A/W was achieved at 50K due to the photo-gating effect. These devices were found to maintain an MWIR photoresponse up to 150K. Our graphene-based photodetector design is expected to contribute to the development of high-performance MWIR image sensors.

In 2019, *Baoyang et al.*[106] blend PEDOT:PSS with other compositions such as non-conductive polymers, the blending can compromise resultant hydrogels' mechanical and/or electrical properties. Here, shows that designing interconnected networks of PEDOT:PSS nanofibrils via a simple method can yield high-performance pure PEDOT:PSS hydrogels. The method involves mixing volatile additive dimethyl sulfoxide (DMSO) into aqueous PEDOT:PSS solutions followed by controlled dry-annealing and rehydration. The resultant hydrogels exhibit a set of properties highly desirable for bioelectronic applications, including high electrical conductivity high stretchability (> 35% strain), low Young's modulus (~2 MPa), superior mechanical, electrical and electrochemical stability, and tunable isotropic/anisotropic swelling in wet physiological environments.

In 2019, Fan *et al.*[107] prepared suspended graphene membranes with attached silicon proof masses as piezoresistive nanoelectromechanical systems accelerometers. Devices were fabricated from the silicon device layer was 15 μm thick, the BOX layer was 2 μm thick and the handle substrate was 400 μm. Next, a photoresist layer was spin-coated on the SiO_2 surface of the silicon device layer and patterned to define the metal electrodes. The cavities were filled with a 50 nm thick layer of titanium (Ti) followed by a 270 nm thick layer of gold (Au) using metal evaporation. They found that the device with dimensions of (40μm×40μm×16.4μm and trench width of 4 μm) exhibit the spectra of the amplified output voltages 0.35 mV at frequency of 160 Hz. Optical microscopy، SEM AFM and Raman spectroscopy characterize the to evaluate graphene membranes and suspended proof.

In 2019, Seyedeh *et al.*[108] prepared fast response ZnO/PVA nanocomposite -based photodiodes modified by graphene quantum dots. a new class of the polymer-based photodetectors is introduced. These device was fabricated by the spin coating. Poly (vinyl alcohol) is used as the host polymer and ZnO/graphene quantum dots utilized as the filler of the polymer matrix. The manufactured photodiode, based on ZnO/GQD/PVA nanocomposite, indicates short rise time of 0.06 s and responsivity of 46.5 AW^{-1}. Also studied using SEM and TEM micrographs confirms that the ZnO nanoparticles are about 50 nm in size and the size of graphene quantum dots ranges from 1 to 5 nm with 2.5 nm average size. Moreover, the SEM image of ZnO/GQD/PVA shows a highly uniform thin film containing the core shell nanoparticles smaller than 100 nm. The absorbance spectra of the ZnO/GQD/PVA shows absorption peaks related to the ZnO are approximately the same for both samples. It can be attributed to the higher numbers of ZnO molecules

In 2020, Ping Fu *et al.* [109] prepared PEDOT:PSS/APA films by blending PEDOT:PSS with APA. The ordered multilayer-structure and fiber-structure were formed via self-assembly between PEDOT:PSS and the triblock copolymer via π-π interactions and hydrogen bonding. A high power factor could be obtained by optimizing the mass ratio of PEDOT:PSS to APA. As a result, PEDOT:PSS/APA thermoelectric films have been successfully prepared via self-assembly of PEDOT:PSS and triblock copolymers based on an aniline oligomer. Hydrogen bonding and π-π interaction are the main driving force to form ordered multilayer-structure films and fibrous-structure films via controlling the ratios of APA and PEDOT:PSS. PEDOT:PSS dominated multilayer-structure films exhibit p-type characteristics, while aniline oligomer based triblock copolymers dominated fibrous-structure films show n-type characteristics. The high power factor and low thermal

conductivity provide good thermoelectric performance for PEDOT:PSS based thermoelectric materials and exhibit great application potential.

In 2020, Wang *et al.* [110] fabrication of p-type PEDOT:PSS films whose optical properties, electrical conductivity, thermal conductivity, and Seebeck coefficient were engineered to perfectly match the n-type indium tin oxide (ITO) counterparts. The dense p-type PEDOT:PSS and n-type ITO thin films show a thermoelectric of merit of zT = 0.30 and 0.29 at 450 K, and a thermal conductivity of 0.22 and 0.32 W m−1 K−1 , respectively. A flexible thermoelectric generator (TEG) module with a high transmittance of >81% in the visible wavelength range of 400–800 nm is fabricated using 10 pairs of p-type PEDOT:PSS and n-type ITO thin film legs. An ultra-high power density of 22.2 W m−2 at a temperature gradient of 80 K was observed, which is the highest power density reported for organic/hybrid-based flexible TEGs so far. Our transparent flexible thin-film p–n junction thermoelectric module with exceptionally high power generation may take a tremendous step forward towards multi-functional wearable devices.

In 2020, Chandio *et al.* [111] studied processing characterization and application of Graphene. The graphene layer has been prepared by using electrochemical approach. For characterization, SEM, UV spectroscopy, AFM Fourier transmission infrared spectroscopy (FTIR) and X-ray diffraction (XRD) were utilised. Following are the observations: folded sheets of graphene were obtained, anamorphous pattern at $2\theta = 26.6^{\circ}$ was observed, the absorption peak of graphene decreased at high wavelengths 266 nm, the graphene peak was also confirmed by FTIR at 1655.5 (C=C) and thickness of flakes were found to be 60nm by AFM.

3.1 Introduction

This chapter includes:

1- Listing the used materials (PEDOT:PSS, Graphene and Isopropyl alcohol) and mention their properties.

2- Describe the procedures used to prepare the substrates.

3- The experimental procedure, which followed to prepare the thin films.

4- Listing the required tests and the devices to evaluate thin film such as XRD, FTIR, DSC, zeta potential, AFM, SEM, Contact Angle, UV and DC.

3.2 Materials

3.2.1 PEDOT:PSS

Highly conductive PEDOT with negatively charged poly (styrenesulfonate), PSS as counter ion was purchased from Ossila (M122 – PH1000) dispersion with the properties maintain in Table (3.1).

Table 3.1: Properties of the used PEDOT:PSS.

Property	Data
Solid content	1.0 – 1.3 wt.% (in water)
Phase	Aqueous solution
Appearance	Dark blue liquid
Viscosity	< 50 mPa.s
Melting point	146 ºC

3.2.2 Graphene

Graphene was purchased from Skyspring with the properties maintain in Table (3.2).

Table 3.2: Properties of the used Graphene.

Property	Data
Thickness	6-8 nm
Phase	Platelet nanopowder
Appearance	Black powder
Density	2.267 g/cm^3
Boiling point	4200 ºC

3.2.3 Isopropyl alcohol

Isopropyl alcohol was purchased from Richest group used as surfactant agents for PEDOT: PSS/Graphene thin films preparation. with the properties maintain in Table (3.3).

Table 3.3: Properties of the used Isopropyl alcohol

Property	Data
Purity %	99.9 %
Phase	Aqueous solution
Appearance	Colorless liquid
Density	0.786 g/cm^3 (20ºC)
Boiling point	86.6ºC

3.3 Preparation Procedures

3.3.1 Preparation of PEDOT: PSS/ Graphene solution

PEDOT: PSS/Graphene solutions were prepared by dispersing (0.5, 1, 1.5 ,2) wt% of Graphene in the PEDOT: PSS polymer using sonication technique for 3 hr at 70 ^{o}C. The resultant homogeneous solutions labeled as S_1, S_2, S_3, S_4 and S_5. And when added Isopropyl alcohol as a surfactant used the same concentration of above samples labeled as Si_1, Si_2, Si_3, Si_4 and Si_5.

3.3.2 Surface modification of glass substrates

Surfaces of glass substrates (7.6 × 2.6 × 0.1) cm^3 were modified by two steps; cleaning and etching.

Cleaning step includes, removing dust and oil by detergent solution, rubbing by tab methanol for 10 min, sonication for 10 min with distilled water and then with acetone as show in Figure (3.1).

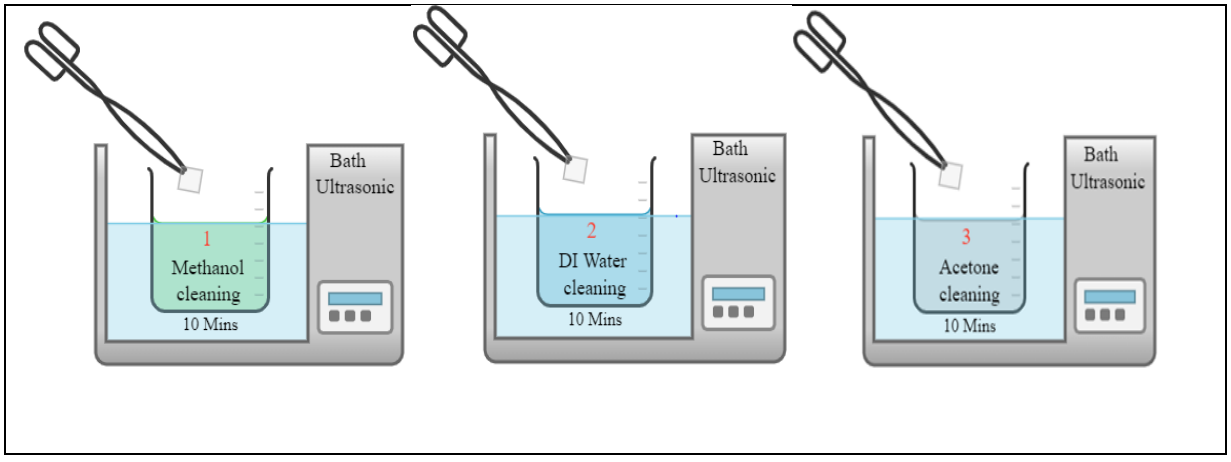

Figure 3.1: Cleaning steps

Etching step carried out using chemical Piranha Solution, which is an aqueous mixture of sulfuric acid (H_2SO_4) and hydrogen peroxide (H_2O_2),

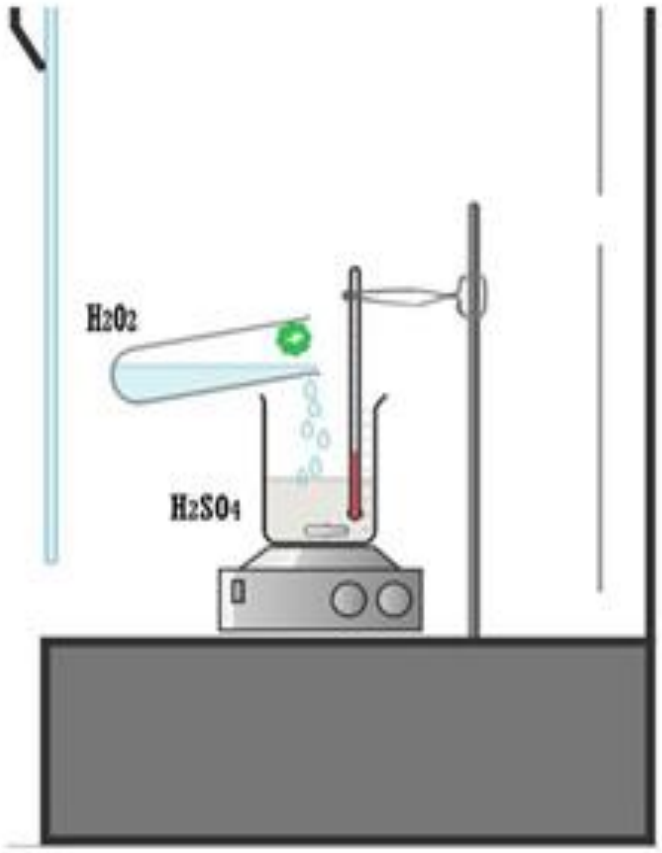

Figure 3.2: Schematic of system to prepare Piranha Solution

The used mixture composed of 3:1 H_2SO_4 and 30% H_2O_2. This mixture prepared in a fume hood by added peroxide to acid and left it stirred for 2 hr as show in Figure (3.2). Then soaked the glass substrates in this solution for 24 hr. After that, the substrate cleaned from the remaining solution and dried in vacuum oven for 10 min at 90^{o}C.

3.3.3 Spin coating process

Thin films of PEDOT:PSS/Graphene were fabricated using spin coating technique (Figure 3.3). This is achieved by dropping of each of the

prepared samples (S_1, S_2, S_3, S_4 and S_5) onto the treated glass substrate at 60 rpm for 20 s.

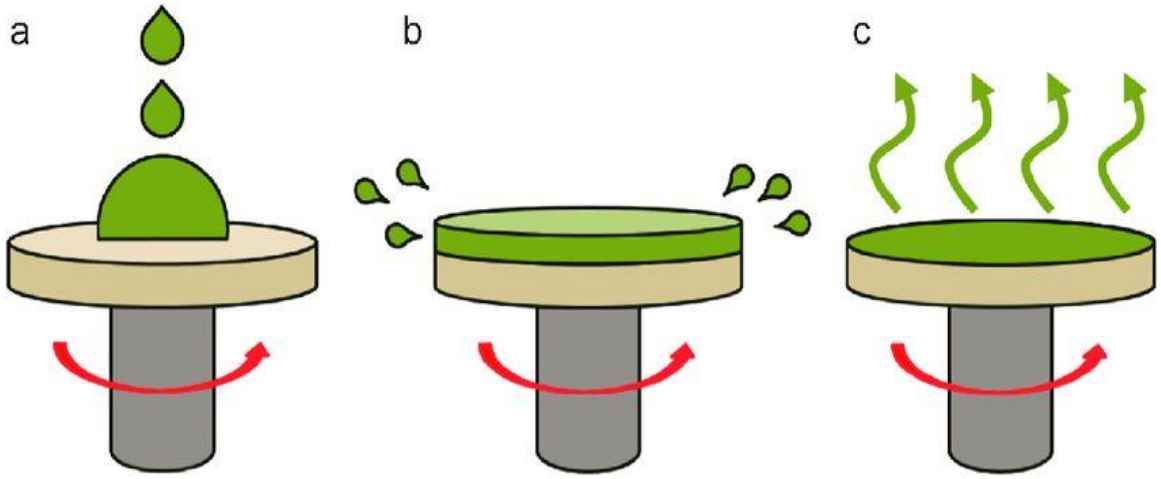

Figure 3.3: Stages of spin coating on substrate.

Thermal annealing was conducted under an air atmosphere at 80◦C for 30 min to obtain PEDOT:PSS/Graphene thin films.

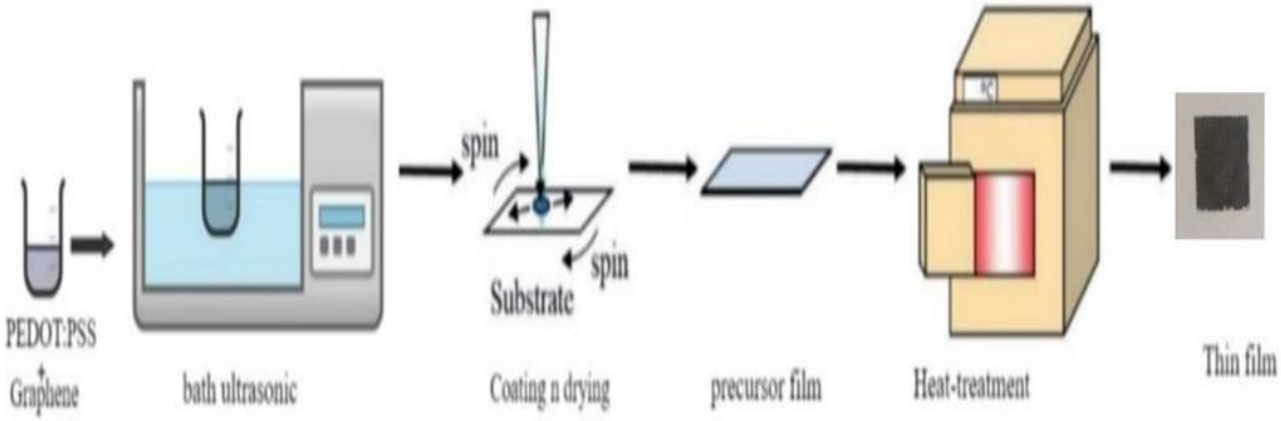

Figure 3.4: Procedure for fabricating thin film

3.3.4 Electrodes deposition for DC measurement

Aluminum sheets were used as a mask. These masks are placed on films to depose the aluminum on the surface of the nanocomposite by using thermal evaporation equipment type (Edward), the electrodes deposited by using aluminum wire placed in (Tangiesten W) boat material under pressure (10-5 Torr), then the aluminum electrodes deposited on the thin films with diameters (0.2) cm as illustrated prepared as in Figure (3.5)

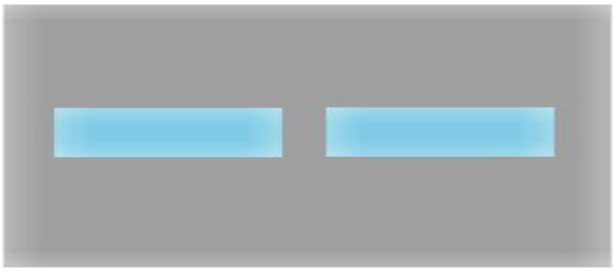

Figure 3.5: The mask, which used for electrical measurement (DC)

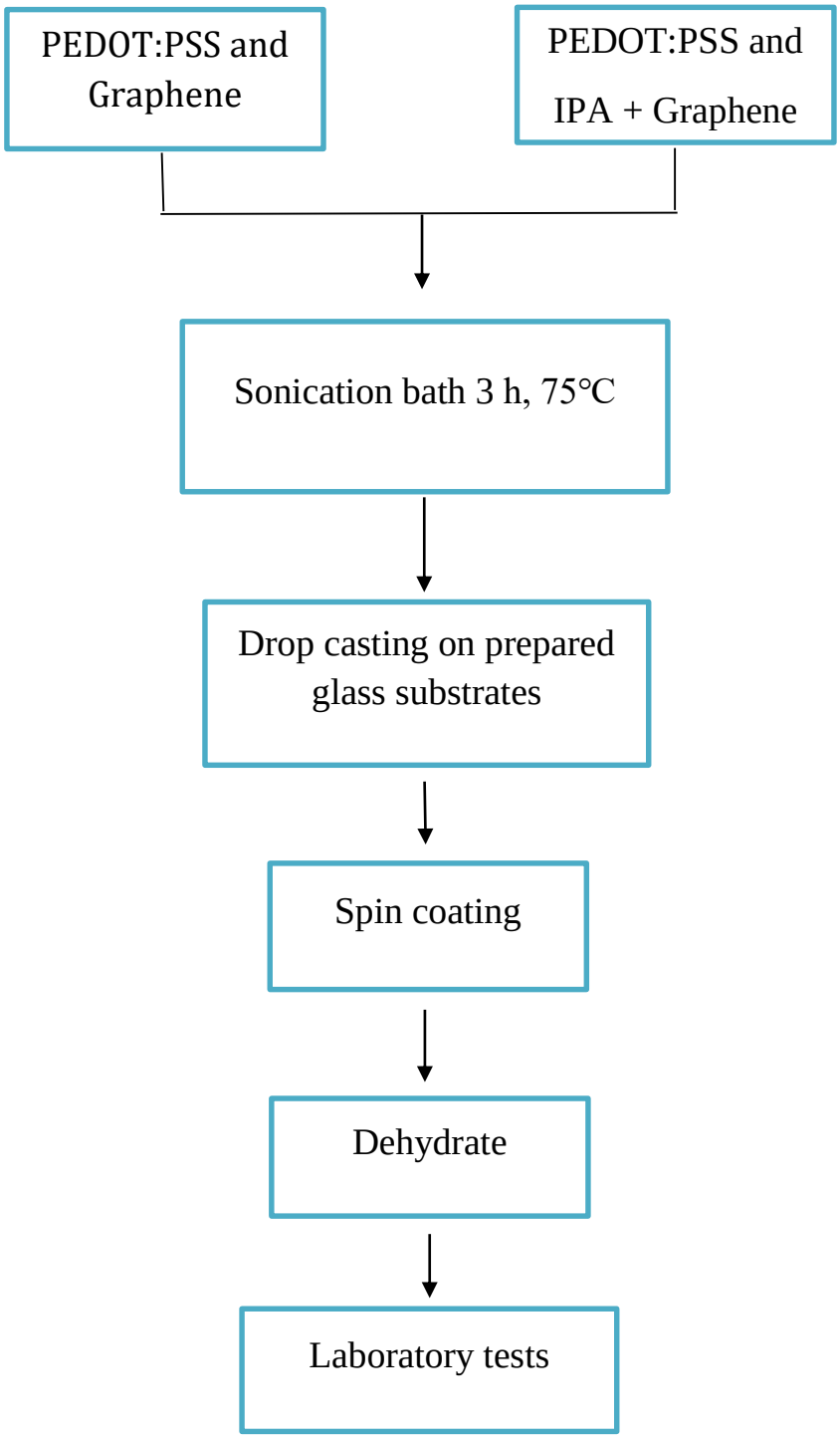

Figure 3.6: General procedure for preparing thin films.

3.4 Tests

The preparation thin film tested by using different techniques as shown in Figure (3.7).

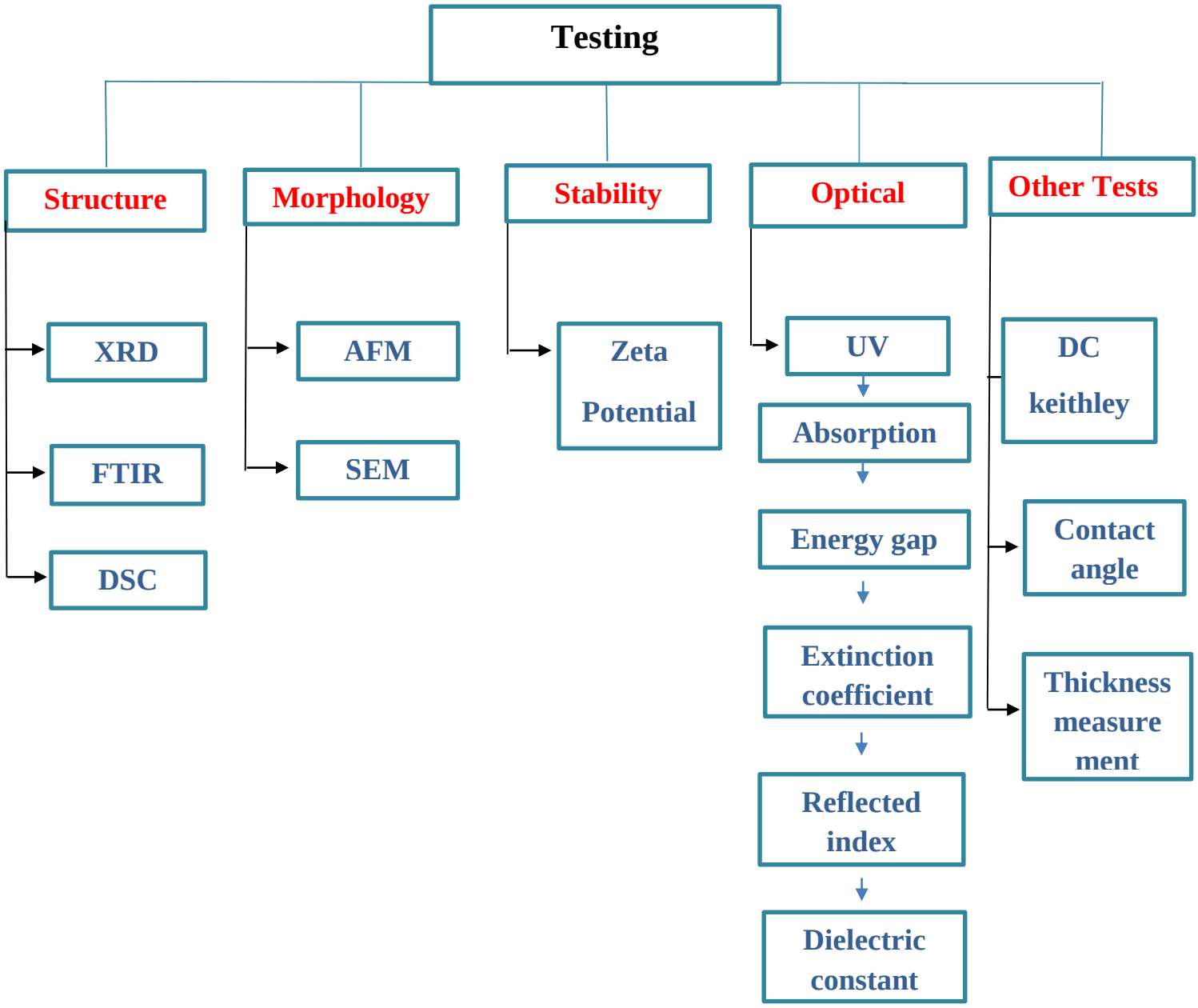

Figure 3.7: Procedure of testing the thin films

2.4.1 Interferometric method for the thickness measurements

For the determination of the thickness of the films deposited, an interferometric Fizeau was used. In Figure (3.8), the system for observing Fizeau fringes is shown schematically, and in Figure (3.9) the Fizeau pattern is shown.

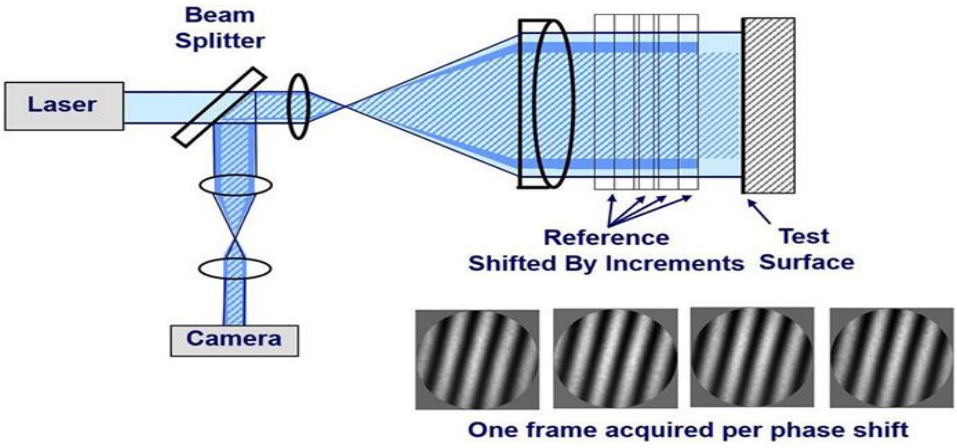

Figure. 3.8: (a) Schematic of the system. (b) The reflection takes place on the two interfacial surfaces

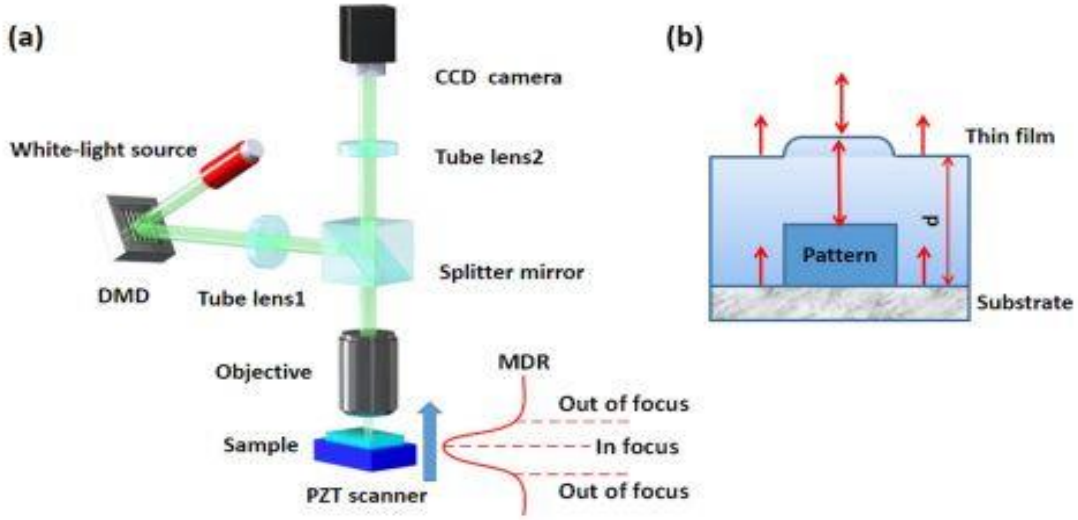

Figure 3.9: Experimental arrangement for observing Fizeau fringes

The thickness of the film is calculated by the optical interferometer process. The approach is based on the interference of the reflection of the light beam from the thin film surface and the bottom of the substrate. It uses He-Ne Laser (600 nm). To calculate the thin film thickness, the following equation :

$$t_t = \frac{\Delta X}{X} \cdot \frac{\lambda}{2} \qquad (3\text{-}1)$$

Where X is the spacing of the fringes, ΔX is the displacement and λ is the laser light wavelength.

3.4.2 X-Ray Diffraction (XRD) Test

It is a rapid analytical technique, primarily used for phase identification of crystalline materials and also can provide information on unite cell dimensions. It is generated in cathode ray tube by heating a filament to produce accelerated electrons toward the target by applying high voltage. Figure (3.10) shows the schematic of x-ray diffraction (XRD).

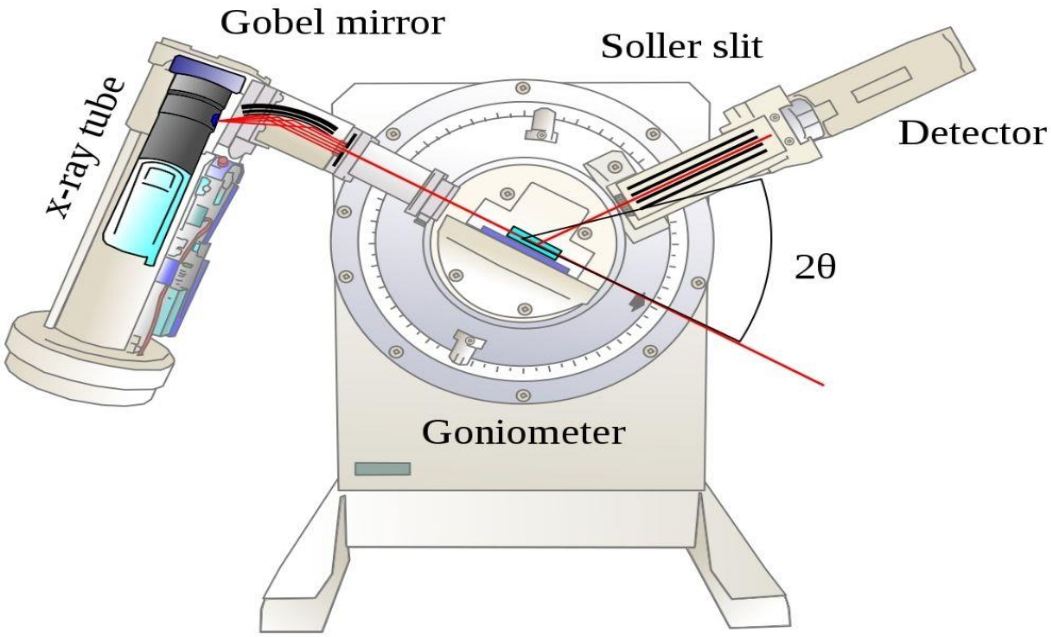

Figure 3.10: A schematic of X-ray diffraction (XRD)

It was proposed that the incident X-ray radiation would produce a Bragg peak if their reflections of the various planes are interfered constructively. The interference is constructive when the phase shift is a multiple of 2π; this condition can be expressed by Bragg's law

$$n\lambda = 2d \sin \Theta \qquad (3\text{-}2)$$

where λ, Θ and n represent X-ray wavelength from Cu target (1.5406 Å), diffraction angle and diffraction order respectively. The direction of crystal planes can be chosen in many different ways as shown in Figure (3.11). The Scherrer equation is a formula that relates the size of crystallites in a solid to the broadening of a peak in a diffraction pattern. It is used in the determination of size of particles of crystals.

$$L_{hkl} = \frac{K\lambda}{\beta \cos\theta} \qquad (3\text{-}3)$$

Where L_{hkl} is the grain size, k is a constant, λ is X-ray wavelength, β is the line broadening at half the maximum intensity, θ is the Bragg angle.

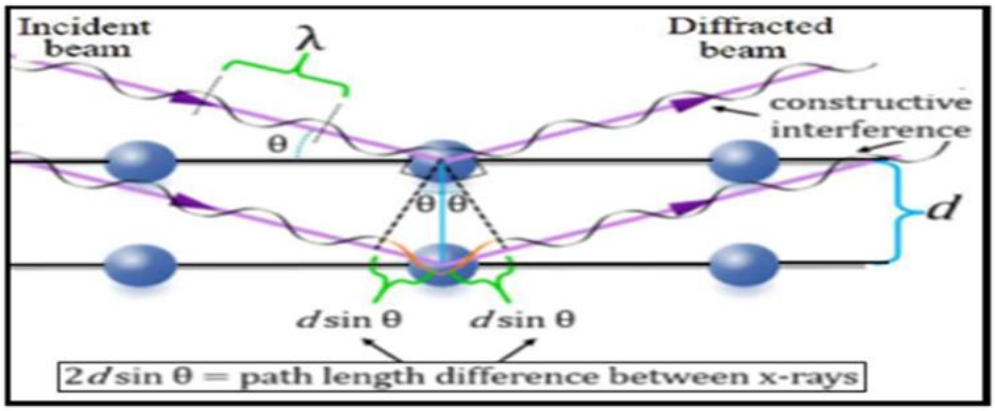

Figure 3.11: Reflection of x-ray beam from a set of atoms plane separated by distance d [71].

3.4.3 Infrared fourier transform spectrometer (FTIR) test

Fourier transforms infrared technique used to characterize the prepared samples using instrument type (IR Affinity-1) made in (Kyoto Japan) located in Polymer and Petrochemicals Department (a schematic shown in Figure 3.12). In order to measure a sample, calibrate the device using the KBr, and then prepare a powder of the sample to be examined, and mixed with KBr (mixing ratio 99% KBr). FTIR spectrum provides a diagram between the permeability or absorption and the number of waves that show the chemical composition of the material. This test carried out according to ASTM E1252 [78] for ABS and ABS/Ag NPs in order to know the bond between the polymer and fillers, if is a chemical or physical bond. Also, this technique used to characterize propolis (P) material.

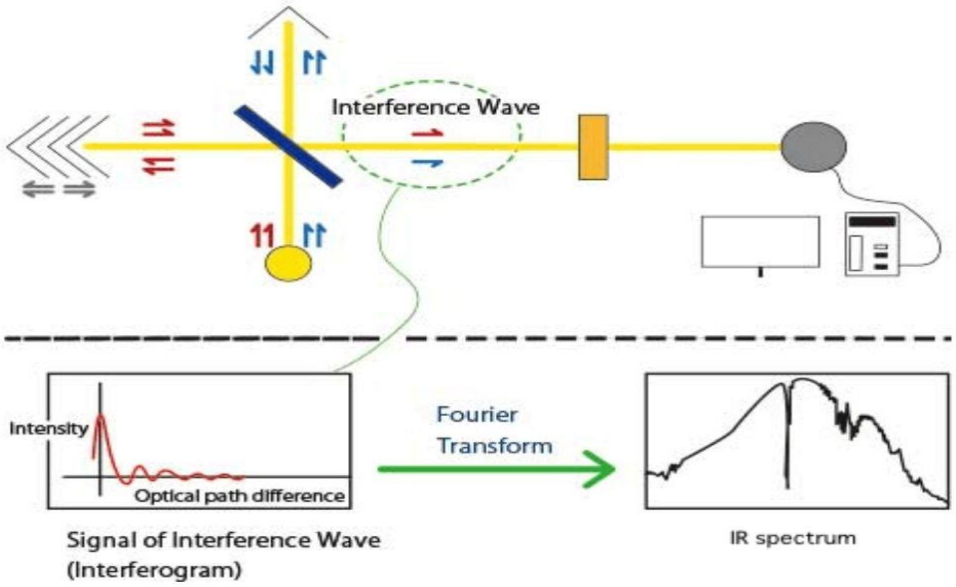

Figure 3.12: Instrument setup for FTIR spectroscopy

3.4.4 Differential Scanning Calorimetry (DSC)

The test was performed according to ASTM D3418-03 using SH1MADZ-4 DSC-60 device (Figure 3.13). The samples of pure materials (PEDOT:PSS) and nano graphene in the powder form was tested under nitrogen gas and heating rate of 10 ˚C / min with heating range from 25 to 400 ˚C

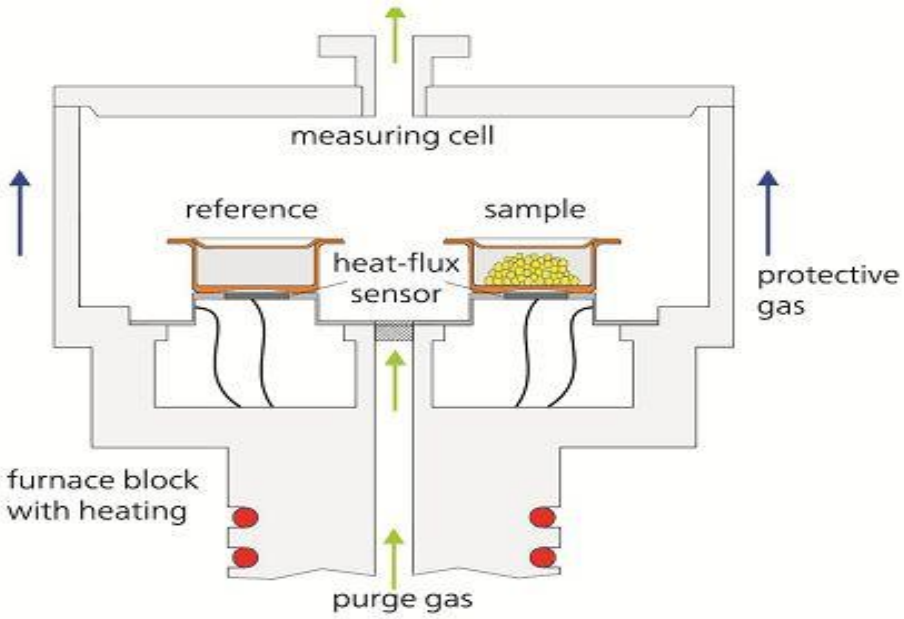

Figure 3.13: schematic of Differential Scanning Calorimetry (DSC)

3.4.5 Zeta potential test

The nanoparticle stability tested by using ZETAPLUS device (Brook haven/USA) by preparing 1ml of PEDOT/Graphene and 1ml of PEDOT:PSS/Graphene and IPA . This test done according to ASTM E2865. The operation principle of this device Similar to particle sizing by dynamic light scattering as shown in Figure (3.14). What is measured is temporal fluctuations in intensity of light scattered by the particles in the dispersion. In light scattering, the fluctuations related to Brownian motion of particles. In PALS for ZP, the fluctuations related to the movement of the particle in the applied field, i.e. to Ua. The zeta potential is then calculated from the UE that is determined by the PALS measurement. As in light scattering. The instrument's autocorrelation and software take care of the data reduction.

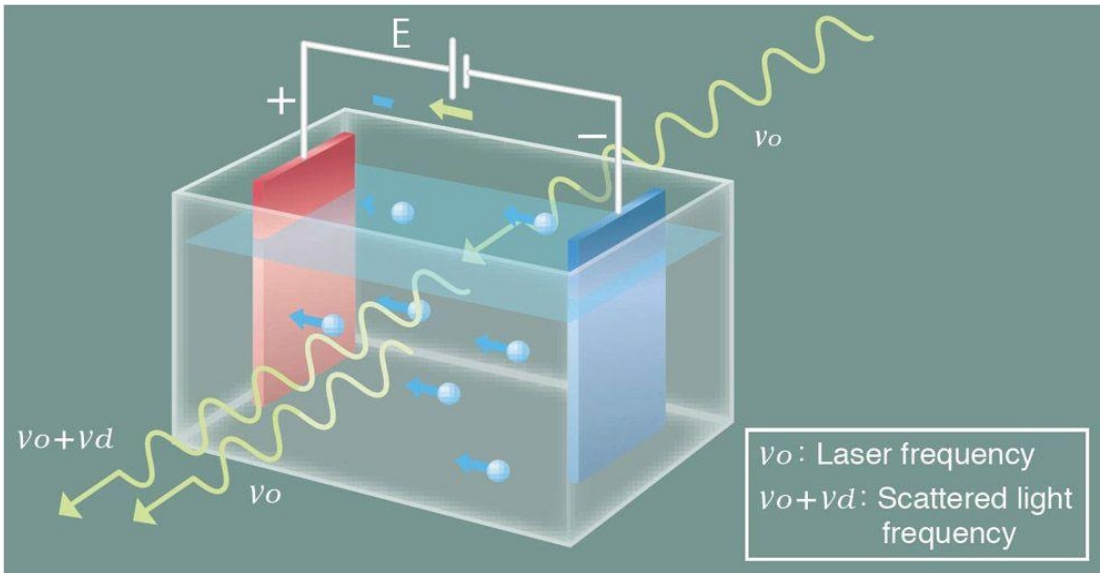

Figure 3.14: The principle of zeta potential.

Stability

Stability of nano partical can be determine by using zeta potential analyzer [112].

The zeta potential is a key indicator of the stability of colloidal dispersions. The magnitude of the zeta potential indicates the degree of electrostatic repulsion between adjacent, similarly charged particles in a dispersion [113]. For molecules and particles that are small enough, a high zeta potential will confer stability, i.e., the solution or dispersion will resist aggregation [114]. When the potential is small, attractive forces may exceed this repulsion and the dispersion may break and flocculate [115]. So, colloids with high zeta potential (negative or positive) are electrically stabilized while colloids with low zeta potentials tend to coagulate or flocculate as outlined in the Table (3.4).

Table 3.4: Stability behavior of particle by zeta potential [116].

Zeta potential [mV]	Stability behavior of the colloid
From 0 to ±5	Rapid coagulation or flocculation
From ±10 to ±30	Incipient instability
From ±30 to ±40	Moderate stability
From ±40 to ±60	Good stability
More than ±61	Excellent stability

3.4.6 Atomic Force Microscope (AFM) test

The surface morphology of the thin film further analyzed using conventional tapping mode probes with constant amplitude (200 mV) of AFM according to ASTM E 2865. The rotated tapping mode etched silicone probe with a 55 resonance frequency of 250 kHz was used. The operation principle of an AFM presented in Figure (3.15).

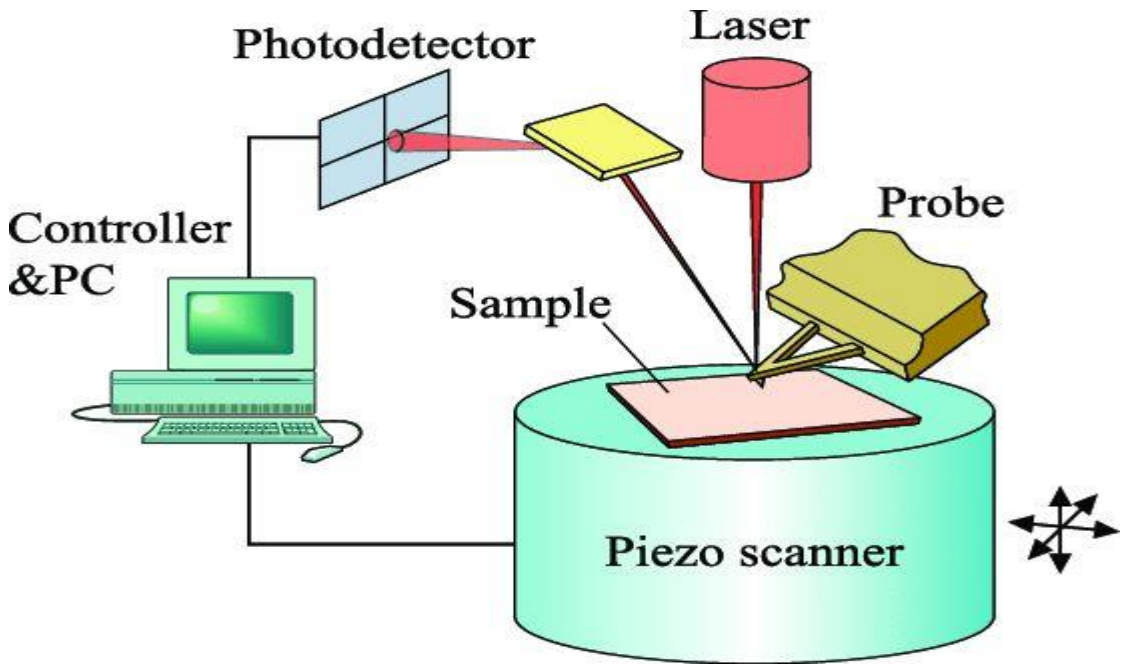

Figure 3.15: The Schematic drawing of AFM.

3.4.7 Scanning electron microscopy (SEM)

Analytical scanning electron microscope (SEM), model (JEOL 6400 F) used to examine the morphology of thin films according to (ASTM 986-04). The third sample used in this test, by adding the drops over the glass slide then placed under the microscope for analysis. Figure (3.16) shows the operating principle of the instrument.

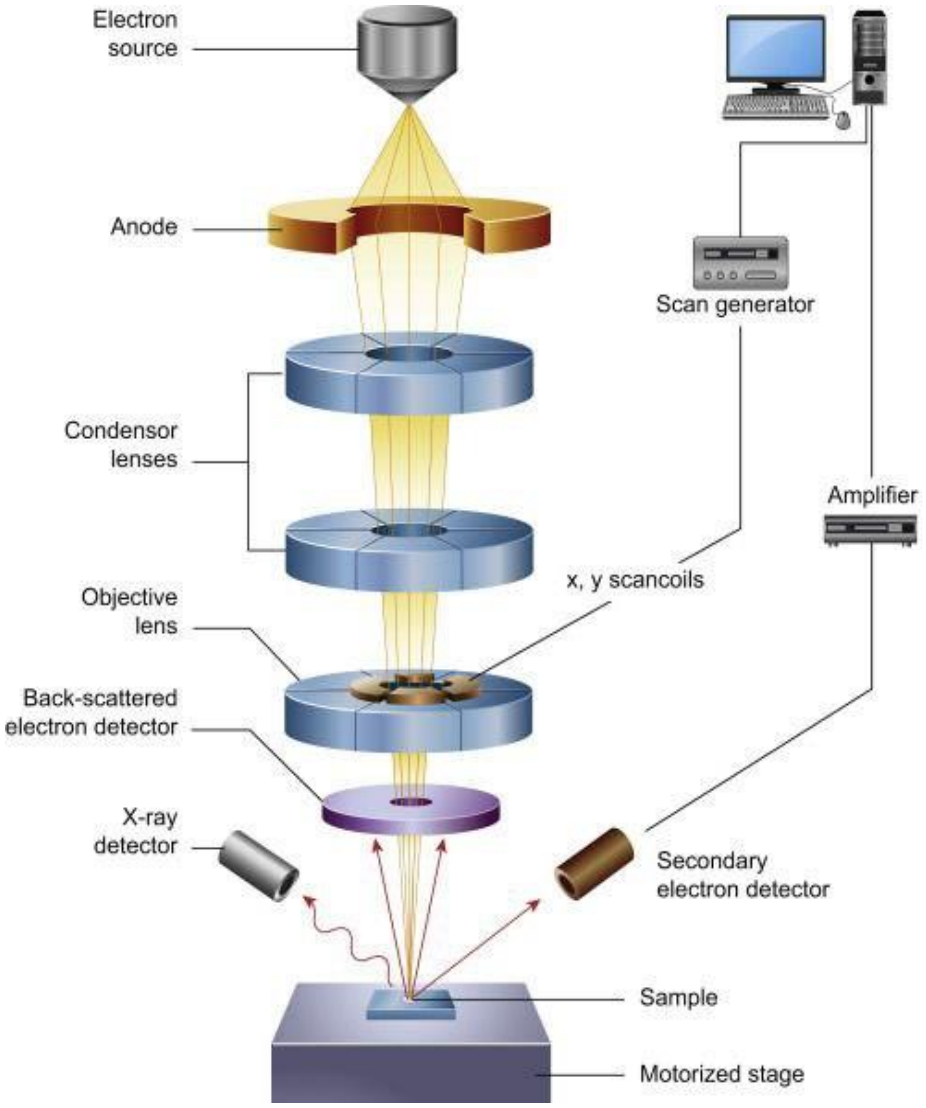

Figure 3.16: The principle of SEM.

3.4.8 Contact angle Test

This test was carried out to evaluate effects of addition on the wettability. The used device is SL 200C - Optical Dynamic I Static Interfacial Tensiometer and Contact Angle Meter which manufactured in KINO Industry Co., Ltd., USA with contact angle range from 0° to 180° (Figure 3.17). This device makes calculation and comparison of left and right contact angle as well as calculate their average value giving a Real time data graph monitoring changes of contact angle with video recording.

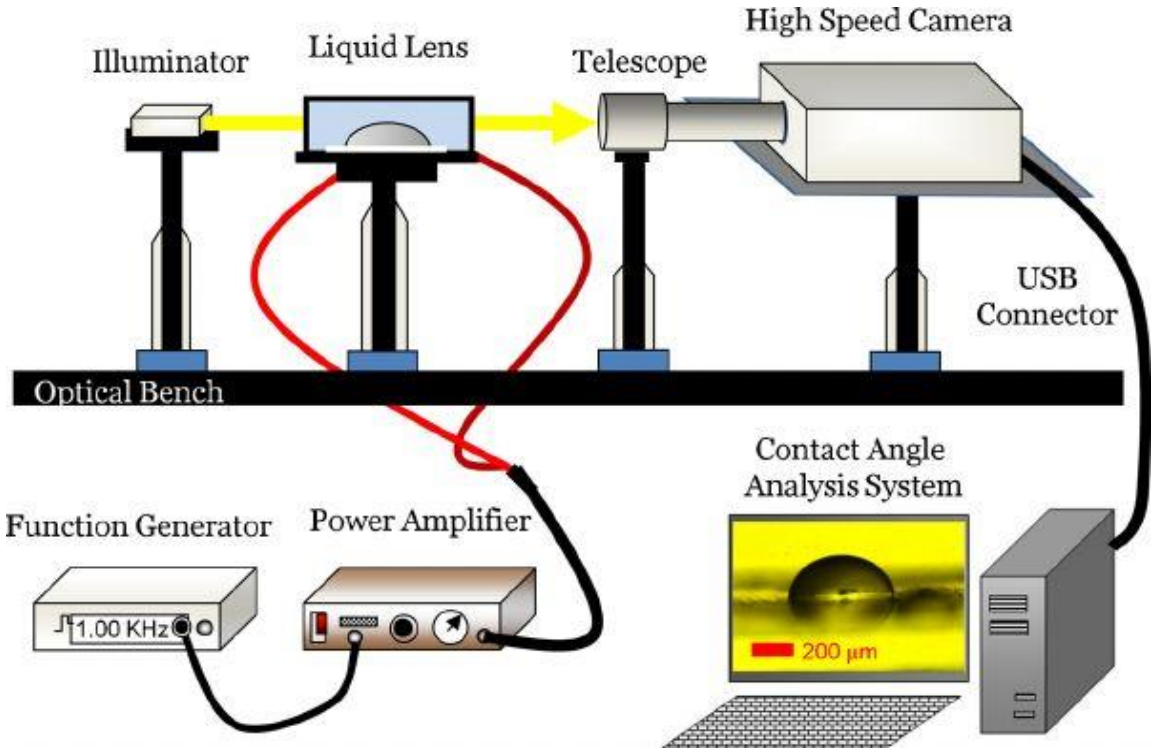

Figure 3.17: The Schematic drawing of Contact angle Test.

3.4.9 Ultraviolet-visible spectrophotometer test

UV-Visible – CECIL 2700 computerized spectrophotometer, it is used to determine the optical properties of samples . The sample is placed in

specific position of UV / VIS device. Figure (3.18) shows the operating principle, where a double beam spectrophotometer utilizes two beams of light: a reference beam and a sampling beam that passes through the sample. Some double beam spectrophotometer have two detectors that allow the two beams to be measured at one time.

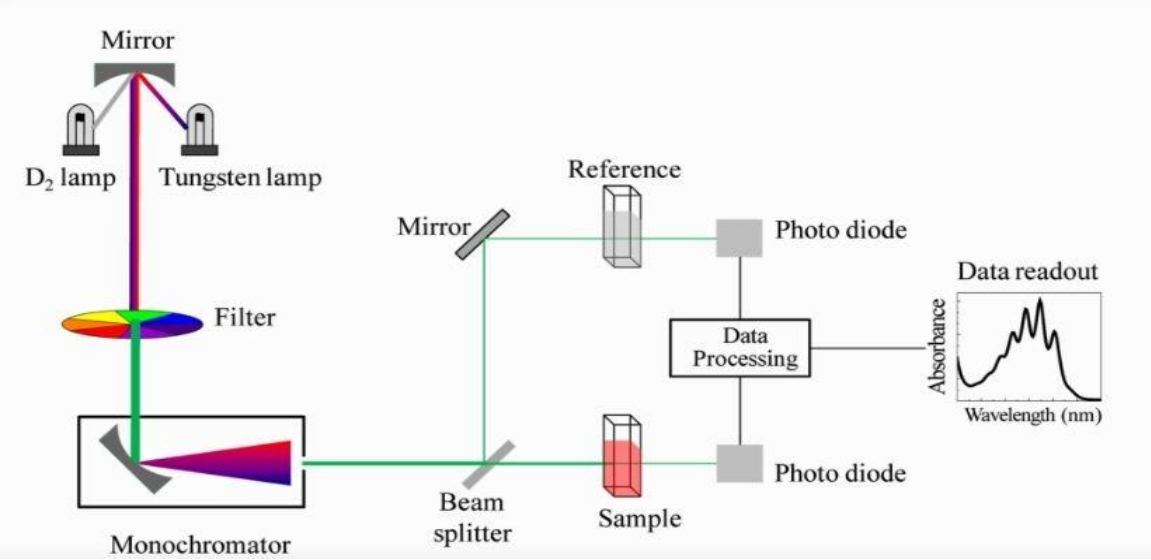

Figure 3.18: The principle of UV.

Optical properties

The study of optical properties is useful for finding the energy gap and optical constants. When light rays fall, a number of processes can occur due to the interaction between the incident light and the material, part of the incident light will be absorbed into the material (absorption), the other part is carried out in the material (transmission), and part is reflected from the surface (reflection). In an ideal semiconductor, the conduction band is empty and separated from the filled valence band by the energy gap. The energy gap means the difference between the energy of a lower level in the conduction

band (E_c) and a higher energy in the valence band (E_v). The first level is called the conduction band edge and the second level is the Valance band edge [117].

When a photon with an energy greater than or equal to the energy gap (between the valence band and the conduction band) falls, it will be absorbed, resulting in the formation of an electron-gap pair [118]

$$\hbar\omega \geq E_g \qquad (3\text{-}4)$$

Where (ω) : is Angular frequency in (rad).

Optical Absorption

When a substance absorbs a photon of energy equal to or greater than the forbidden energy gap of the substance, the electron can move from the valence band to the conduction band. The characteristic and common feature of the absorption scheme of all semiconductor materials is the rapid increase in absorption when the energy of the absorbed radiation becomes equal to the energy gap separating between the valence and conduction bands, which is called (the fundamental edge of absorption).

The position and composition of this edge gives valuable information about the properties of the energy bands and their composition at the top and bottom. The absorption edge can also be defined as the region of the incident rays spectrum at which electrons begin to move, which is equal in magnitude to the difference between the location of the lowest point in the conduction band and the highest point in the valence band.

and when E_g^{opt} it is equal to $\hbar\omega_o$ we get :

$$\omega_o = \frac{E_g^{opt}}{\hbar} \qquad (3\text{-}5)$$

Where ω_o : critical angular frequency (rad)

The relationship between the photon wavelength (λ) and energy gap (E_g) will be defined as follows:

$$\lambda_c(\mu m) = \frac{1.24(eV\mu m)}{E_g(eV)} \qquad (3\text{-}6)$$

Where λ_c : is the critical wavelength

The absorption edge can be divided into three main regions, as shown in Figure (3.19), which are [119]

(A) High Absorption Region

It is the transition region between the extended levels of the valence and conduction bands, and the value of the absorption coefficient is $\alpha \geq 10^4$ cm^{-1}.

(B) Exponential Region

It is the transition region between the local planes at the edges of the beams and the value of the absorption coefficient ranges in it ($1 < \alpha < 10^4$) cm^{-1}

(C) Weak Absorption Region

This region is attributed to the deep states in the middle of the energy gap caused by impurities and the value of the absorption coefficient is very small $\alpha < 1$ cm^{-1}.

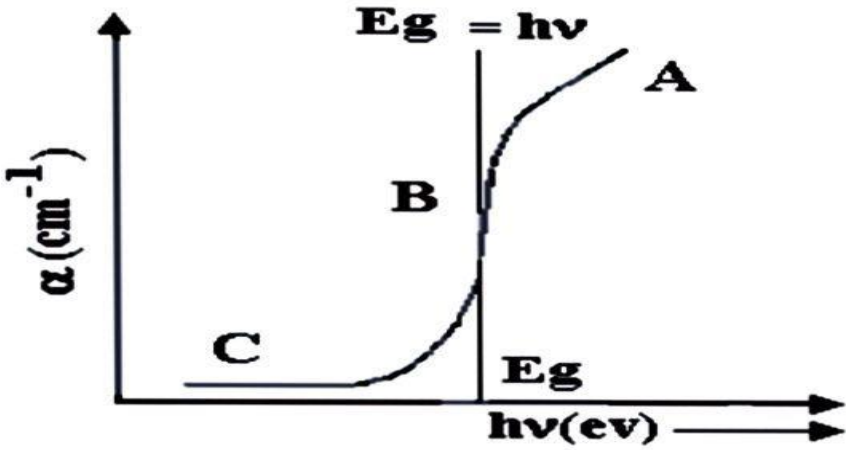

Figure 3.19: shows the main regions of the optical absorption edge.

Direct Transition

When the position of the peak energy of the valence band (Ev) in the wave vector space (K) matches the position of the bottom of the conduction band (Ec), then the semiconductor is said to have a direct gap, which means that a photon with energy (Eg=Ec-Ev), can excite An electron is directly at the top of the completely filled valence band to a vacant quantum state at the bottom of the conduction band through a vertical transition process in the wave space ($\Delta K = 0$) [120]. Conduction can occur without a change in the momentum and energy of the crystal as in the following relationships:

$$E_f = E_i + \hbar\omega \qquad (3\text{-}7)$$

$$\hbar K_f = \hbar K_i + \hbar\bar{q}$$

where:

Ei, the initial energy of the electron in the valence beam, E_f, the final energy of the electron in the conduction beam, the energy of the incident photon (eV),

K_i the initial wave vector of the transmitted electron, the final wave vector of the transmitted electron, the wave vector of the incident photon.

$$\alpha(\hbar\omega) = A'(\hbar\omega - E_g)^r \qquad (3\text{-}8)$$

where :

r: exponential modulus, A': proportionality constant, E_g: energy gap, α: absorption coefficient.

Absorption Coefficient (α)

It is defined as the relative number of photons absorbed per unit distance or propagation through the semiconductor and is given in units (cm^{-1}), and (α) depends on the photon energy (hν) and the energy gap (Eg) [121]. Most of the absorbed photons (63%) occur at a distance (1/α) and this distance is called the penetration depth. When the energy of the incident photon is less than the energy gap, the photon is transmitted and the permeability of the film is given by the following relationship:

$$T_{op} = (1-R)^2 e^{-\alpha t} \qquad (3\text{-}10)$$

T_{op} : Transmission

It is defined as the ratio between the intensity of the transmitted ray to the intensity of the incident ray, and it is written in the following form:

$$T_{op} = \frac{I_t}{I_o} \qquad (3\text{-}11)$$

R : reflectivity

Defined as the ratio between the intensity of the reflected beam to the intensity of the beam falling and write the following formula:

$$R = \frac{I_r}{I_o} \qquad (3\text{-}12)$$

t : thickness of the film

and from the solution of equation:

$$I = I_o \exp(-\alpha t) \qquad (3\text{-}13)$$

get the relationship of Transmission (T_{op}) with Absorbance (A):

$$A = \mathrm{Log}_{10} \frac{1}{T_{op}} \qquad (3\text{-}14)$$

$$T_{op} = e^{-2.303A} \qquad (3\text{-}15)$$

Substituting (T_{op}) from equation (3-8) into equation (3-13), we get:

$$e^{-2.303A} = (1-R)^2 e^{-\alpha t} \qquad (3\text{-}16)$$

$$A = \frac{1}{2.303}[\alpha t - 2\ln(1-R)] \qquad (3\text{-}17)$$

In order to get rid of the limit (1-R), which represents the reflectivity of the film, two films are prepared from the same material. The reflectivity is equal under the same conditions. If the thickness of the first film is (t_1) and its reflectivity is (R_1), its absorbance is:

$$A_1 = 1/2.303[\alpha t_1 - 2\ln(1-R_1)] \qquad (3\text{-}18)$$

For another film, thickness (t_2) and reflectivity (R_2), then:

$$A_2 = 1/2.303[\alpha t_2 - 2\ln(1-R_2)] \qquad (3\text{-}19)$$

By subtracting equation (3-17) from equation (3-16), we get the calculated absorption coefficient from the absorption spectrum.

$$\alpha t = 2.303 A \qquad (3\text{-}20)$$

$$\alpha = 2.303\frac{A}{t} \qquad (3\text{-}21)$$

Extinction Coefficient (k)

Represents the extinction of the electromagnetic wave inside the material, and the Extinction coefficient is defined as the relative loss in energy experienced by the electromagnetic wave when it passes through the material, and it represents the imaginary part of the refractive index. The extinction coefficient is related to the absorption coefficient by the following relationship:

$$k = \frac{\alpha\lambda}{4\pi} \qquad (3\text{-}22)$$

Refractive Index (n)

Is the ratio between the speed of light in free space (c) to speed in the middle (v). The refractive index is given by the following equation:

$$n = \left[\left(\frac{1+R}{1-R}\right)^2 - (k^2+1)\right]^{1/2} - \frac{R+1}{R-1} \qquad (3\text{-}23)$$

$$n = \frac{c}{v} = \sqrt{\varepsilon_\tau} \qquad (3\text{-}24)$$

where ε_τ is the dielectric constant

Dielectric Constan

The process of energy loss in the material occurs due to the interaction between the light and the charges of the medium and the resulting polarization of the charges of that medium. This polarization is usually described by the complex dielectric constant of the medium, which is expressed by the following equation

$$\varepsilon = \varepsilon_1 - i\,\varepsilon_2 \qquad (3\text{-}25)$$

ε: the complex dielectric constant, ε2 , ε1: the real and imaginary portions of the dielectric constant, respectively. The complex dielectric constant is related to the refractive index in its complex form by the following relationship:

$$\varepsilon = N^2 \qquad (3\text{-}26)$$

Since N: is represented by the complex refractive index, which is known by the following formula:

$$N = n - i\,k \qquad (3\text{-}27)$$

n : the real part of the complex refractive index.

From equations (3-23), (3-24), (3-25), we can conclude:

$$(n - k)^2 = \varepsilon_1 - i\,\varepsilon_2 \qquad (3\text{-}28)$$

From equation (3-23), the partial real and imaginary complex dielectric constant can be written in the following form:

$$\varepsilon_1 = n^2 - k^2 \qquad (3\text{-}29)$$

$$\varepsilon_2 = 2\,n\,k \qquad (3\text{-}30)$$

3.4.10 Direct-current Characteristics (DC)

The resistivity measurement is one of the most important analysis used to prove the existence of conductivity of the prepared sample. The closed cycle system used to determine the resistivity of the sample by using four probe technique .The silver paste used during the measurement to connect the sample under the four probe technique. The DC. power supply was used to supply the sample with the constant current and the voltage was measured by a digital nano voltmeter type (Keithely), The electrical resistance of the electrospun films has been measured as a function of temperature in the range (30 -100) ^{o}C. The full setup of this experiment is mentioned in Figure (3.20). Then the resistivity was measured according to the following equation

$$\rho=(R.w.t)/L \qquad (3\text{-}31)$$

and EC determined as:

$$\sigma=1/\rho \qquad (3\text{-}32)$$

Such that:

ρ: film resistivity (Ωcm^{-1}), R: resistance (Ω), σ: electric conductance (S/cm)

t: thickness, w and L: electrodes dimensions

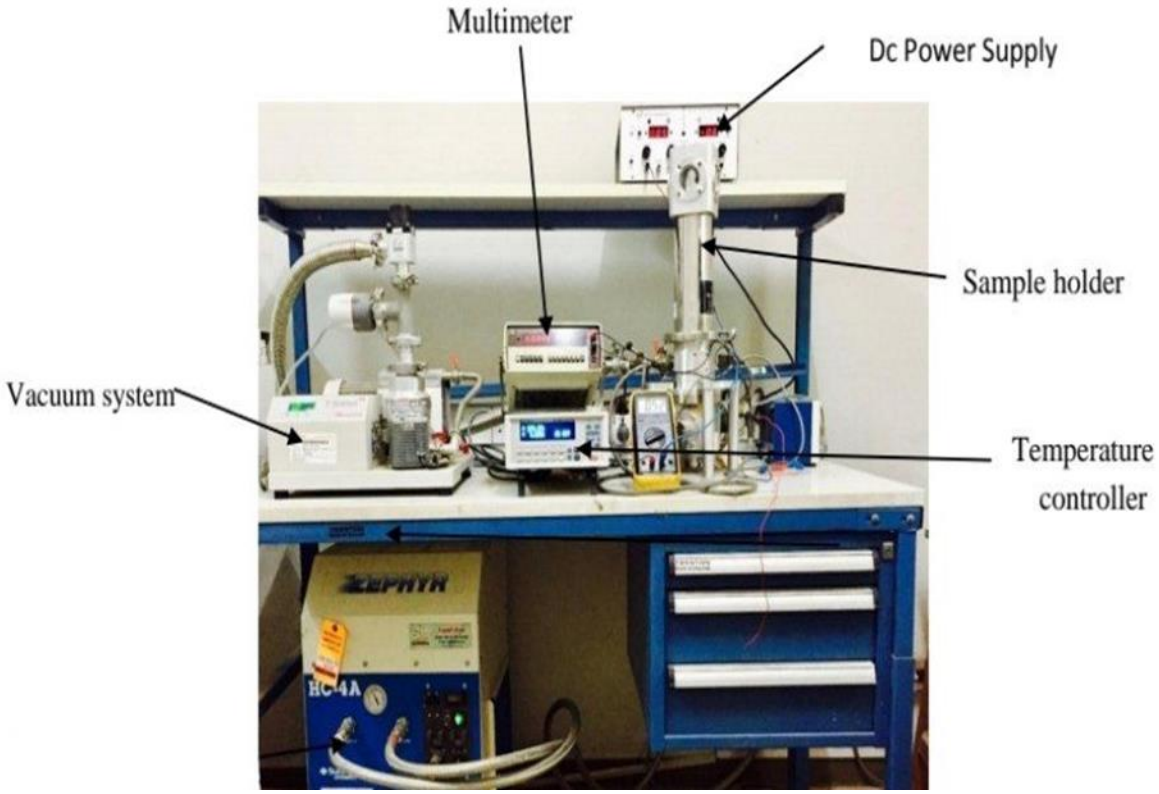

Figure 3.20: The system for resistivity measurement

4.1 Introduction

This chapter illustrates the results obtained through the results of X-ray diffraction, morphology, wettability and tests of the optical and electrical properties of thin films deposited on prepared glass substrates by spin coating method with different concentrations of preparing nano thin films from PEDOT:PSS/Graphene. In addition, the effects of Isopropyl alcohol (IPA) as a surfactant agent was studied in order to improve the conductivity of prepared films. This chapter includes the following axes:

1. Studying the structural properties by XRD, FTIR and DSC techniques
2. Studying the morphological properties by AFM and SEM techniques
3. Studying the optical properties of thin films, which included measuring the transmittance and absorption spectrum as a function of wavelength, calculating the permissible energy gap, as well as knowing the optical constants such as the absorption coefficient and refractive index.
4. Studding the electrical properties by DC.

4.2 Structural Results

4.2.1 XRD results

XRD analysis, by way of the study of the crystal structure, is used to identify the crystalline phases present in a material and thereby reveal chemical composition information.

According to Figure (4.1), the diffraction angle of pure PSS: PEDOT polymer (S_1 sample) is at $2\theta = 24^{o}$ the diffract gram indicates that PSS: PEDOT polymer have semi- amorphous structure due to the absence of sharp peaks. This scattering, which correspond to the (020) crystalline plane of the orthorhombic unit cell of PEDOT crystals [122].

In contrast, all the remaining samples (S_2-S_5) have crystalline structures and their diffraction positions shifted to the $2\theta = 26^{\circ}$. This shifting proves the

dispersion of Graphene sheets within the PSS: PEDOT structure because Graphene scattered the X-ray at 2θ = 26.228 (according to the JCPDS Card No, 75-1621) from its 002 plane within its hexagonal crystalline structure [123]. This shifting action means, that Graphene sheets caused a real change in the lattice parameters of the sample structures.

Also, it is observed that the intensity of diffraction peaks increases with increasing of Graphene concentration. That means, that the extent of crystallinity of the particular plane proportional linearly with the Graphene amounts.

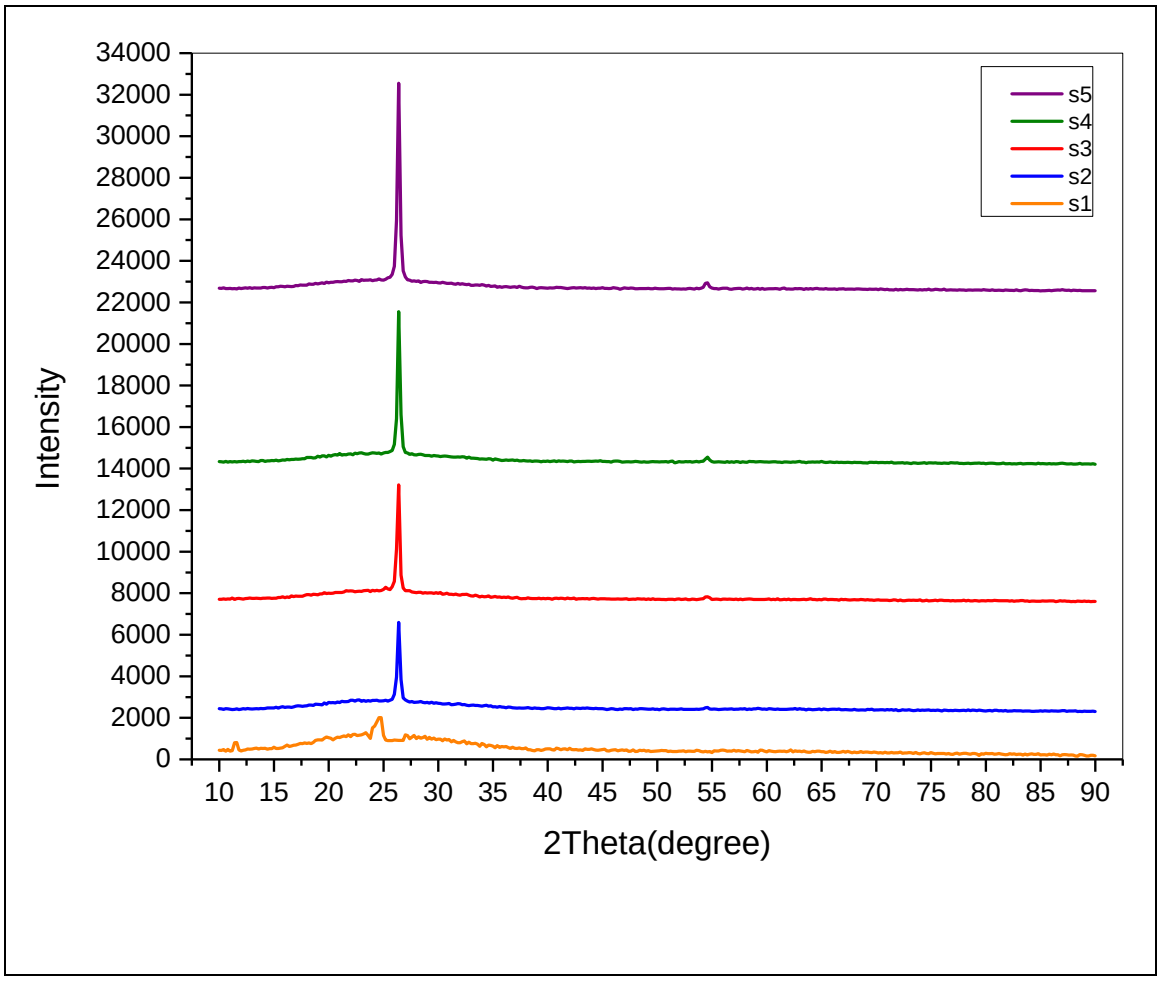

Figure 4.1: X-ray diffraction spectra for pure PEDOT:PSS polymer and the prepared samples

Table 4.1: XRD parameters for samples

Samples	2θ (deg)	d-Spacing (Aº)	β (deg)	Crystallite size (nm)	Scattering Function (s)
S_1	24.5346	3.62541	14	0.101	0.27583
S_2	26.4208	3.36933	1	1.4236	0.29667
S_3	26.4318	3.37071	0.7	2.0338	0.29679
S_4	26.4859	3.37509	0.6	2.3726	0.29849
S_5	26.6517	3.66845	0.5	2.8487	0.29921

From table 1, the d-spacing parameter calculated from (Bragg's Law (3-2)) experienced some ups and downs, which gives an indicator about the dispersion of Graphene sheets within the polymeric structure.

A great improvement occurred in the crystallite size (calculated from Scherer's equation (3-3)) with the Graphene addition, where this size increased from 0.101 to 2.8487 nm. This gives another indicator about the slight exfoliation of Graphene sheets, and these sheets are agglomerated due to slight penetration of fluid and polymeric chains among these sheets. Similar findings obtained from the decreasing in the β parameter, which is the line broadening at half the maximum intensity (FWHM). As β decreased, as the crystalline degree increased.

Slight increment; 8.5% occurred in the scattering function; s (s = 2 sin ɵ /λ), which, indeed proportional to the increment in the solid portion in the film components due the addition of solid Graphene sheets.The increments of each of the L, β and s coincide with the increment of the crystalline peak intensities with the Graphene additions.

4.2.2 FTIR results

The characteristic peaks of both the PSS:PEDOT polymer and the Graphene sheets were investigated by FTIR results. Band at 1620 cm^{-1} refers to the stretching vibration mode C=C for conjugated alkene structure within the PSS:PDOT polymer. Weak band around 1980 cm^{-1} indicates the C-H bending mode in the aromatic compounds. Strong band around 3300 cm^{-1} is due to the O-H stretching mode. Band ar ound 880 cm^{-1} represents the C=C bending mode, while band around 3000 cm^{-1} represents the C-H stretching mode [124].

FTIR results (Figure 4.2), also show that there is no chemical reaction between Graphene and the polymer. There is only hydrogen bonding between water (already present in the polymer), Graphene and PSS:PEDOT polymer. The weak band at 1380 cm^{-1} belongs to the C – O…H bond, which formed due to the interaction between surface of grapheme sheet and the carboxyl group (OH^-) in water. These interactions enhances the dispersion and the stability and the dispersion of Graphene sheets within the PEDOT: PSS solution.

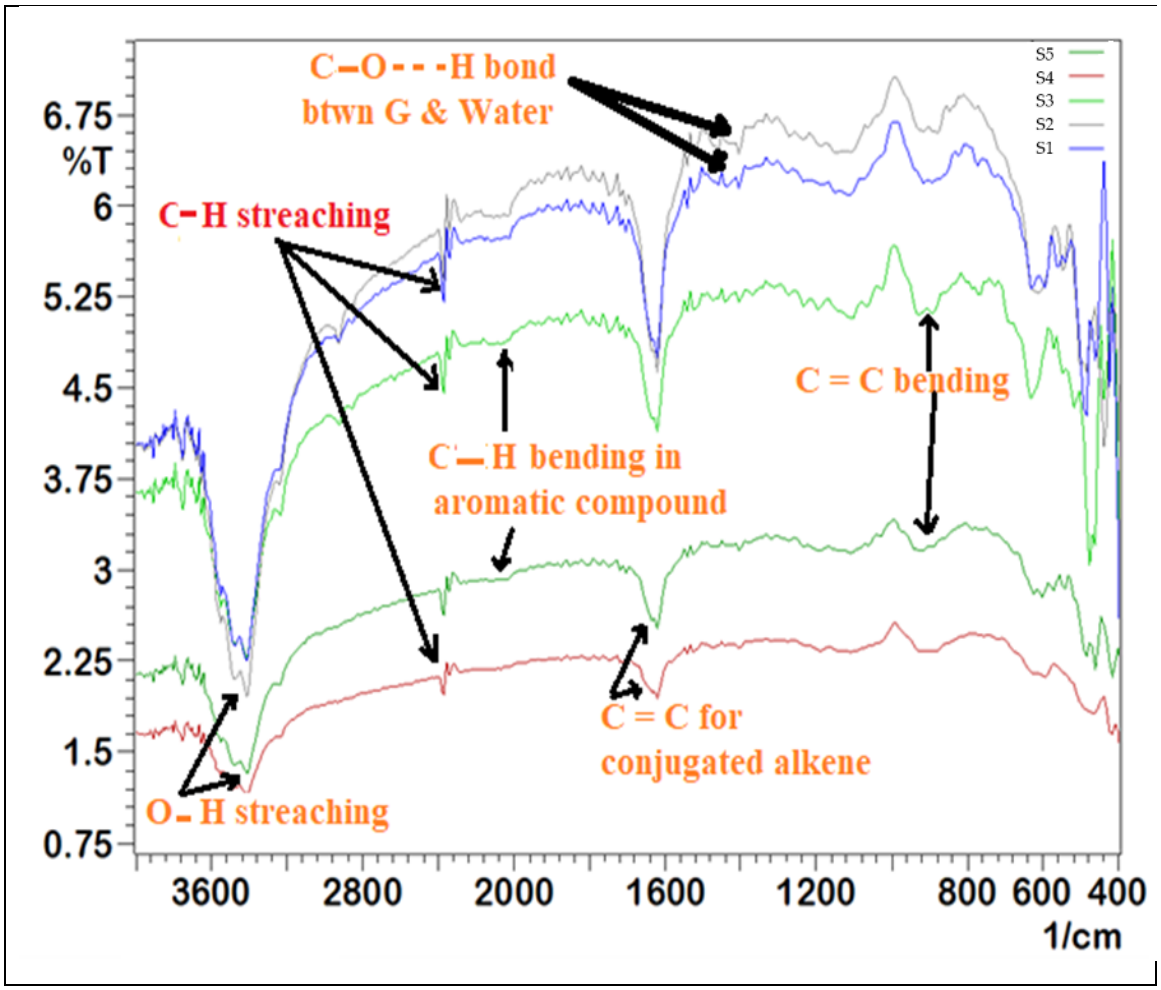

Figure 4.2: FTIR spectra of PEDOT:PSS and its composites with Graphene

4.2.2.1 Proposed interaction model

The proposed mechanism of the interaction among components of the prepared samples, takes place according to the following steps:

1- Hydrogen bonding between water molecule and PEDOT:PSS polymer because this polymer is already contains 30% water molecules within its structure.

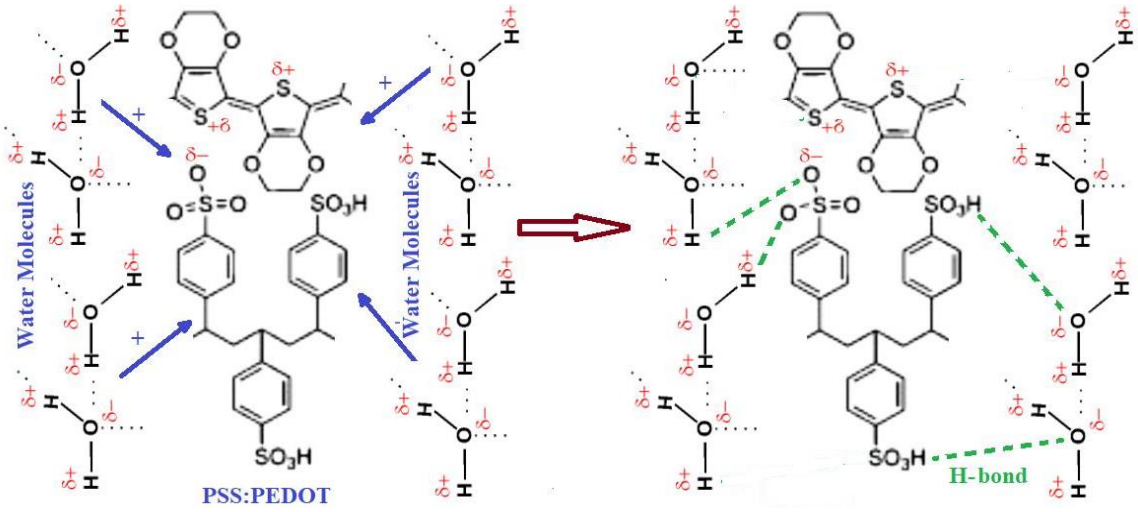

2- The Graphene sheet is indeed contains small amounts of oxygen (about 1%). These oxygen sites are capable to form hydrogen bonds between Graphene sheet and the water molecules, which is available within the polymer structure.

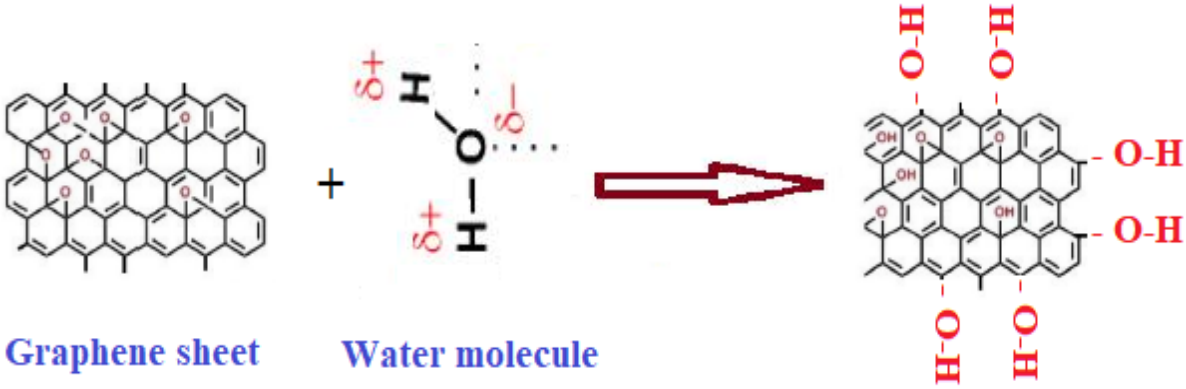

3- Carbon atoms at the edges of the Graphene sheet are unsaturated, therefore, these sites are active and can react with the water molecules creating hydroxyl groups (OH^-) on the sheet surface. These hydroxyl groups can create hydrogen bonds with SO_3^- groups within the PEDOT:PSS polymer.

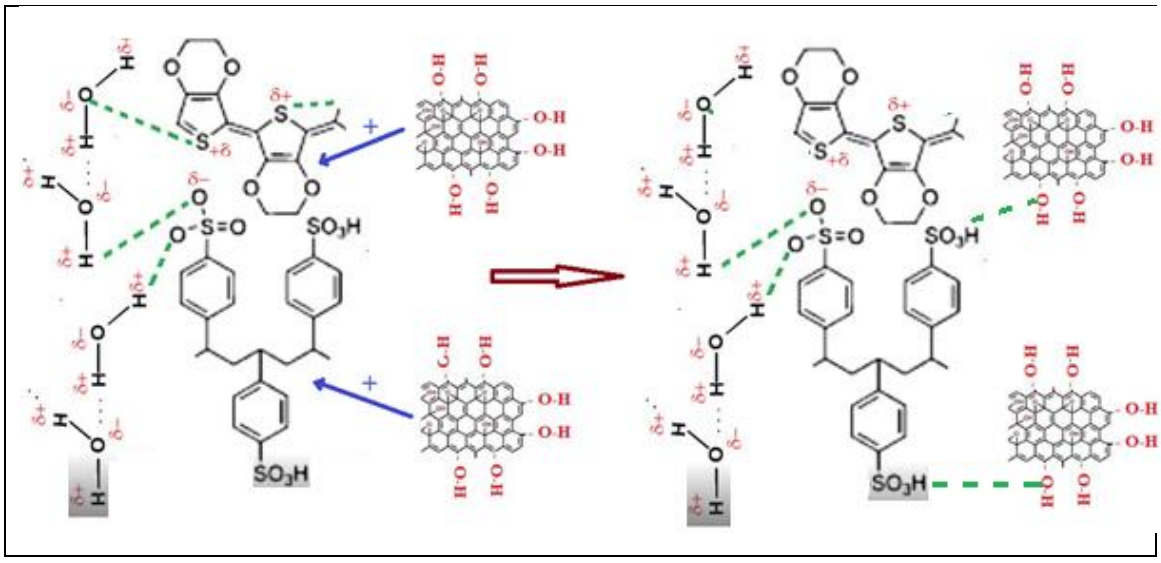

Figure 4.3: Proposed interaction model due to the nano graphene addition to the PEDOT:PSS

Figure (4.4) shows the FTIR spectra of the prepared samples containing different amounts of isopropyl alcohol (IPA). The addition of IPA is adopted in order to enhance the dispersion level of Graphene sheet. FTIR results, shows no new peek compared with the FTIR spectrum of Graphene PEDOT:PSS. This is because of the structures similarity, where IPA contain from carbon, oxygen and hydrogen atoms only and the bonds arises among these three atoms are already exist among polymer atoms. The intensity of the hydroxyl group (OH^-) at 3200-3600 cm-1 increased due to the presence of this group in the IPA structure.

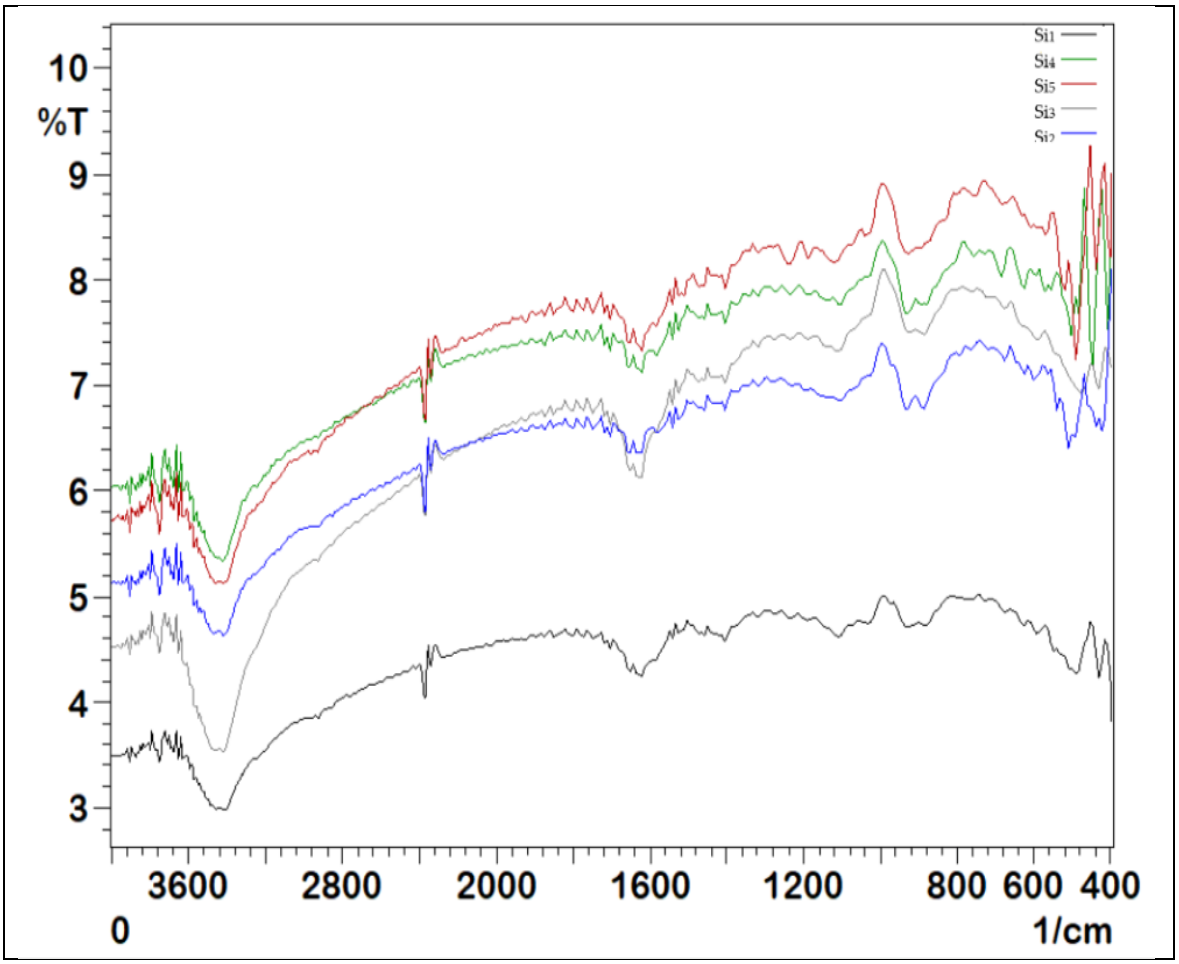

Figure 4.4: FTIR spectra of PEDOT:PSS and its composites with Graphene and IPA

4.2.3 DSC results

Figure (4.5) shows the DCS analysis of pure PEDOT:PSS and (PEDOT:PSS/Graphene) mixtures.

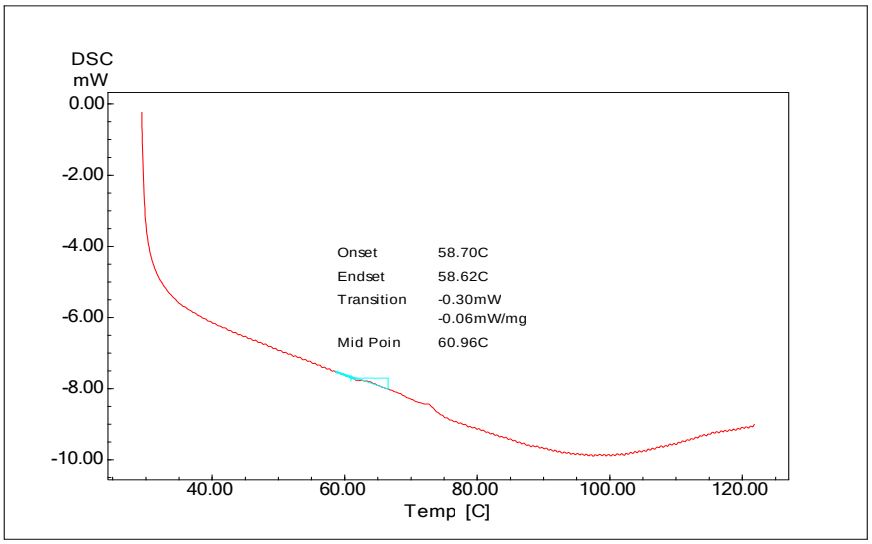
DSC
mW
0.00
-2.00
-4.00
-6.00
-8.00
-10.00
Onset 58.70C
Endset 58.62C
Transition -0.30mW
-0.06mW/mg
Mid Poin 60.96C
40.00
60.00
80.00
100.00
120.00
Temp [C]

S1

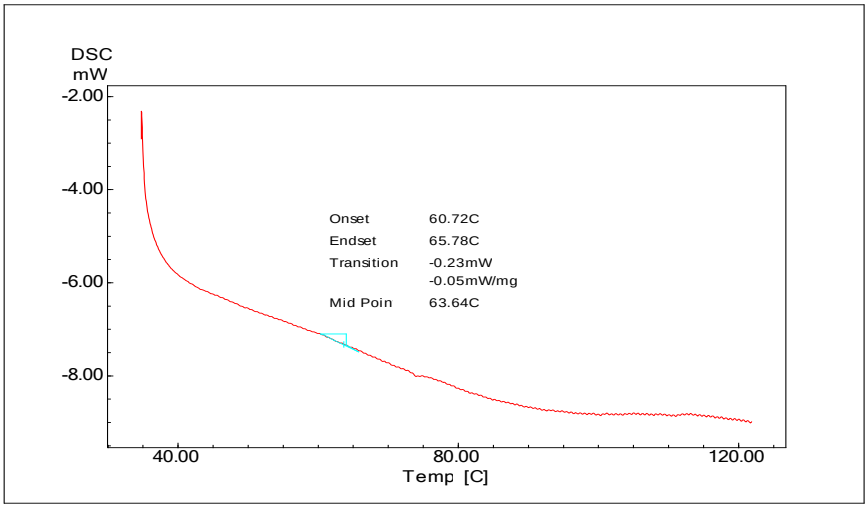
DSC
mW
-2.00
-4.00
-6.00
-8.00
Onset 60.72C
Endset 65.78C
Transition -0.23mW
-0.05mW/mg
Mid Poin 63.64C
40.00
80.00
120.00
Temp [C]

S2

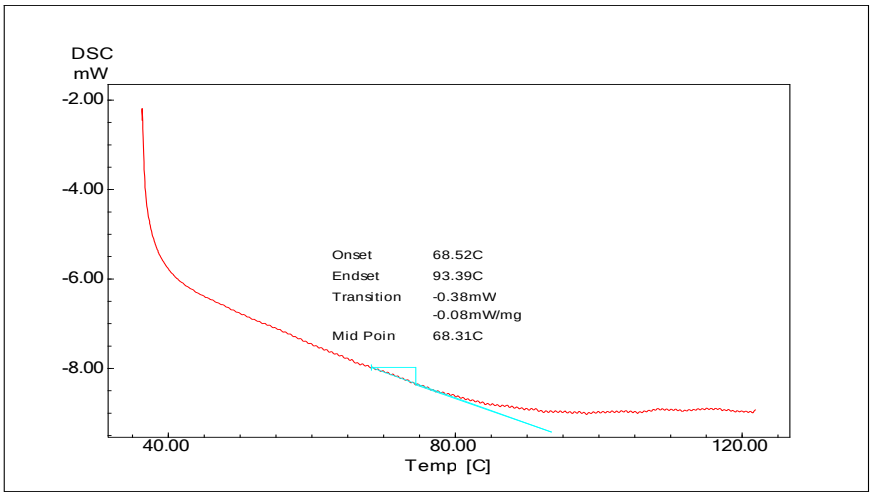
DSC
mW
-2.00
-4.00
-6.00
-8.00
Onset 68.52C
Endset 93.39C
Transition -0.38mW
-0.08mW/mg
Mid Poin 68.31C
40.00
80.00
120.00
Temp [C]

S3

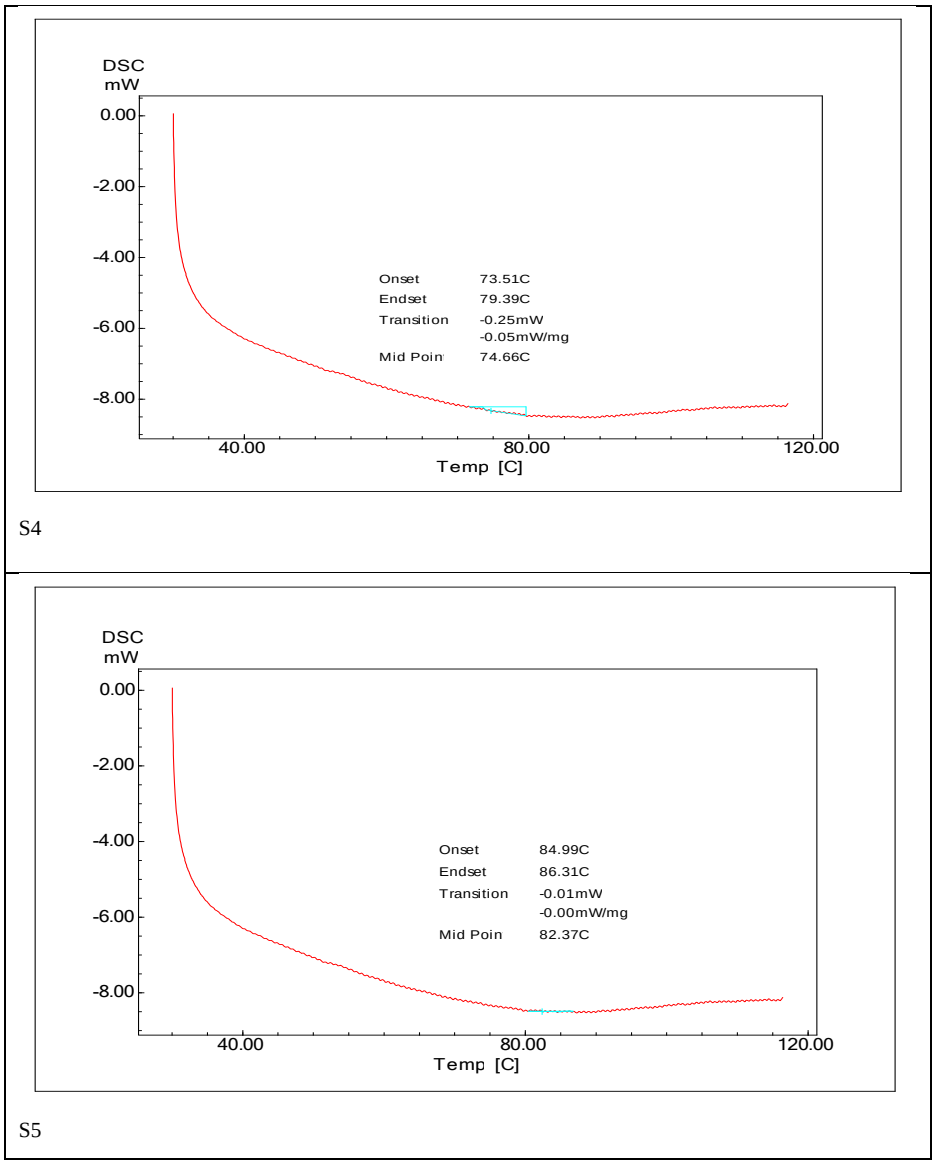

Figure 4.5: DSC results of PEDOT:PSS and its composites with Graphene.

It is clear from Figures (4.5), that T_g values increased linearly from 60.69^{o}C (for pure polymer [125]) up to 82.37 ^{o}C (for sample with 2 wt% Graphene); 35%. This is because that Graphene is a solid material and has compact structure compared with the semi-crystalline structure of PEDOT:PSS. This increment in T_g give an indicator about the improvement of the mechanical properties of the prepared samples as well as the thermal stability. When Graphene amounts increased within the composite structure, the steric hindrance increased, so the polymeric chain restricted and can not be sliding above each others, which leads to increase both of T_g and T_m.

The addition of IPA to the Graphene: PEDOT:PSS solution increased the Tg from 58.54^{o}C to 76.62 ^{o}C (Figure 4.6). This is due to the increment in the polarity with IPA addition which increased the hydrogen bonding among the polymeric samples. These extra bonding, prevent the polymeric chains movements.

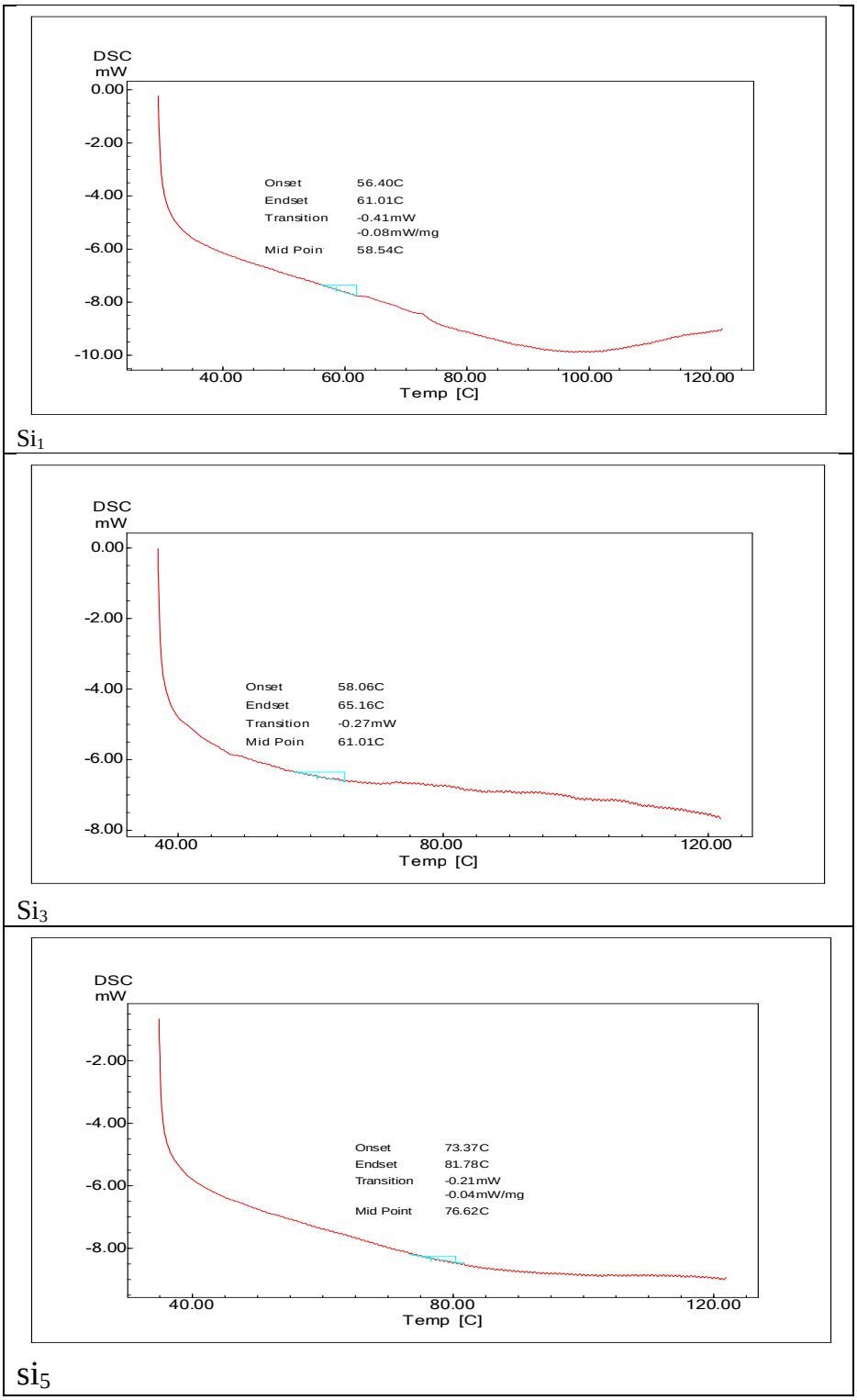

Figure 4.6: DSC results of PEDOT:PSS and its composites with Graphene and IPA.

4.2.4 Zeta potential

Figure 4.7 shows the zeta potential test for the PEDOT:PSS containing 1.5wt% G. The value of current sample is -48.04 mV; which means that, the sample with good stability according to the Table 3.4. This value indicates, that the degree of electrostatic repulsion between adjacent particles are so high that there is a high dispersion level of Graphene particles within the film components and the repulsion is high enough to prevent rapid coagulation and to resist the aggregation. This dispersion level points to that, the repulsion forces exceed the attractive forces among the Graphene particles, which leads finally to resist the coagulation and aggregation tendencies.

The mobility of this sample; -2.27 (μ/s)/(V/cm), give another indicator about the good dispersion of the Graphene component in the sample.

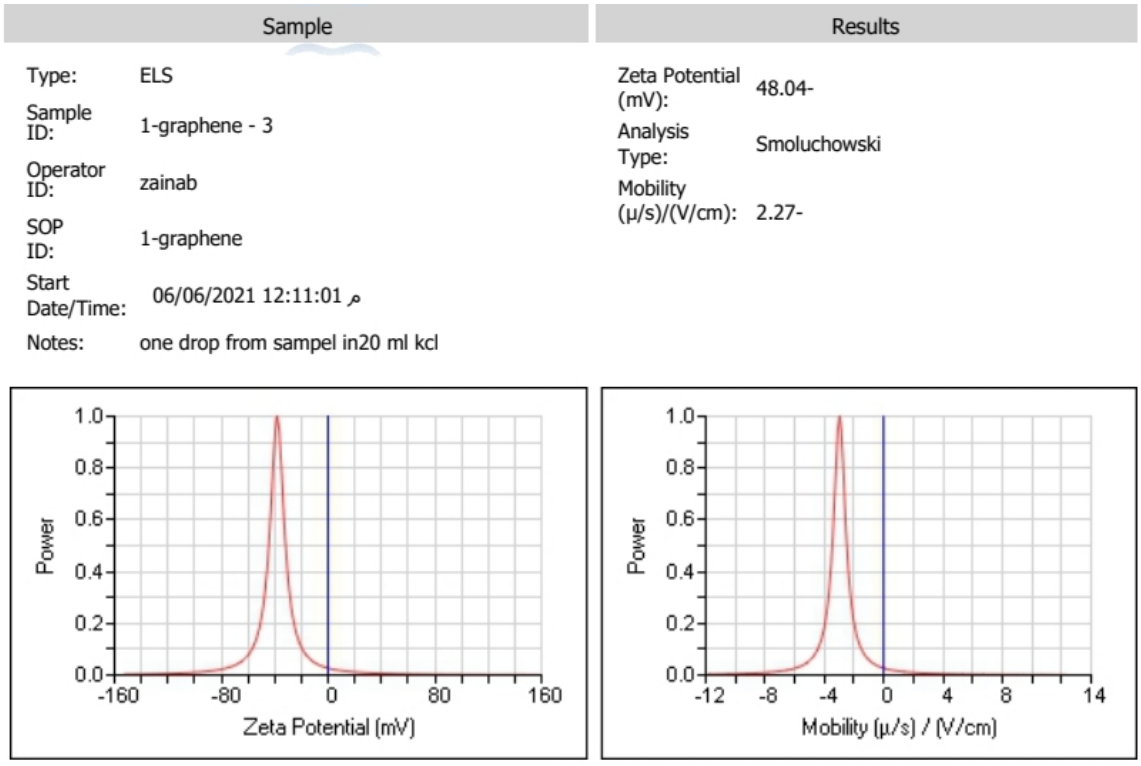

Figure 4.7: a- Zeta potential b- mobility of PEDOT:PSS containing 1.5wt% Graphene

The new value of zeta potential ; -168.38 mV as shown in Figure (4.8) proved that the IPA addition enhances the electrostatic repulsion force among the Graphene sheets, preventing them from settling and aggregation. This leads finally to obtain an excellent stability according to Table 3.4. The addition of IPA increased the polarity of the solution due to the extra dipole moment entered to this solution. This new dipole moment belongs to the IPA component, which is 1.66 D, where PEDOT:PSS solution contains already 30% water with 1.85 D as a dipole moment. The increment of solution polarity (due to IPA addition) increased the zeta potential from -48.04 to -168.38 mV for the same sample; which contains 1.5 wt% Graphene. As well as the mobility altered from -2.27 to -1.6 (μ/s)/(V/cm).

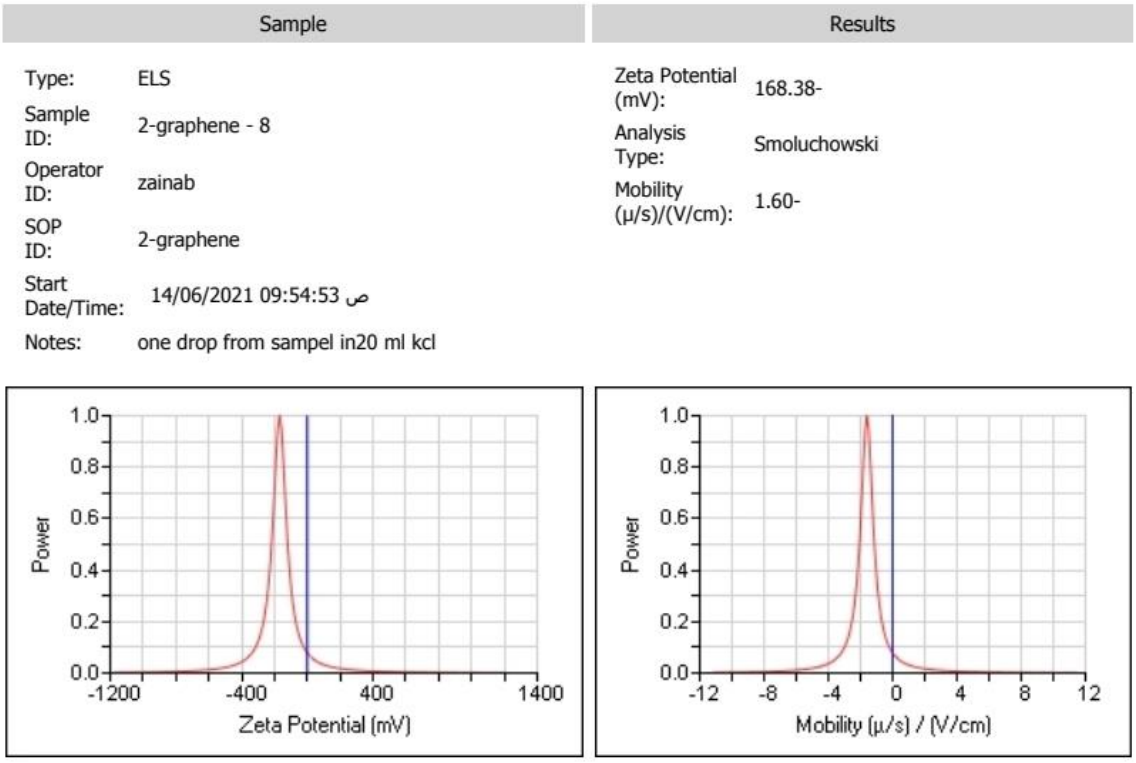

Figure 4.8: a- Zeta potential b- mobility of PEDOT:PSS/IPA containing 1.5wt% Graphene

4.3 morphological result for PEDOT:PSS/Graphene

4.3.1 AFM results

4.3.1.1 PEDOT:PSS/Graphene for glass substrate

To get further information for the effect of graphene on the morphology, 3D AFM images were taken and are presented in Figure (4.9). Also, table 4.2 shows the roughness parameters, which extracted from the 2D AFM images. Image of the pure polymer, shows that, PEDOT:PSS film is smooth with an roughness average (S_a) of 1.05 nm, and when Graphene was added, the surface topography changed and S_a increased to 1.43nm, 1.83nm, 2.27 nm and 2.74 nm for 0.5, 1, 1.5 and 2 wt% Graphene additions respectively. That means that the final roughness increment is 91.6%. Similar increment (but with less extent) in the density of summits (S_{ds}), where this roughness parameter increase by 45% with Graphene addition. This is due to the settling of some of Graphene sheets on the film surface during its formation process.

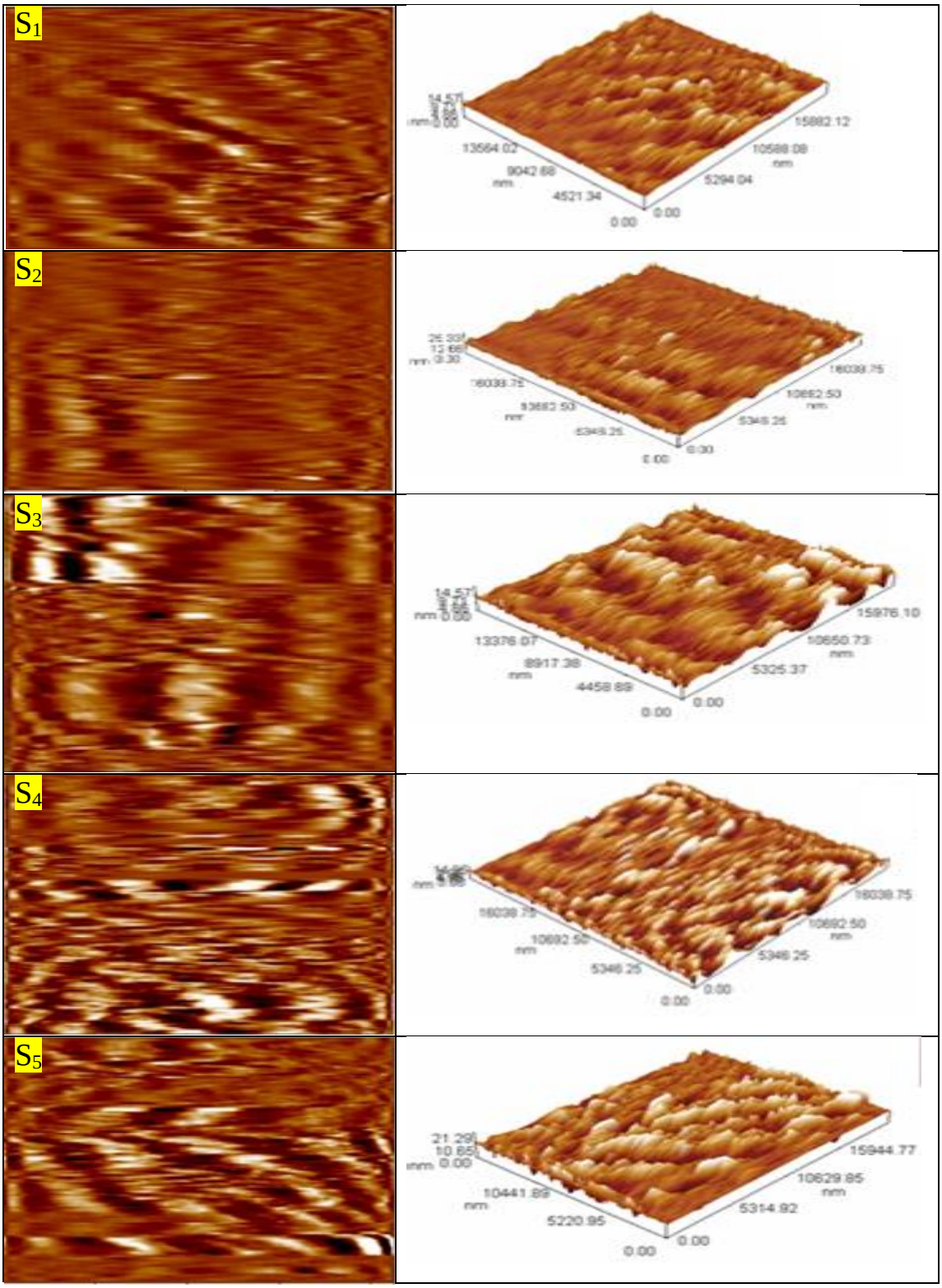

Figure 4.9: AFM images of the PEDOT:PSS/Graphene films

Table 4.2: AFM parameters of PEDOT:PSS/Graphene

Samples	S_a (nm)	S_{ds}	S_{bi}	S_{ci}
S_1	1.05	0.165	0.216	1.52
S_2	1.43	0.169	0.298	1.53
S_3	1.83	0.199	0.754	1.59
S_4	2.27	0.217	0.864	1.62
S_5	2.74	0.239	1.35	1.63

The surface bearing index (S_{bi}) increased from 0.216 (for pure polymer) to 1.35 at the final Graphene addition; increased by 525%. Thus, the durability and the mechanical strength of the prepared films improved clearly and significantly**,** because the S_{bi} parameter is a function of the mechanical properties. This is because, that the mechanical properties of Graphene sheets is higher than the liquid polymer.

The core fluid retention index (S_{ci}) increased only by 7.23% (from 1.52 to 1.63), which means there is a slight increment in the fluid absorption capacity with Graphene addition. That means, that the exfoliation gap between the Graphene sheet is so small, that a small voids created among these sheets. These spaces are barely sufficient to accommodate only the PSS:PEDOT polymeric chains and do not allow high amount of fluid to penetrate the composite structure.

Figure (4.10). Also, table 4.3 shows the roughness parameters, shows PEDOT:PSS with IPA film is smooth with an roughness average (Sa) of 1.19 nm, and when Graphene concentration was increase, the surface topography changed and Sa increased to 3.2nm, and this applies to S_{ds} and S_{bi} also. Compered to films without IPA, there is a slight increase in roughness and other parameters.

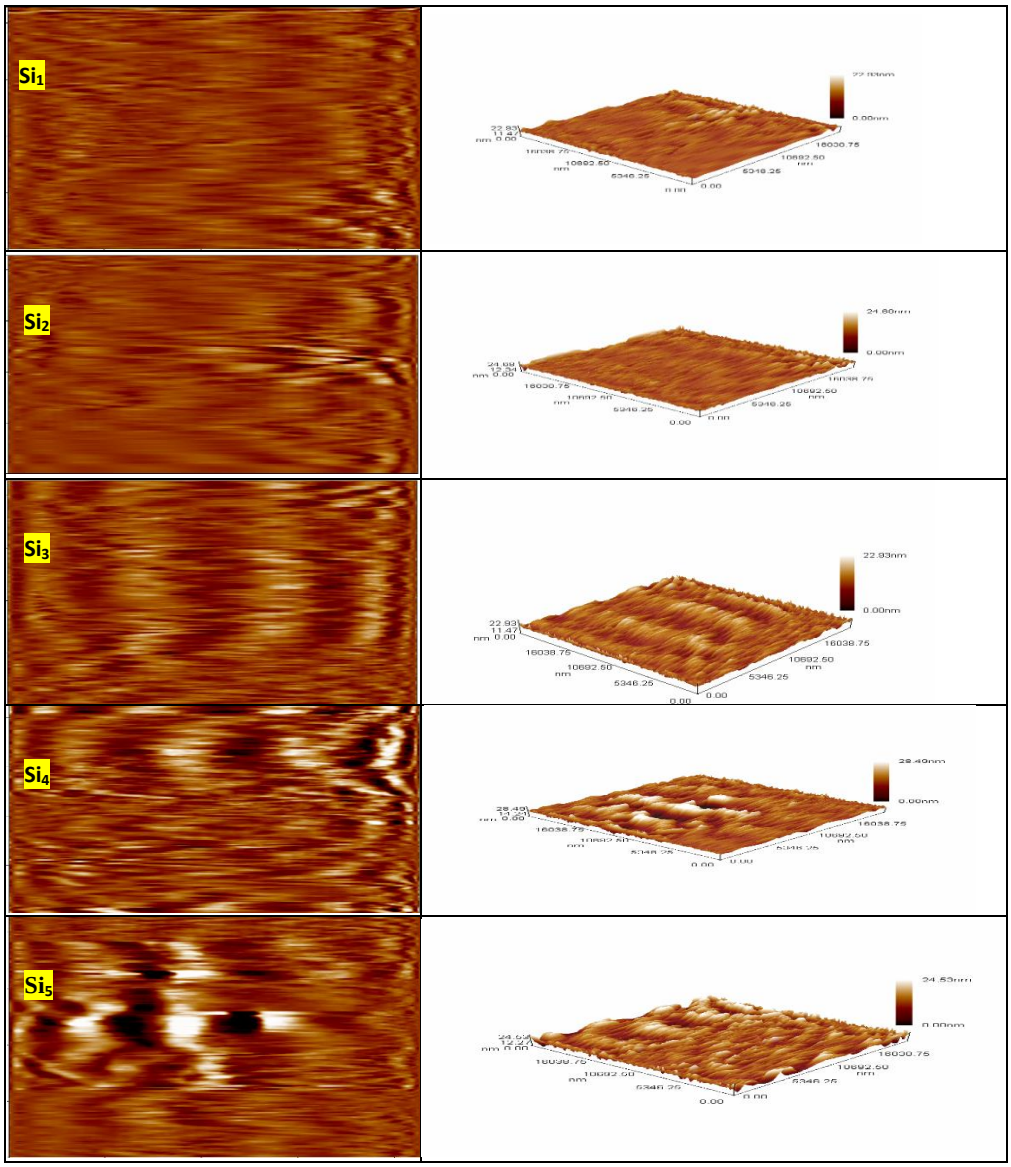

Figure 4.10: AFM images of the PEDOT:PSS/Graphene and IPA films

Table 4.3: AFM parameters of PEDOT:PSS/Graphene and IPA

Samples	S_a (nm)	S_{ds}	S_{bi}	S_{ci}
S_1	1.19	0.16	0.19	1.45
S_2	1.29	0.269	0.227	1.46
S_3	1.97	0.226	0.388	1.53
S_4	3.08	0.254	0.704	1.57
S_5	3.2	0.268	1.773	1.61

4.3.2 SEM Results

Figure (4.11) shows the SEM images of the prepared nanocomposite films at 5.00 kx magnification power. This high magnification power allows only to mointer small regions in the samples, not the full network film structures. The white color refers the summits, while the black color points to the bottom of the surface. SEM images showed that, the PEDOT:PSS films without Graphene has a comparatively smoother surface than the PEDOT:PSS with Graphene. These results matched with the previous AFM results. The PEDOT:PSS forms a core-shell structure resulting in PEDOT being surrounded by PSS [126]. The conformation of PEDOT:PSS will be changed from a coiled to a linear/extended-coil structure owing to the Graphene addition. Images, also shows the good desperation of Graphene particles within the PEDOT: PSS structure.

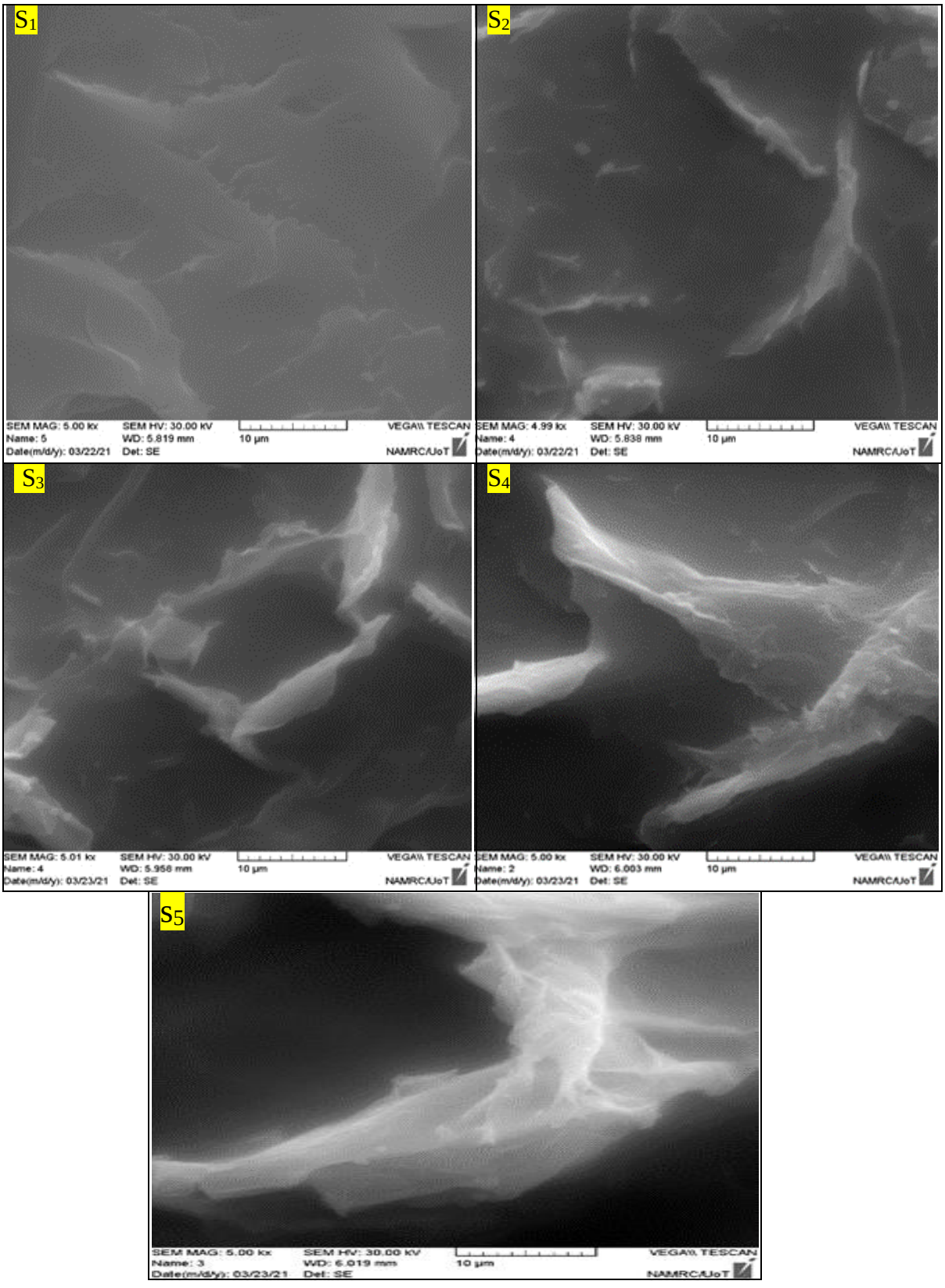

Figure 4.11: SEM images of S_1, S_2, S_3, S_4 and S_5 samples

4.3.3 Surface wettability for PEDOT:PSS/Graphene

The wettability of the prepared films was evaluated by contact angle measurement using circle fitting mode. This test carried out with water (25ºC), where the contact angle measured after 1 and 240 second as shown in Figure (4.12). Results showed that for all sample, the contact angle with pure PEDOT:PSS (S_1) shows a good absoring of water; thus increasing the surface wettability.

With graphene, the prepared surfaces tend to be more crystalline (as shown in XRD results). This high crysttilinty decreased the voids amoung the polymeric chains, which restricts the pentration of water molecules within polymeric surfaces. For pure PEDOT:PSS , the effect of wetting time is to decrease the contact angle with fluid, where the contact angle decreased for pure polymer from 74.645º to 18.59º at 240s.

From these figure, it is clear that the contact angles for pure PEDOT:PSS are lower at the beginning than for Graphene nanocomposites. This means that the surface of the pure PEDOT:PSS has higher wettability than the PEDOT:PSS and Graphene . The nanoparticles addition causes a decrease in surface wettability by forming nanoroughnesses on the surface of films with hydrophobic properties. Decreasing in wettiblity of nanocomposites indicates an increased hydrophobicity of it.

Time	1 second	240 second
S_1	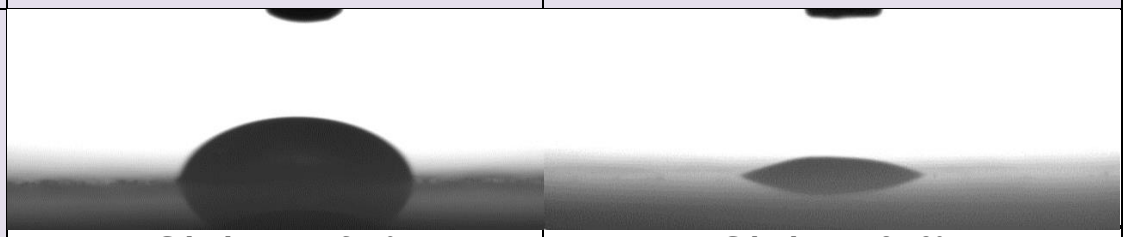 CA_AV = 74.645º	CA_AV = 18.59º
S_2	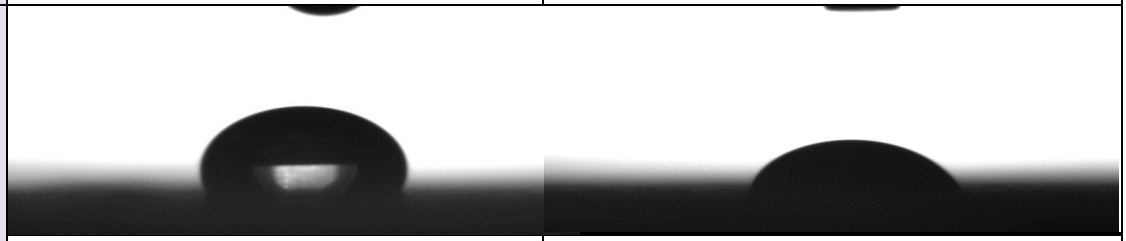 CA_AV =81.704 º	CA_AV = 59.044º
S_3	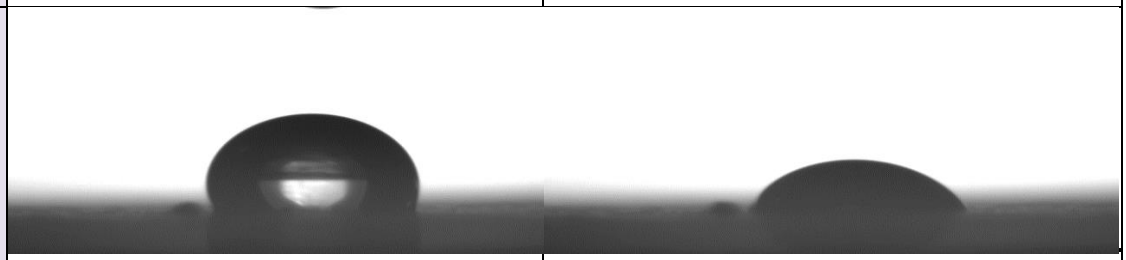 CA_AV =88.168 º	CA_AV =72.236 º
S_4	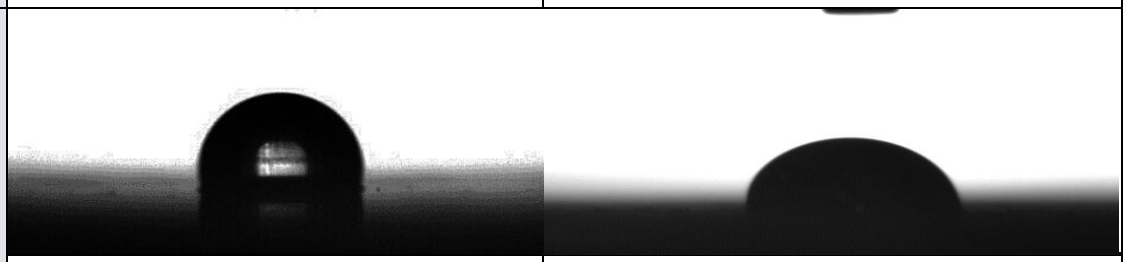 CA_AV = 93.616º	CA_AV =77.970º
S_5	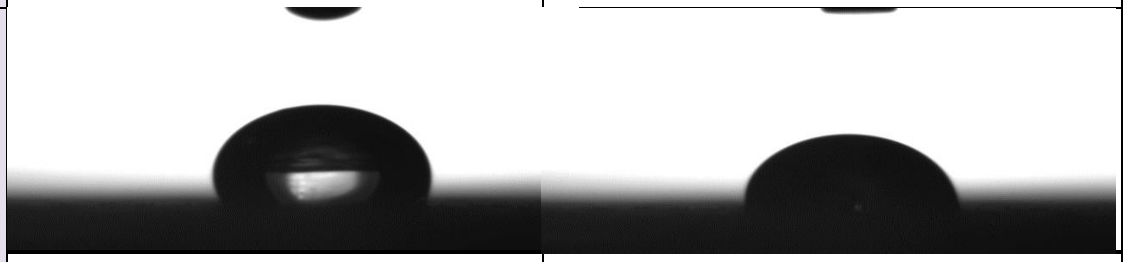 CA_AV =136.624 º	CA_AV = 89.039º

Figure 4.12: Contact angles for samples (PEDOT:PSS and Graphene) at different times.

4.4 UV- VIS Spectroscopy results

4.4.1 Absorption

Figure (4.13) shows the absorption of the prepared samples at UV, VIS and IR regions of the electromagnetic spectrum.

At UV region, the absorbency increased as the Graphene content increased, which means that Graphene addition caused changes in the electronic energy levels within the polymeric composite structure. These changes allows to the structures to absorb the harmful UV radiation and dissipated it as slight, harmless heat. This is a good benefit, which emphasizes that the composite films have the ability to avoid the UV-degradation risks and remains in service for longer periods.

Same behavior occurs in the visible region (400-800 nm), where the absorbance increased linearly with the Graphene content, but with less intensities. This is because, that the radiations in the VIS region are with low energies and longer wavelengths. Also, it is clear that the absorbance along the VIS region is quite steady, which means that the prepared films absorbs all colors within this region by the same rate.

In IR region, also, Graphene addition and IPA increased the absorbency, which allowed to the chemical functional groups to be detected. This means that, Graphene resulted in changed of both vibrational and rotational movements of the molecules within the composite structures.

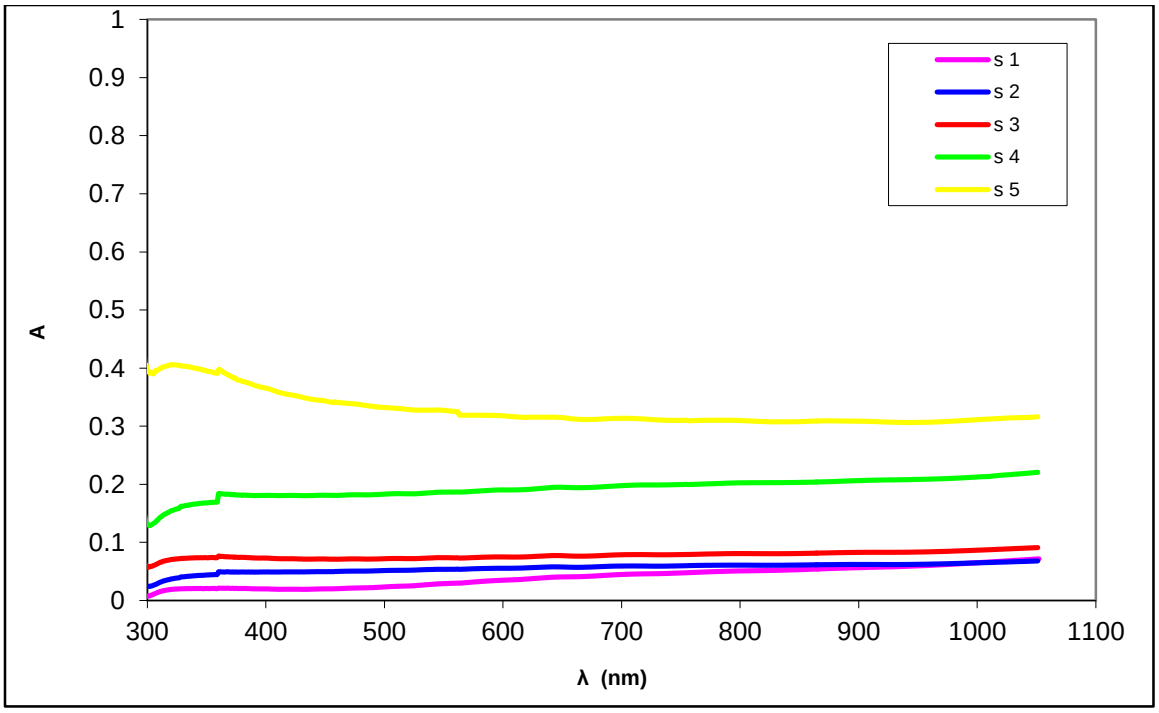

Figure 4.13: UV-absorbance of S_1,S_2,S_3,S_4 and S_5 samples

Also, with the addition of IPA, an increase in absorption is observed with an increase in graphene concentrations

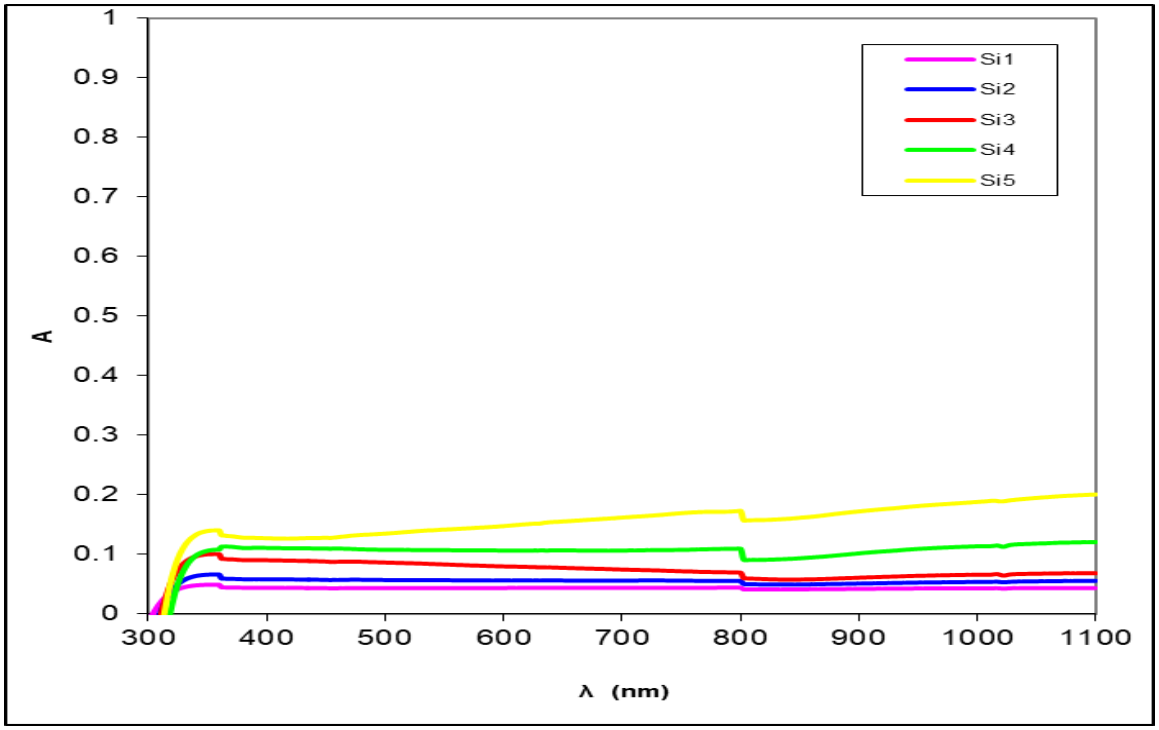

Figure 4.14: UV-absorbance of Si_1,Si_2,Si_3,Si_4 and Si_5 samples

4.4.2 Energy gap

The optical energy gap is defined as the lowest energy required to transfer an electron from the top of the valence band to the bottom of the conduction band. The energy gap is one of the most important constants in semiconductor physics, as the use of semiconducting materials in optical applications such as solar cells, photovoltaic cells, sensors, detectors, photodiodes and coating solar collectors depends on determining this constant. Electromagnetic and as needed to control and control how much photons are absorbed, transmitted, or reflected from the photons falling on the membrane[180].

The PEDOT:PSS films are semiconductors with a direct energy gap of about 2.8. The value of the optical energy gap for permissible direct transitions was calculated through equation (3-8), and the absorption coefficient (α) is related to the energy of the incident photon through the same relationship, so it is drawn The relationship between 2(υhα) and photon energy (υh), then we extend a part of the straight line from the curve to intersect the photon energy axis at (0 = 2(υhα)),

The value of the energy gap for the allowed direct transitions Through Figure (4.15), notice when increase in the percentage of Graphene, the energy gap decreased (S_1, S_2, S_3, S_4, S_5), respectively, as a result of the generated of nanoscale energy levels of graphene inside the energy gap, and the width of these levels increases with the increase in the percentage of Graphene, which leads to a decrease In the width of the gap, we also notice a decrease in the value of the energy gap when increasing the value of the Graphene, as shown in Figure, and this decrease is due to the change in the crystalline structure of the films in terms of increased crystallization as well as a noticeable increase

in roughness and grain size, and this is consistent with the results XRD,AFM and SEM.

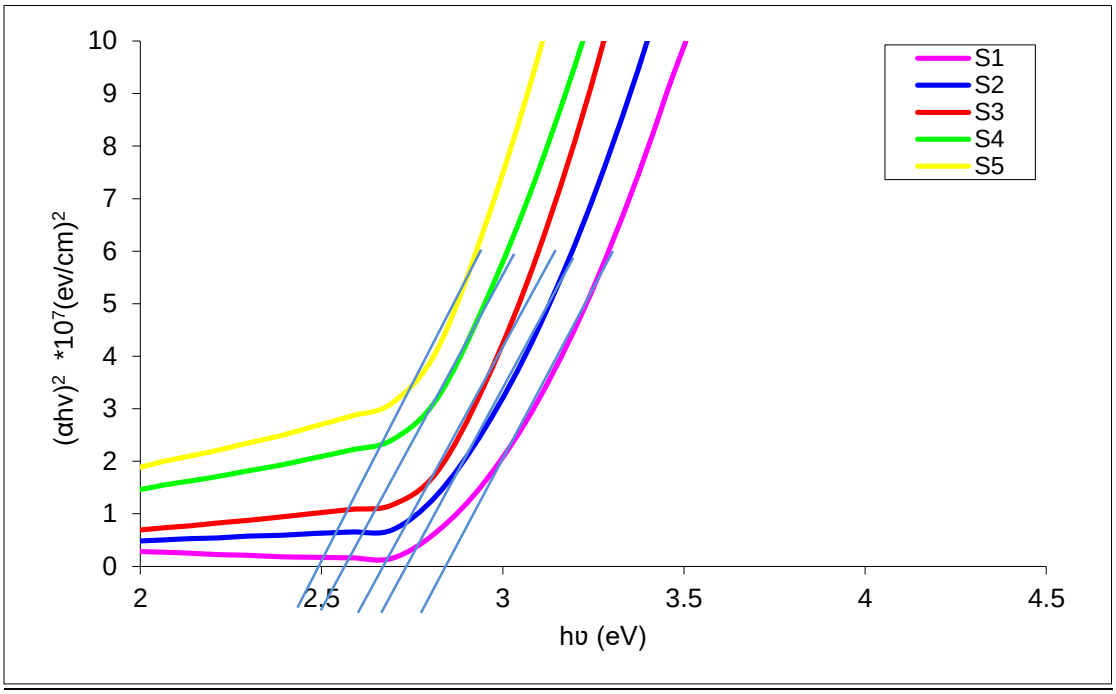

Figure 4.15: energy gap of S_1,S_2,S_3,S_4 and S_5 samples

Figure (4.16) it is noticed from the energy gap behavior that samples with different grafting rates lead to a decrease in the energy gap as a result of the generation of secondary levels within the energy gap between the highest edge of the valence band and the lowest edge of the conduction band and this behavior did not change from what it was without the presence of the IPA but the addition of the IPA, It led to a decrease in the value of the energy gap as a result of obtaining homogeneity and high geometric arrangement between the polymer and graphene, and this is evident from the Zeta potential and AFM tests.

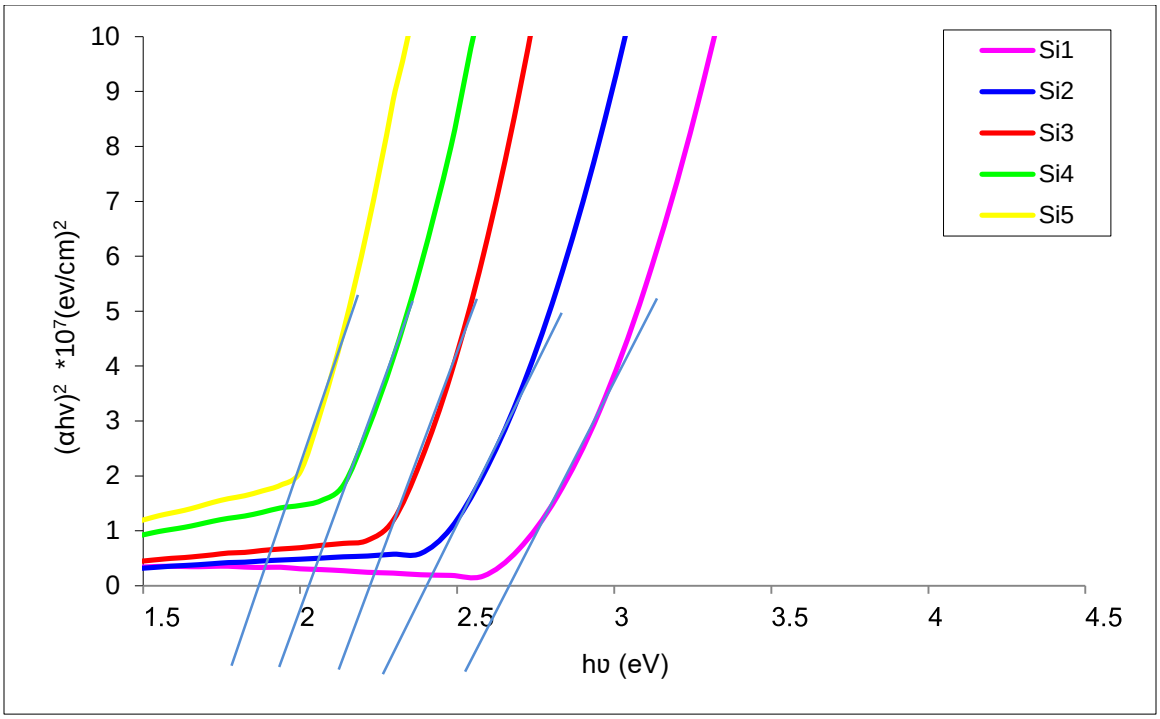

Figure 4.16: energy gap of Si_1,Si_2,Si_3,Si_4 and Si_5 samples

4.4.4 Extinction coefficient

The extinction coefficient represents the amount of energy absorbed in the thin film. It also represents the imaginary part of the complex refractive index. The extinction coefficient was calculated from the relationship (3-22) and the extinction coefficient is related to the absorption coefficient as shown in the previous relationship.

Figures (4.17) and (4.18) shows the change of the extinction coefficient as a function of the photon energy of the processed films, whereby the increase in the Graphene ratio increases the extinction coefficient. There is a gradual increase in the values of the extinction coefficient at photon energies higher than the absorption edge. This increase indicates the occurrence of electronic transitions between the valence and conduction bands, which led to an increase in the absorption coefficient and then an increase in the extinction coefficient

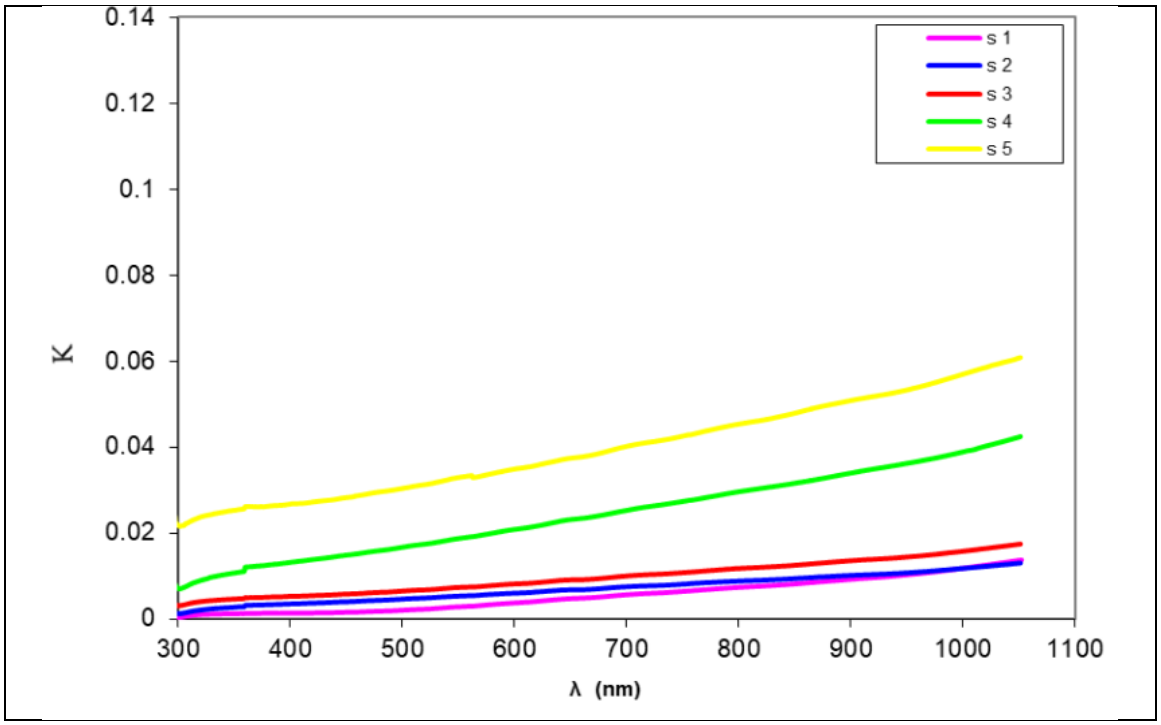

Figure 4.17: Extinction coefficient of S_1,S_2,S_3,S_4 and S_5 samples

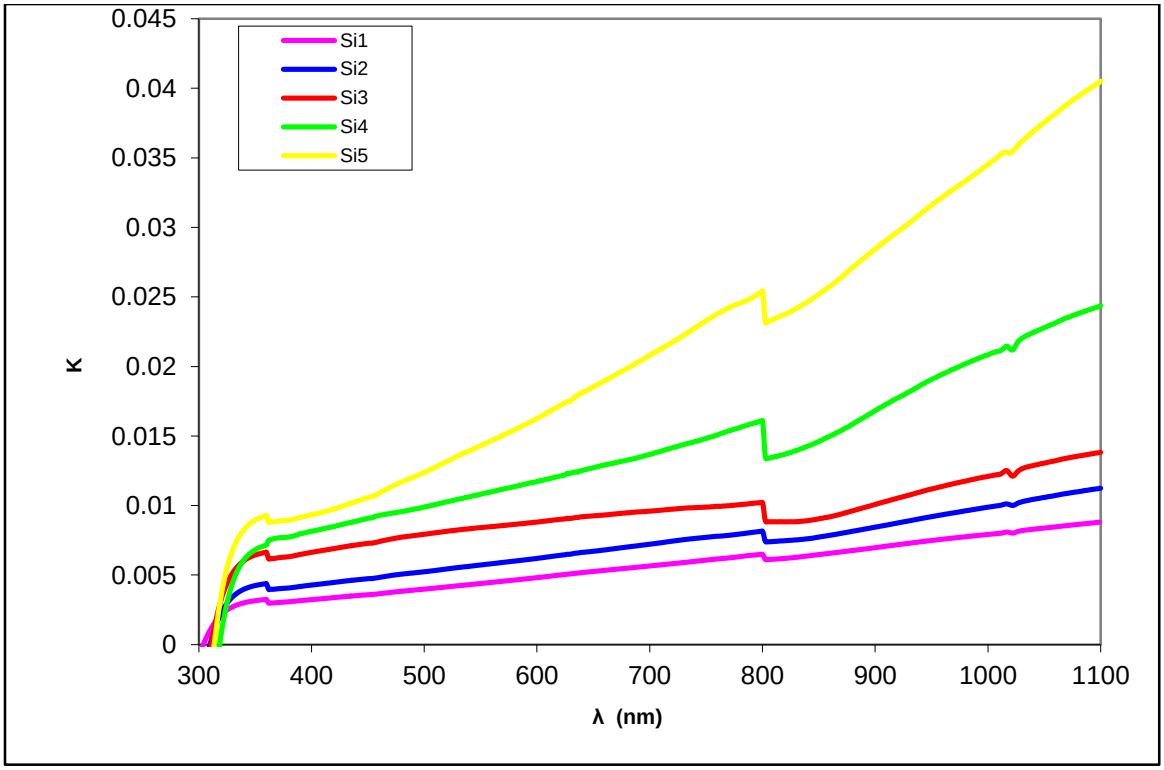

Figure 4.18: Extinction coefficient of Si_1,Si_2,Si_3,Si_4 and Si_5 samples

4.4.5 Reflective index

The refractive index is defined as the ratio between the speed of light in a vacuum to its speed inside the material. The refractive index is related to the reflectivity of the film according to the equation (3-23) through which the refractive index values were calculated.

Figure (4.19) and (4.20) represents the change of the refractive index as a function of the photon energy of Pure PEDOT:PSS and with the additions in different proportions, the nature of the refractive index curve is similar to the nature of the reflectivity curve due to the correlation of the reflectivity with the refractive index, and it is noted that the increase in the proportion of graphene leads to an increase in the refractive index and the reason is due to the change in the reflectivity of the membrane due to the decrease in the porosity of the membrane.

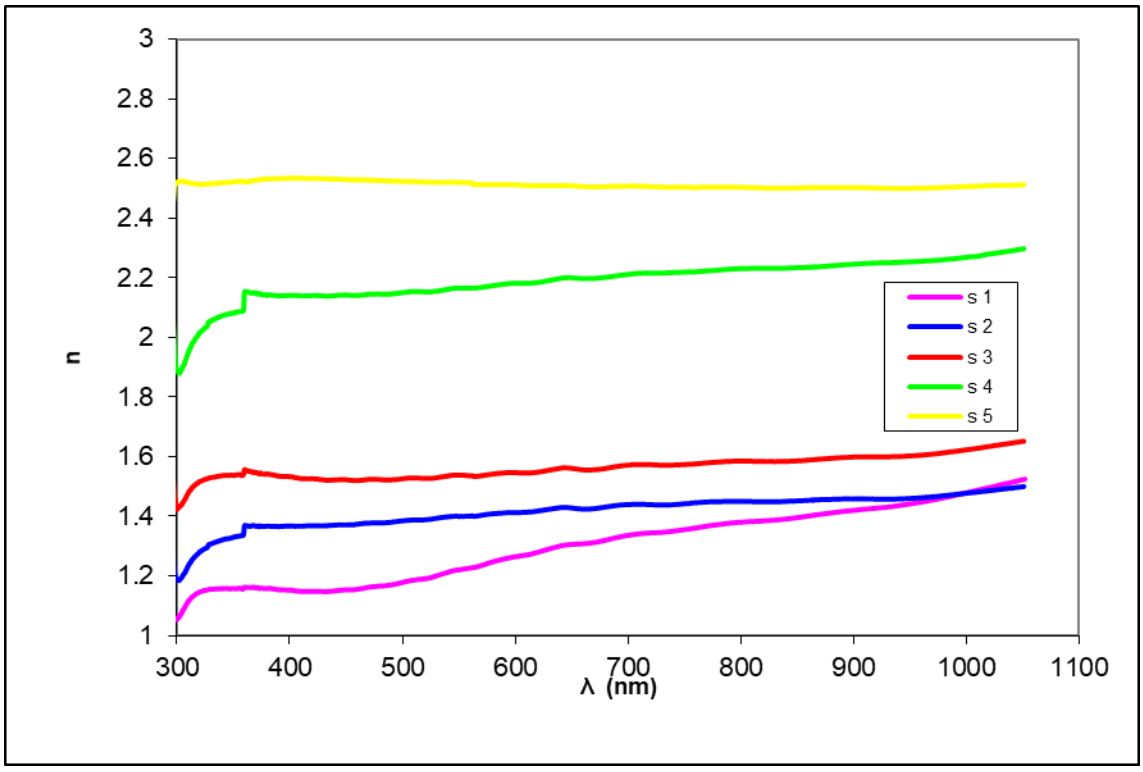

Figure 4.19: Reflected index of S_1,S_2,S_3,S_4 and S_5 samples

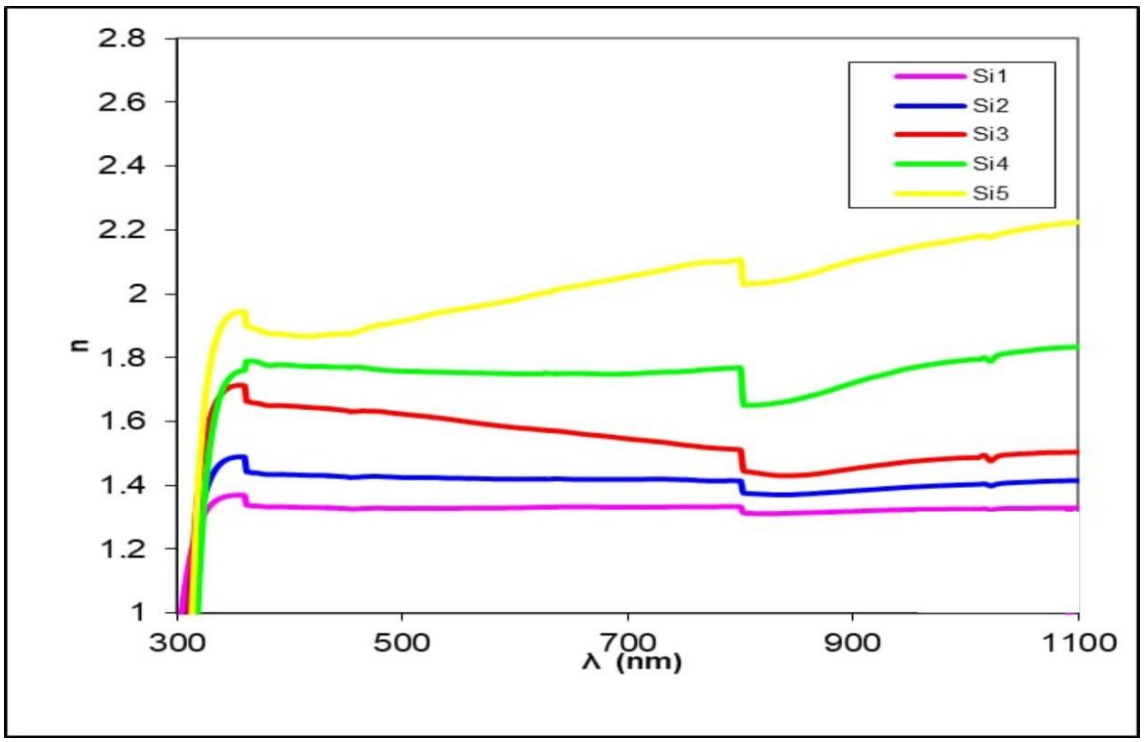

Figure 4.20: Reflected index of Si_1,Si_2,Si_3,Si_4 and Si_5 samples

4.4.6 Dielectric constant

The interaction between the light and the charges of the medium is due to the process of absorbing energy in the material and then the process of polarization of the charges of that medium. This polarization is usually described by the complex dielectric constant of that medium [181].

Figure (4.22) shows the change of the real part of the dielectric constant as a function of the energy of the pure photon. Notes that the behavior of the curve is somewhat similar to the behavior of the refractive index curve. The real dielectric constant was calculated from the relationship (3-29). We note that the effect of the extinction coefficient is very small compared to the effect of the refractive index, and it can be neglected, especially at low photon energies. As for increasing graphene, we notice that the nature of the true

dielectric constant curve in general has not changed in form and this is due to Relationship of the real part of the dielectric constant to the refractive index.

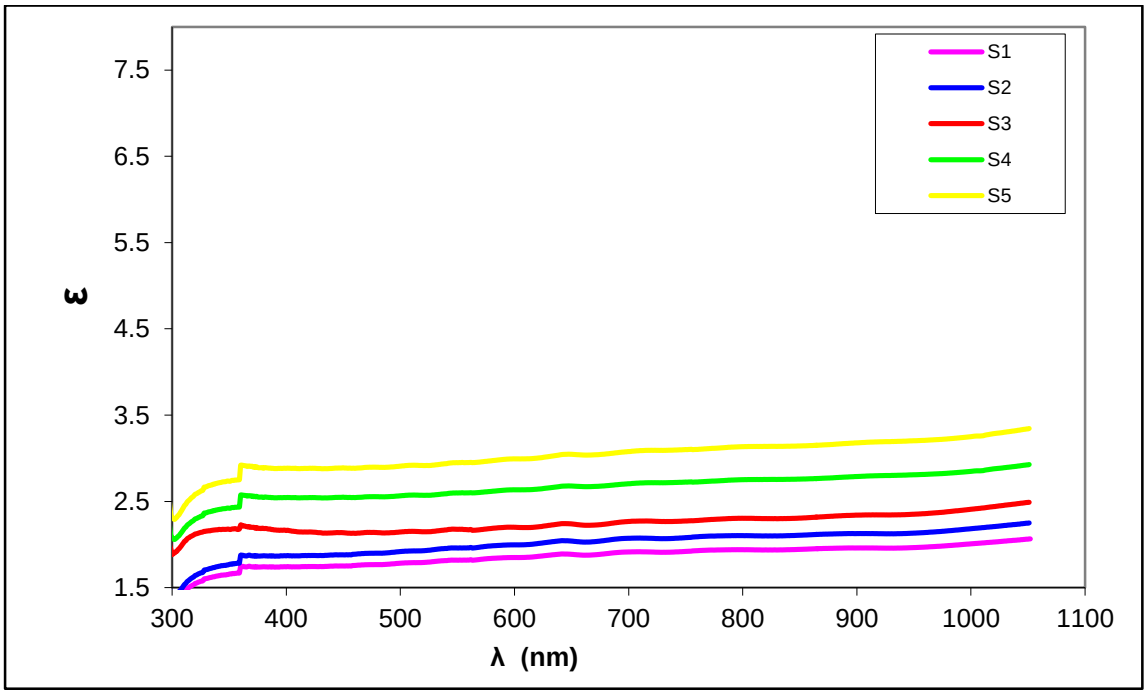

Figure 4.21: Dielectric constant of S_1,S_2,S_3,S_4 and S_5 samples

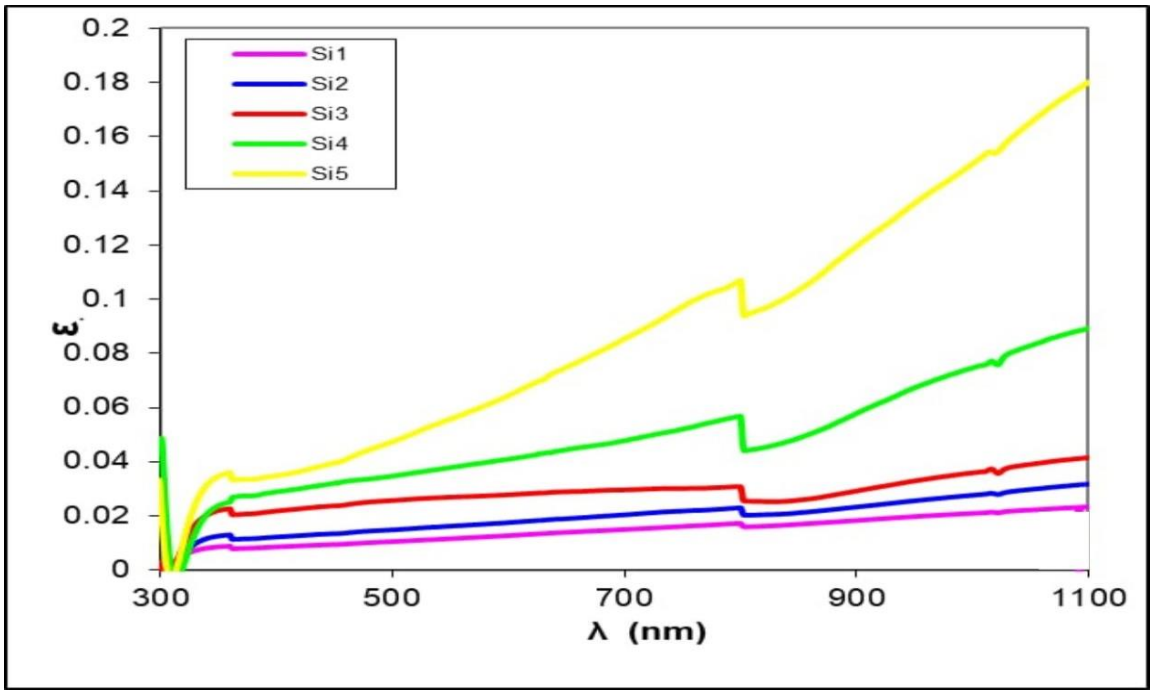

Figure 4.22: Dielectric constant of Si_1,Si_2,Si_3,Si_4 and Si_5 samples

4.5 DC results

Figure (4.23) shows that the conductivity increased with increasing temperature, this is because of the increasing of charge carriers in the conduction band [127]. The results of this test show decreasing the electric resistance (increase in the electrical conductivity) with increasing the temperature from 30 to 100 C° in a behavior similar to that of semiconductors because they have resistance with a negative thermal coefficient. The electrical conductivity increasing due to increasing the density and mobility of charge carriers. Increasing the electrical conductivity with increasing the wt. % of graphene. The maximum electrical conductivity resulted with 2wt.% of graphene which represented the maximum addition.

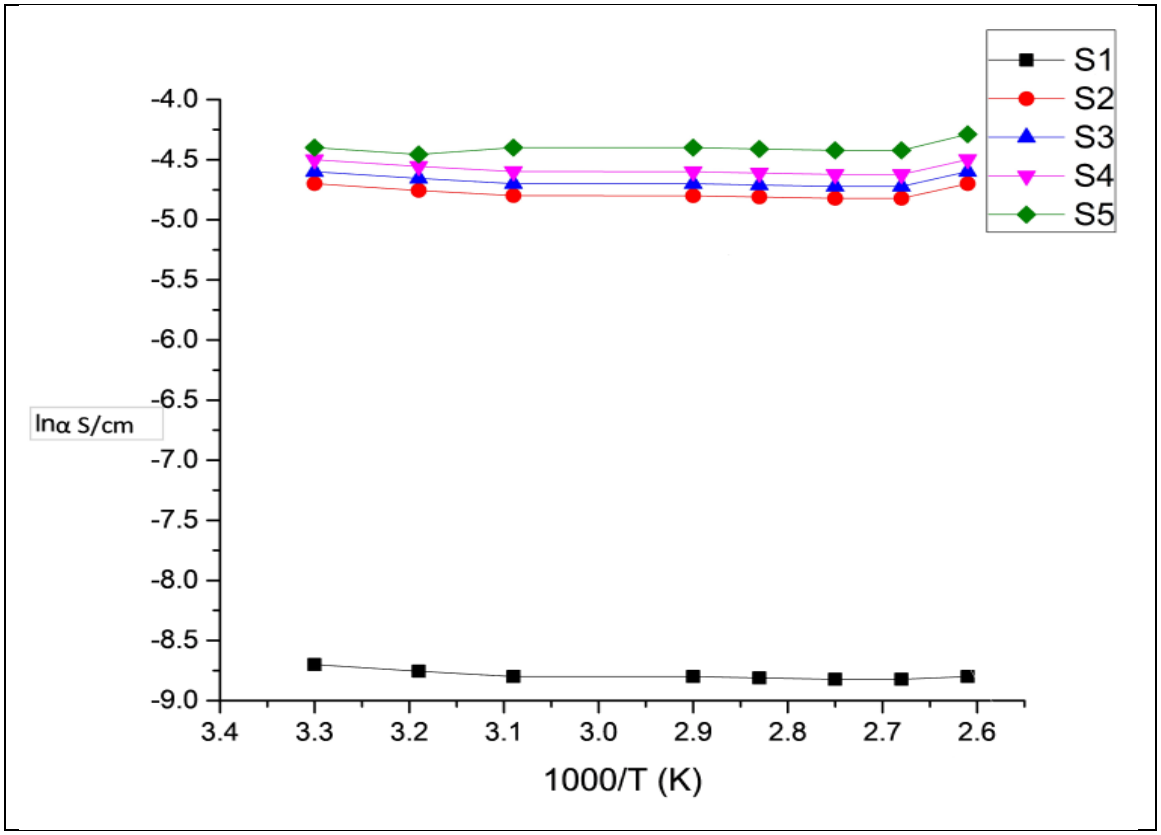

Figure 4.23: ln σ against (1000/T) of PEDOT:PSS/Graphene films

while when adding the IPA as shown in figure (4.24) the conductivity is electrical Significantly higher increase with increasing temperature, due to the decrease in the value of the energy gap as shown in Figure (4.16), and this helps to obtain electro-optical applications.

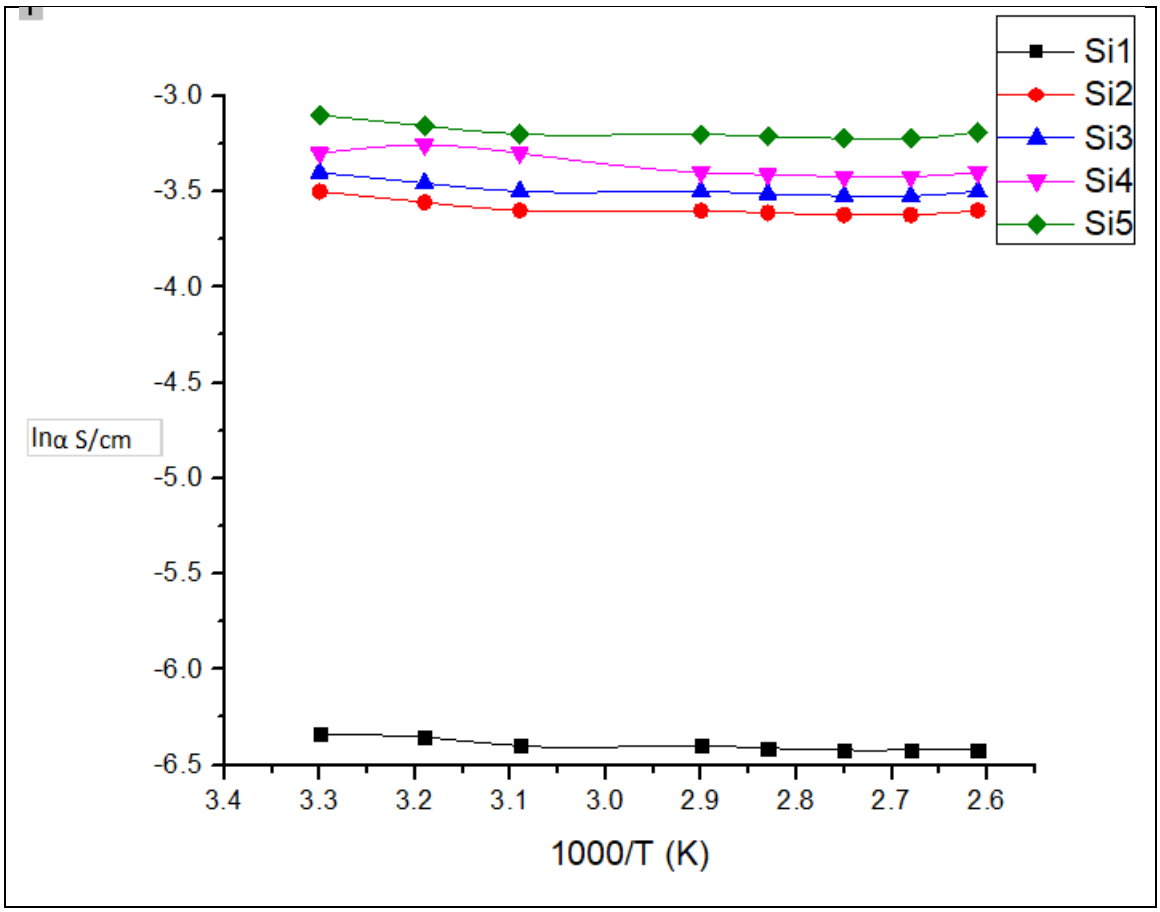

Figure 4.24: ln σ against (1000/T) of PEDOT:PSS/Graphene and IPA films

5. 1 Conclusions

1. X-ray results showed that, the addition of graphene shifted the diffraction position up word, the crystallin degree increased linearly with graphene concentration, crystalline size increased and the scattering function increased by 8.5%

2. FTIR results proved, there is no chemical reaction, and there is only interaction, which enhance the desperation and the stability of graphene sheets.

3. Base on FTIR results, the proposed interaction model suggests that the interaction its take place by three steps.

4. DSC results proved, that there is about 35% increasing in the Tg value, which points to an expected improvement in thermal stability and mechanical properties.

5. Zeta potential test showed that, there is enough electrostatic repulsion among graphene sheets, which enhance its stability and dispersion.

6. Graphene addition increases the surface roughness parameter, when S_a increased.

7. Graphene addition convert the structure from hydrophilic to hydrophobic.

8. IPA addition (compared with neat samples) causes no new bonds also

9. UV- VIS Spectroscopy showed that the prepared films have an absorption in the range 300-900 and the highest absorption in the range 300-400 , adding graphene increased the absorbance while the transmittance decreased.

10. The pure and doped PEDOT:PSS film has an optical energy gap for the direct electronic transitions, and the value of the energy gap for the pure PEDOT:PSS film is (2.8 eV), this value decreases with the increase of the

graphene concentration, and this reason is due to the levels of graphene impurities within the energy gap.

11. Graphene enhance he conductivity of polymer as shown by the results of the DC

5.2 Recommendations

There are recommendations that may be useful for further work in this field, which are:

1. Using another conductive polymer such as P_3HT (Poly(3-hexylthiophene)).
2. Doping with metals, such as gold or copper.
3. Possibility of using the prepared films in smart material applications like robot.
4. Study of electronic and mechanical properties.
5. Study addition of other surfactant with various number of hydroxyl group, such as Glycolic acid ($2OH^-$) or Glycerol ($3OH^-$).
6. Study the thermal stability by TGA technique.

References

[1] Ozaydin-Ince, G., Coclite, A. M., & Gleason, K. K. (2011). CVD of polymeric thin films: applications in sensors, biotechnology, microelectronics/organic electronics, microfluidics, MEMS, composites and membranes. Reports on Progress in Physics, 75(1), 016501.

[2] Chen, N., Kim, D. H., Kovacik, P., Sojoudi, H., Wang, M., & Gleason, K. K. (2016). Polymer thin films and surface modification by chemical vapor deposition: Recent progress. Annual review of chemical and biomolecular engineering, *7*, 373-393.

[3] Lin, Z., Huang, Y., & Duan, X. (2019). Van der Waals thin-film electronics. Nature Electronics, 2(9), 378-388.

[4] Akraa, M., Hasan, A. S., & Kadhim, M. J. H. (2020). Spectroscopy Characterization of Ethylene Vinyl Acetate Degradation by Different Kinds of Accelerated Aging. Baghdad Science Journal, 17(3), 0795-0795.

[5] Guo, X., Xu, Y., Ogier, S., Ng, T. N., Caironi, M., Perinot, A., ... & Yan, F. (2017). Current status and opportunities of organic thin-film transistor technologies. *IEEE transactions on electron devices*, *64*(5), 1906-1921.

[6] Ati, A. A., Abdalsalam, A. H., & Hasan, A. S. (2021). Thermal, microstructural and magnetic properties of manganese substitution cobalt ferrite prepared via co-precipitation method. Journal of Materials Science: Materials in Electronics, 32(3), 3019-3037.

[7] Yoo, D., Kim, J., & Kim, J. H. (2014). Direct synthesis of highly conductive poly (3, 4-ethylenedioxythiophene): poly (4-styrenesulfonate)(PEDOT: PSS)/graphene composites and their applications in energy harvesting systems. *Nano Research*, *7*(5), 717-730.

[8] Huang, X., Yin, Z., Wu, S., Qi, X., He, Q., Zhang, Q., ... & Zhang, H. (2011). Graphene-based materials: synthesis, characterization, properties, and applications. *small*, *7*(14), 1876-1902.

[9] Said, S. M., Rahman, S. M., Long, B. D., & Sabri, M. F. M. (2015). Preparation of TEG material based on conducting polymer PEDOT: PSS through treatment by nitric acid. *WIT Trans. Ecol. Environ*, *206*, 251-258.

[10] Zhang, G. J., Cai, M., & Hu, A. (2013). Energy consumption and the unexplained winter warming over northern Asia and North America. *Nature Climate Change*, *3*(5), 466-470.

[11] Arshad, M., Zubair, M., Rahman, S. S., & Ullah, A. (2020). Polymers for advanced applications. In Polymer Science and Nanotechnology (pp. 325-340). Elsevier.

[12] Lyu, M. Y., & Choi, T. G. (2015). Research trends in polymer materials for use in lightweight vehicles. International journal of precision engineering and manufacturing, 16(1), 213-220.

[13] Lalwani, G., Patel, S. C., & Sitharaman, B. (2016). Two-and three-dimensional all-carbon nanomaterial assemblies for tissue engineering and regenerative medicine. Annals of biomedical engineering, 44(6), 2020-2035.

[14] Müller, K., Bugnicourt, E., Latorre, M., Jorda, M., Echegoyen Sanz, Y., Lagaron, J. M., ... & Schmid, M. (2017). Review on the processing and properties of polymer nanocomposites and nanocoatings and their applications in the packaging, automotive and solar energy fields. Nanomaterials, 7(4), 74.

[15] Delides, C. G. (2016). Everyday Life Applications of Polymer Nanocomposites. no. October.

[16]Soule‹ D. E., McClure, J. W., & Smith, L. B. (1964). Study of the Shubnikov-de Haas effect. Determination of the fermi surfaces in graphite. Physical Review, 134(2A), A453.

[17]Kroto, H. W., Heath, J. R., O'Brien, S. C., Curl, R. F., & Smalley, R. E. (1985). C 60: buckminsterfullerene. nature, 318(6042), 162-163.

[19] Patil, A., Lopez, G., Foxe, M., Childres, I., Roecker, C., Boguski, J., ... & Chen, Y. P. (2010). Graphene field effect transistors for detection of

ionizing radiation. In IEEE Nuclear Science Symposuim & Medical Imaging Conference (pp. 674-676). IEEE.

[20] Georgiou, T., Britnell, L., Blake, P., Gorbachev, R. V., Gholinia, A., Geim, A. K., ... & Novoselov, K. S. (2011). Graphene bubbles with controllable curvature. Applied Physics Letters, 99(9), 093103.

[21] Kuilla, T., Bhadra, S., Yao, D., Kim, N. H., Bose, S., & Lee, J. H. (2010). Recent advances in graphene based polymer composites. Progress in polymer science, 35(11), 1350-1375.

[22] Poh, T. Y., Ali, N. A. T. B. M., Mac Aogáin, M., Kathawala, M. H., Setyawati, M. I., Ng, K. W., & Chotirmall, S. H. (2018). Inhaled nanomaterials and the respiratory microbiome: clinical, immunological and toxicological perspectives. Particle and fibre toxicology, 15(1), 1-16.

[23] Delides, C. G. (2016). Everyday Life Applications of Polymer Nanocomposites. no. October.

[24] Shameli, K., Bin Ahmad, M., Jazayeri, S. D., Sedaghat, S., Shabanzadeh, P., Jahangirian, H., ... & Abdollahi, Y. (2012). Synthesis and characterization of polyethylene glycol mediated silver nanoparticles by the green method. International journal of molecular sciences, 13(6), 6639-6650.

[25] Han, J.T. and Cho, K. (2006). Nanoparticle-induced Enhancement in Fracture Toughness of Highly Loaded Epoxy Composites Over a Wide Temperature Range, Journal of Materials Science, 41(13): 42394245.

[26] Wu, C.L., Zhang, M.Q., Rong, M.Z. and Friedrich, K. (2002). Tensile Performance Improvement of Low Nanoparticles Filled-polypropylene Composites, Composites Science and Technology, 62(10): 13271340.

[27] Jordan, J., Jacob, K. I., Tannenbaum, R., Sharaf, M. A., & Jasiuk, I. (2005). Experimental trends in polymer nanocomposites—a review. Materials science and engineering: A, 393(1-2), 1-11. [28] Y.-P. Wu, Q.-X. Jia, D.-S. Yu, and L.-Q. Zhang, Polym. Test. 23, 903 (2004).

[29] Hu, H., Onyebueke, L., & Abatan, A. (2010). Characterizing and modeling mechanical properties of nanocomposites-review and evaluation.

Journal of minerals and materials characterization and engineering, 9(04), 275.

[30] Tronto, J., Bordonal, A. C., Naal, Z., & Valim, J. B. (2013). Conducting polymers/layered double hydroxides intercalated nanocomposites. Materials Science-Advanced Topics, 3-30.

[31] Collins, M. N., Nechifor, M., Tanasă, F., Zănoagă, M., McLoughlin, A., Stróżyk, M. A., ... & Teacă, C. A. (2019). Valorization of lignin in polymer and composite systems for advanced engineering applications–a review. International journal of biological macromolecules, *131*, 828-849.

[32] Mylvaganam, K., Chen, Y., Liu, W., Liu, M., & Zhang, L. (2015). Hard thin films: Applications and challenges. In Anti-Abrasive Nanocoatings (pp. 543-567). Woodhead Publishing.

[33] Kern, W. (2012). *Thin film processes II* (Vol. 2). Elsevier.

[34] Benelmekki, M., & Erbe, A. (2019). Nanostructured thin films–background, preparation and relation to the technological revolution of the 21st century. In Frontiers of Nanoscience (Vol. 14, pp. 1-34). Elsevier.

[35] Wang, J., Huang, Z., Duan, H., Yu, S., Feng, X., Wang, G., ... & Wang, T. (2011). Surface stress effect in mechanics of nanostructured materials. Acta Mechanica Solida Sinica, 24(1), 52-82.

[36] Seshan, K. (Ed.). (2001). Handbook of thin film deposition processes and techniques. William Andrew.

[37] Kelly, P. J., & Arnell, R. D. (2000). Magnetron sputtering: a review of recent developments and applications. Vacuum, 56(3), 159-172.

[38] Vickers, N. J. (2017). Animal communication: when I am calling you, will you answer too. Current biology, 27(14), R713-R715.

[39] Hishimone, P. N., Nagai, H., & Sato, M. (2020). Methods of Fabricating Thin Films for Energy Materials and Devices. In Lithium-ion Batteries-Thin Film for Energy Materials and Devices. IntechOpen.

[40] Bednorz, J. G., & Müller, K. A. (1986). Possible high T c superconductivity in the Ba− La− Cu− O system. Zeitschrift für Physik B Condensed Matter, 64(2), 189-193.

[41] Willmott, P. R., & Huber, J. R. (2000). Pulsed laser deposition and vaporization. Rev. Mod. Phys, 72, 315-28.

[42] Lu J, Elam JW, Stair PC. Atomic layer deposition - sequential self-limiting surface reactions for advanced catalyst "bottom-up" synthesis. Surface Science Reports. 2016;71:410-472. DOI: 10.1016/j. surfrep.2016.03.003

[43] Johnson, R. W., Hultqvist, A., & Bent, S. F. (2014). A brief review of atomic layer deposition: from fundamentals to applications. Materials today, 17(5), 236-246.

[44] Fahlman, B. D. (2018). What is "materials chemistry"?. In Materials chemistry (pp. 1-21). Springer, Dordrecht.

[45] Jones, A. C. (2002). Molecular design of improved precursors for the MOCVD of electroceramic oxides. Journal of Materials Chemistry, 12(9), 2576-2590.

[46] Livage, J. (1996). Sol-gel chemistry and electrochemical properties of vanadium oxide gels. Solid state ionics, 86, 935-942.

[47] Dimitriev, Y., Ivanova, Y., & Iordanova, R. (2008). History of sol-gel science and technology. Journal of the University of Chemical technology and Metallurgy, 43(2), 181-192.

[48] Nagai, H., & Sato, M. (2012). Heat treatment in molecular precursor method for fabricating metal oxide thin films. Heat Treatment—Conventional and Novel Applications; Czerwinski, F., Ed, 297-322.

[49] Fotovvati, B., Namdari, N., & Dehghanghadikolaei, A. (2019). On coating techniques for surface protection: A review. *Journal of Manufacturing and Materials Processing*, *3*(1), 28.

[50] Yilbas, B. S., Al-Sharafi, A., & Ali, H. (2019). Chapter 3-Surfaces for Self-Cleaning. Self-Cleaning of Surfaces and Water Droplet Mobility; Yilbas, BS, Al-Sharafi, A., Ali, H., Eds, 45-98.

[51] He, Z., Ma, M., Lan, X., Chen, F., Wang, K., Deng, H., ... & Fu, Q. (2011). Fabrication of a transparent superamphiphobic coating with improved stability. Soft Matter, 7(14), 6435-6443.

[52] Brinker, C. J., & Scherer, G. W. (2013). Sol-gel science: the physics and chemistry of sol-gel processing. Academic press.

[53] Sahu, N., Parija, B., & Panigrahi, S. (2009). Fundamental understanding and modeling of spin coating process: A review. Indian Journal of Physics, 83(4), 493-502.

[54] Steele, A., Bayer, I., & Loth, E. (2009). Inherently superoleophobic nanocomposite coatings by spray atomization. Nano letters, 9(1), 501-505.

[51] Urban, G. (2016). Jacob Fraden: Handbook of modern sensors: physics, designs, and applications.

[52] Marcaník, M., Šustek, M., Tomášek, P., & Jašek, R. (2017). Utilization of 3D sensors in robotics. In MATEC Web of Conferences. EDP Sciences.

[53] Sinha, G. R. (2020). Advances in Modern Sensors; Physics, design, simulation and applications.

[54] Heerens, W. C. (1986). Application of capacitance techniques in sensor design. Journal of physics E: Scientific instruments, 19(11), 897.

[55] Zhao, W., & Chen, G. (2009, April). Comparison of active and passive damping methods for application in high power active power filter with LCL-filter. In 2009 International Conference on Sustainable Power Generation and Supply (pp. 1-6). IEEE.

[56] Tseng, K. C., Huang, C. C., & Lian, F. L. (2009, February). Analysis of sensor characteristics and error eliminations of a wheeled mobile robot with range sensors. In 2008 IEEE International Conference on Robotics and Biomimetics (pp. 228-233). IEEE.

[57] Fraden, J. (2016). Sensor Characteristics. In Handbook of Modern Sensors (pp. 35-68). Springer, Cham.

[58] Kumar, V. J. (2017). Sensors and Their Characteristics. In Advanced Interfacing Techniques for Sensors (pp. 1-71). Springer, Cham.

[59] Bengtsson, L. E. (2012). Lookup table optimization for sensor linearization in small embedded systems.

[60] Arshak, K., & Twomey, K. (2002). Thin films of In2O3/SiO for humidity sensing applications. Sensors, 2(6), 205-218.

[61] Sureshkumar, N., & Dutta, A. (2020). Environmental gas sensors based on nanostructured thin films. In Multilayer Thin Films-Versatile Applications for Materials Engineering. IntechOpen.

[62] Amjadi, M., Kyung, K. U., Park, I., & Sitti, M. (2016). Stretchable, skin-mountable, and wearable strain sensors and their potential applications: a review. Advanced Functional Materials, 26(11), 1678-1698.

[63] Schmaljohann, F., Hagedorn, D., & Löffler, F. (2015). Thin film sensors for measuring small forces. Journal of Sensors and Sensor systems, 4(1), 91-95.

[64] Navale, S. T., Mane, A. T., Chougule, M. A., Shinde, N. M., Kim, J., & Patil, V. B. (2014). Highly selective and sensitive CdS thin film sensors for detection of NO 2 gas. RSC Advances, 4(84), 44547-44554.

[65] Kim, G. H., Shao, L., Zhang, K., & Pipe, K. P. (2013). Engineered doping of organic semiconductors for enhanced thermoelectric efficiency. *Nature materials*, *12*(8), 719-723.

[66] Rwei, S. P., Lee, Y. H., Shiu, J. W., Sasikumar, R., & Shyr, U. T. (2019). Characterization of solvent-treated PEDOT: PSS thin films with enhanced conductivities. Polymers, *11*(1), 134.

[67] Rivnay, J., Inal, S., Collins, B. A., Sessolo, M., Stavrinidou, E., Strakosas, X., ... & Malliaras, G. G. (2016). Structural control of mixed ionic and electronic transport in conducting polymers. *Nature communications*, *7*(1), 1-9.

[68] Zhang, S., Yu, Z., Li, P., Li, B., Isikgor, F. H., Du, D., ... & Ouyang, J. (2016). Poly (3, 4-ethylenedioxythiophene): polystyrene sulfonate films with low conductivity and low acidity through a treatment of their solutions with probe ultrasonication and their application as hole transport layer in polymer solar cells and perovskite solar cells. Organic Electronics, 32, 149-156.

[69] Yan, H., Jo, T., & Okuzaki, H. (2009). Highly conductive and transparent poly (3, 4-ethylenedioxythiophene)/poly (4-styrenesulfonate)(PEDOT/PSS) thin films. Polymer journal, 41(12), 1028-1029.

[70] Ahonen, H. J., Lukkari, J., & Kankare, J. (2000). n-and p-doped poly (3, 4-ethylenedioxythiophene): two electronically conducting states of the polymer. *Macromolecules*, *33*(18), 6787-6793.

[71] Rattan, S., Singhal, P., & Verma, A. L. (2013). Synthesis of PEDOT: PSS (poly (3, 4-ethylenedioxythiophene))/poly (4-styrene sulfonate))/ngps (nanographitic platelets) nanocomposites as chemiresistive sensors for detection of nitroaromatics. Polymer Engineering & Science, *53*(10), 2045-2052.

[72] Ghosh, S., & Inganäs, O. (1999). Self-assembly of a conducting polymer nanostructure by physical crosslinking: applications to conducting blends and modified electrodes. Synthetic Metals, 101(1-3), 413-416.

[73] Zheng, W., & Wong, S. C. (2003). Electrical conductivity and dielectric properties of PMMA/expanded graphite composites. *Composites Science and Technology*, *63*(2), 225-235.

[74] Rattan, S., Singhal, P., & Verma, A. L. (2013). Synthesis of PEDOT: PSS (poly (3, 4-ethylenedioxythiophene))/poly (4-styrene sulfonate))/ngps (nanographitic platelets) nanocomposites as chemiresistive sensors for detection of nitroaromatics. *Polymer Engineering & Science*, *53*(10), 2045-2052.

[75] Zhu, Z., Yang, G., Li, R., & Pan, T. (2017). Photopatternable PEDOT: PSS/PEG hybrid thin film with moisture stability and sensitivity. Microsystems & nanoengineering, 3(1), 1-9.

[76] Balamurugan, A., Ho, K. C., & Chen, S. M. (2009). One-pot synthesis of highly stable silver nanoparticles-conducting polymer nanocomposite and its catalytic application. *Synthetic Metals*, *159*(23-24), 2544-2549.

[77] Mauger, S. A., Chang, L., Rochester, C. W., & Moulé, A. J. (2016). Directional dependence of electron blocking in PEDOT: PSS. *Organic Electronics*, *13*(11), 2747-2756.

[78] Elmahmoudy, M. (2017). *Micro-and nano-patterning of conducting polymers for biomedical applications* (Doctoral dissertation, Université de Lyon).

[79] Liu, J., Pathak, S., Stergiopoulos, T., Leijtens, T., Wojciechowski, K., Schumann, S., ... & Snaith, H. J. (2015). Employing PEDOT as the p-type charge collection layer in regular organic–inorganic perovskite solar cells. *The journal of physical chemistry letters*, *6*(9), 1666-1673.

[80] Huo, L., Liu, T., Sun, X., Cai, Y., Heeger, A. J., & Sun, Y. (2015). Single-Junction organic solar cells based on a novel wide-bandgap polymer with efficiency of 9.7%. *Advanced Materials*, *27*(18), 2938-2944.

[81] Cho, Y. J., Yook, K. S., & Lee, J. Y. (2014). A universal host material for high external quantum efficiency close to 25% and long lifetime in green fluorescent and phosphorescent OLEDs. Advanced Materials, 26(24), 4050-4055.

[82] Kaltenbrunner, M., Adam, G., Glowacki, E. D., & Drack, M. (2012). Schwö diauer. *R., and Bauer, S*.

[83] Amenaghawon, A. N., Anyalewechi, C. L., & Kusuma, H. S. (2021). Polysaccharides for inorganic nanomaterials synthesis. In *Green Sustainable Process for Chemical and Environmental Engineering and Science* (pp. 201-225). Elsevier.

[84] Georgiou, T., Britnell, L., Blake, P., Gorbachev, R. V., Gholinia, A., Geim, A. K., ... & Novoselov, K. S. (2011). Graphene bubbles with controllable curvature. Applied Physics Letters, 99(9), 093103.

[85] Singh, V., Joung, D., Zhai, L., Das, S., Khondaker, S. I., & Seal, S. (2011). Graphene based materials: past, present and future. Progress in materials science, 56(8), 1178-1271.

[86] Tiwari, S. K., Sahoo, S., Wang, N., & Huczko, A. (2020). Graphene research and their outputs: Status and prospect. Journal of Science: Advanced Materials and Devices, 5(1), 10-29.

[87] Geim, A.K., 2009. Graphene: Status and prospects. Science 324 (5934), 1530–1534

[88] Reina, A., Jia, X., Ho, J., Nezich, D., Son, H., Bulovic, V., ... & Kong, J. (2009). Large area, few-layer graphene films on arbitrary substrates by chemical vapor deposition. Nano letters, 9(1), 30-35.

[89] Park, S. J., & Seo, M. K. (2011). Comprehension of nanocomposites. In *Interface Science and Technology* (Vol. 18, pp. 777-819). Elsevier.

[90] Balandin, A. A., Ghosh, S., Bao, W., Calizo, I., Teweldebrhan, D., Miao, F., & Lau, C. N. (2008). Superior thermal conductivity of single-layer graphene. Nano letters, 8(3), 902-907.

[91] Abbott's, I. E. (2007). Graphene: exploring carbon flatland. Phys. Today, 60(8), 35.

[92] Chakraborty, M., & Hashmi, M. S. J. (2018). Graphene as a material–an overview of its properties and characteristics and development potential for practical applications.

[93] Abbott's, I. E. (2007). Graphene: exploring carbon flatland. Phys. Today, 60(8), 35.

[129] Si, Y., & Samulski, E. T. (2008). Synthesis of water soluble graphene. *Nano letters*, *8*(6), 1679-1682.

[130] Li, X., Wang, X., Zhang, L., Lee, S., & Dai, H. (2008). Chemically derived, ultrasmooth graphene nanoribbon semiconductors. science, 319(5867), 1229-1232.

[95] Allen, M. J., Tung, V. C., & Kaner, R. B. (2010). Honeycomb carbon: a review of graphene. Chemical reviews, 110(1), 132-145.

[94] Ventura, G., & Martelli, V. (2009). Thermal conductivity of Kevlar 49 between 7 and 290 K. Cryogenics, 49(12), 735-737.

[96] Jin, C., Lan, H., Peng, L., Suenaga, K., & Iijima, S. (2009). Deriving carbon atomic chains from graphene. *Physical review letters*, *102*(20), 205501.

[97] Logsdon, J. E., & Loke, R. A. (2000). Isopropyl alcohol. Kirk-Othmer Encyclopedia of Chemical Technology.

[98] Hansen, C. M. (2007). Hansen solubility parameters: a user's handbook. CRC press.

[99] U.S. Pat. 3,256,250 (June 14, 1966), V. J. Frilette (to Socony Mobil Oil).

[100] Fu, P., Qiao, X., Yao, J. A., Li, H., Zhang, Y. F., Lin, Z. D., ... & Du, F. P. (2020). Constructing ordered-structure organic thermoelectric films via supramolecular self-assembly of PEDOT: PSS and conjugated triblock copolymer. *Synthetic Metals*, *269*, 116536.

[101] Thomas, J. P., & Leung, K. T. (2016). Mixed co-solvent engineering of PEDOT: PSS to enhance its conductivity and hybrid solar cell properties. *Journal of Materials Chemistry A*, *4*(44), 17537-17542.

[102] Said, S. M., Rahman, S. M., Long, B. D., & Sabri, M. F. M. (2015). Preparation of TEG material based on conducting polymer PEDOT: PSS through treatment by nitric acid. WIT Trans. Ecol. Environ, 206, 251-258.

[103] Park, S., Kim, Y., Jung, H., Park, J. Y., Lee, N., & Seo, Y. (2017). Energy harvesting efficiency of piezoelectric polymer film with graphene and metal electrodes. Scientific reports, 7(1), 1-8.

[104] Yamaguchi, H., Aizawa, K., Chonan, Y., Komiyama, T., Aoyama, T., Sakai, E., ... & Sato, N. (2018). Highly Flexible and Conductive Glycerol-Doped PEDOT: PSS Films Prepared Under an Electric Field. Journal of Electronic Materials, 47(6).

[105] Fukushima, S., Shimatani, M., Okuda, S., Ogawa, S., Kanai, Y., Ono, T., & Matsumoto, K. (2018). High responsivity middle-wavelength infrared graphene photodetectors using photo-gating. Applied Physics Letters, 113(6), 061102.

[106] Lu, B., Yuk, H., Lin, S., Jian, N., Qu, K., Xu, J., & Zhao, X. (2019). Pure pedot: Pss hydrogels. *Nature communications*, *10*(1), 1-10.

[107] Fan, X., Forsberg, F., Smith, A. D., Schröder, S., Wagner, S., Östling, M., ... & Niklaus, F. (2019). Suspended graphene membranes with attached silicon proof masses as piezoresistive nanoelectromechanical systems accelerometers. Nano letters, 19(10), 6788-6799.

[108] Mousavi, S. S., Sajad, B., & Majlesara, M. H. (2019). Fast response ZnO/PVA nanocomposite-based photodiodes modified by graphene quantum dots. Materials & Design, 162, 249-255.

[109] Wang, X., Suwardi, A., Lim, S. L., Wei, F., & Xu, J. (2020). Transparent flexible thin-film p–n junction thermoelectric module. *NPJ Flexible Electronics*, *4*(1), 1-9.

[110] Zhang, Y., Chen, L., Hu, X., Zhang, L., & Chen, Y. (2015). Low work-function poly (3, 4-ethylenedioxylenethiophene): Poly (styrene sulfonate) as electron-transport layer for high-efficient and stable polymer solar cells. *Scientific reports*, *5*(1), 1-12.

[111] Chandio A. D., Abro S. H., Rasheed A., Zehra K., Ansari M. B., Salman W., Hazimmoria. (2020). "Processing Characterisation and Application of Graphene" SindhUniv. Res. Jour. (Sci. Ser.), Vol.52, No.2, pp.173-180.

[112] Andrés, M. T., Chung, W. O., Roberts, M. C., & Fierro, J. F. (1998). Antimicrobial Susceptibilities ofPorphyromonas gingivalis, Prevotella intermedia, and Prevotella nigrescens spp. Isolated in Spain. *Antimicrobial agents and chemotherapy*, *42*(11), 3022-3023.

[113] Yu, W., & Xie, H. (2012). A review on nanofluids: preparation, stability mechanisms, and applications. *Journal of nanomaterials*, *2012*, 1.

[114] Singh, C., Purohit, S., Singh, M., & Pandey, B. L. (2013). Design and evaluation of microspheres: A Review. Journal of drug delivery research, 2(2), 18-27.

[115] Thota, S., Kusuma, B., Rarevati, M., Narendra, P., & Babu, S. M. (2021). Formulation and Evaluation of ethyl cellulose microspheres containing diclofenac sodium. International Journal of Research in Pharmaceutical Sciences and Technology, 2(4).

[116] Danaei, M., Dehghankhold, M., Ataei, S., Hasanzadeh Davarani, F., Javanmard, R., Dokhani, A., ... & Mozafari, M. R. (2018). Impact of Particle Size and Polydispersity Index on the Clinical Applications of Lipidic Nanocarrier Systems. *Pharmaceutics*, *10*(2), 57.

[117] Kittel, C. (1976). Introduction to solid state physics.

[118] M. Quillec, "Materials of Opoelectronics", Springer-Verlag, Berlin Heidelberg, New York (1996).

[119] R.Grigorvici , " Amorphous and Liquid Semiconductor " Ed. by. Tauc , Plenum Press , London , (1974) .

[120] Streetman, B. G., & Banerjee, S. (2006). *Solid state electronic devices* (Vol. 10). Upper Saddle River, NJ: Pearson/Prentice Hall.

[121] Peinke, J., Parisi, J., Rössler, O. E., & Stoop, R. (1992). Semiconductor physics. In *Encounter with Chaos* (pp. 9-41). Springer, Berlin, Heidelberg.

[122] Wang, X., Kyaw, A. K. K., Yin, C., Wang, F., Zhu, Q., Tang, T., ... & Xu, J. (2018). Enhancement of thermoelectric performance of PEDOT: PSS films by post-treatment with a superacid. RSC advances, 8(33), 18334-18340.

[123] Du, F. P., Cao, N. N., Zhang, Y. F., Fu, P., Wu, Y. G., Lin, Z. D., ... & Cheng, C. (2018). PEDOT: PSS/graphene quantum dots films with enhanced thermoelectric properties via strong interfacial interaction and phase separation. Scientific reports, 8(1), 1-12.

[124] Mecozzi, M., & Sturchio, E. (2017). Computer assisted examination of infrared and near infrared spectra to assess structural and molecular changes in biological samples exposed to pollutants: a case of study. *Journal of Imaging*, *3*(1), 11.

[125] Zhou, J., Anjum, D. H., Chen, L., Xu, X., Ventura, I. A., Jiang, L., & Lubineau, G. (2014). The temperature-dependent microstructure of PEDOT/PSS films: insights from morphological, mechanical and electrical analyses. Journal of Materials Chemistry C, 2(46), 9903-9910.

[126] Ju, D., Kim, D., Yook, H., Han, J. W., & Cho, K. (2019). Controlling electrostatic interaction in PEDOT: PSS to overcome thermoelectric tradeoff relation. *Advanced Functional Materials*, *29*(46), 1905590.

[127]. 14. A.R. Blythe" Electrical Properties of Polymers", United States of America by Cambridge University Press, New York, First Edition, pp. (90-93) (1977).

جمهورية العراق
وزارة التعليم العالي والبحث العلمي
جامعة بابل
كلية هندسة المواد
قسم هندسة المواد البوليمرات والصناعات البتروكيمياوية

دراسة مقارنة بين الافلام الرقيقة للمركبات النانوية ل (PEDOT:PSS-Graphene) و (PEDOT:PSS/Graphene with Isopropy lalcohol) بتقنية الطلاء بالدوران

رسالة
مقدمة الى كلية هندسة المواد/ جامعة بابل وهي جزء من متطلبات نيل درجة الماجستير في هندسة المواد/ البوليمر

من قبل الباحثة

سرى كامل جبر زامل

(بكالوريوس في هندسة المواد 2017)

بإشراف

أ.د. عودة جبار بريهي
أ.م.د. علي صلاح حسن

1443 هـ **2021م**

الخلاصة

تم تصنيع متحسس ضوئي قليل الكلفة ويعمل بطول موجي طويل بتقنية الطلاء الدوراني (Spin Coating)وعلى ركيزة زجاجية (Glass substrate). يتكون المتحسس من متراكب بوليمري نانوي مكون من بوليمرPEDOT: PSS ومضافا اليه الكرافين النانوي (Nano Graphene) بنسب وزنية مختلفة (0.5, 1 ,1.5 ,2). كما أضيف كحول الايزوبروبيل (Isopropyl Alcohol; IPA) كمادة مشتتة (Surfactant) لتحسين انتشارية مالئ الكرافين النانوي ضمن الطور الرئيسي للمتراكب وتم مقارنتها مع المركب الاولي.

لضمان التلاصق الجيد بين الركيزة الزجاجية ومكونات المتراكب النانوي، فقد تم تهيئة سطح الركيزة وفق السياقات العالمية كما وتم تحفيرها كيميائيا (Chemical Etching) باستخدام محلول Piranha المكون من بيروكسيد الهيدروجين (H_2O_2) وحامض الكبريتيك المركز(H_2SO_4). للتأكد من نجاح عملية التحفير، فقد تم اجراء فحوصات الخشونة (Roughness) وقابلية التبلل (Wettability) قبل وبعد عملية تحفير الركائز المحضرة. اعتمدت الطريقة البصـــرية لــقياس سمك الاغشية المحضرة و للتأكد من ان كافة الافلام المحضرة ذات سمك متساوي (Even Thickness).

أجري اختبار جهد زيتا (Zeta Potential Test) للتأكد من دور المادة المشتتة المقترحة (IPA) لزيادة انتشارية مالئ الكرافين النانوي، اذ تستخدم المادة المشتتة هذه لأول مرة مع الكرافين النانوي وقد تم اقتراحها للتغلب على مشكلة ترسب الكرافين بعد بضعة ساعات من تحضير العالق مما كان يحول دون استخدام العالق ذاته في اليوم التالي من العمل المختبري.

وظفت مطيافية الأشعة تحت الحمراء (FTIR) لتحديد نوع الترابط بين المكونات ولاقتراح موديل للترابط (ان وجد) ، فيما استخدمت تقنية حيود الأشعة السينية (XRD) لدراسة المتغيرات البلورية. تم رصد تأثير المالئ النانوي على التحولات الحرارية (Thermal Transitions) باستخدام مسعر المسح التفاضلي (DSC) كما تم دراسة الخواص المورفولوجية بمجهري المسح الالكتروني (SEM) والقوى الذرية (AFM). أما الخواص البصرية فقد درست بمطيافية الأشعة المرئية فوق البنفسجية (UV-Visible spectrometer). قيست التوصيلية الكهربائية بجهاز DC Keithley، فيما درست قابلية التبلل (Wettability) وفق مبدء زاوية التلامس (Contact angle).

أكدت النتائج نجاح عمليتي التهيئة السطحية والتحفير الكيميائي في تغيير طوبغرافية وخشونة سطح الركيزة وبما يضمن تلاصق كفوء لها مع المتراكب النانوي، كما تبين ان لطريقة الطلاء الدوراني المتبعة القدرة على انتاج افلام باسماك متقاربة، اذ بلغت 245 ±5 نانومتر. بينت النتائج كذلك قدرة المادة المشتتة المقترحة (IPA) على احداث التغيير المنشود في منع ترسب مالئ الكرافين النانوي وزيادة استقرارية العالق من حالة الاستقرارية الجيدة (Good Stability) الى حالة الاستقرارية الممتازة (Excellent)

Stability، اذ تغير جهد زيتا من -48.04 الى -168.38 ملي فولت كما وتغيرت التحركية (Mobility) من -2.27 الى -1.6 (V/cm) / (µ/s).

أظهرت نتائج مطيافية الاشعة تحت الحمراء عدم حدوث تفاعل كيميائي بين مكونات المتراكب والاقتصار فقط على حدوث ترابطات هيدروجينية (Hydrogen Bonding's) وعليه تم اقتراح موديل للتجاذب بين المكونات يتحقق بثلاث خطوات، اذ تنشأ في البداية اواصر هيدروجينية بين بوليمرPEDOT:PSS والماء المجهز معه وعندما يضاف الكرافين يحصل ترابط جديد بين الاوكسجين (الموجود بنسبة 1% في صفائح الكرافين) مع الهيدروجين المتوفر في البوليمر وبذا تزداد الفعالية السطحية للكرافين (لامتلاكه لمجاميع الهيدروكسيل توا) مما يؤهله للترابط مع الماء المتوفر.

أحدث اضافة الكرافين تأثيرات ملحوضة على البلورية، اذ حولت التركيب شبه المتبلور (Semi - crystalline) للبوليمر النقي الى تركيب متبلور وكلما زادت نسبة المالئ ازدادت حدة نبضات التبلور وظهرت في مواقع جديدة مما يعزز دور المالئ كعامل تنوية (Nucleating Agent) اذ ظهرت مستويات تبلور جديدة عند الموقع $2\Theta = 55^0$. تعززت زيادة البلورية من خلال الحسابات المرافقة كحجم التبلور (Crystallite Size) وفق حعادلة شيرر (Scherrer equation) الذي ازداد من 0.1 الى 2.8487 نانومتر ودالة الاستطارة (Scattering function) التي ازدادت من 0.25783 الى 0.29921. كما احدثت اضافة الكرافين زيادة درجة الانتقال الزجاجي (T_g) بنسبة 35% وتحولا من الوضع المحب للماء (Hydrophillic nature) الى الطبيعة الكارهة للماء، اذ تغيرت زاوية التلامس من 74.645^0 الى 136.624^0.

أظهرت نتائج AFM ازدياد معاملات الخشونة اذ ازداد متوسط الخشونة (S_a) بنحو 92٪ ومعامل كثافة القمم (S_{ds}) بنسبة 45٪ وقد تطابقت هذه النتائج مع صور SEM والتي أظهرت أن أفلام PEDOT: PSS بدون الكرافين لها سطح أكثر سلاسة نسبيًا من أسطح المتراكبات النانوية. زاد مؤشر الاحتفاظ بالسوائل (Sci) بنسبة 7.23٪ بسبب نشوء حجيرات صغيرة جدا تخزن السوائل في المتراكب نتيجة للتأصر الهيدروجيني أنف الذكر ، في السياق نفسه. ازداد مؤشر تحمل السطح (Surface Bearing Index ; S_{bi}) بنسبة عالي جدا (525٪) وبما يشير الى التحسن المتوقع في المواصفات الميكانيكية للافلام المحضرة.

أثبتت مطيافية لأشعة المرئية ـ فوق البنفسجية أن إضافة الكرافين تزيد من الامتصاصية في كافة مناطق الطيف الثلاث (منطقة الأشعة فوق البنفسجية ، منطقة الأشعة تحت الحمراء والمنطقة المرئية) وتكون الزيادة على أوجها في منطقة الأشعة فوق البنفسجية مما يشير إلى امكانية المتحسس المحضر مقاومة تدهور الأشعة فوق البنفسجية (لأنه سيمتصها ويبددها بداخله على شكل حرارة طفيفة) وامكانيته العمل ضمن طول موجي طويل يشمل المناطق الثلاث. أثبتت المطيافية ذاتها، انخفاض فجوة الطاقة (Band gab energy) وخصوصا بعد اضافة المادة المشتتة وان قيم الفجوة تقع ضمن نطاق عمل المتحسسات ، كما

بينت هذه المطيافية تغيرات واضحة في معاملات الاثارة والتخميد وثابت العزل(Dielectric Constant).
بينت قياسات التوصيلة الكهربائية زيادة ملحوضة باضافة الكرافين النانوي.